Utrecht University

Institute for Theoretical Physics

Master's Thesis

Cosmological Phase Transitions and Gravitational Wave Production in Conformal Extensions of the Standard Model

Author:
Jonas Rezacek

Supervisor:
Dr. Tomislav Prokopec

July 15, 2018

Abstract

This thesis concerns the analysis of the first-order electroweak phase transition in a conformal extension of the standard model (SM). The model we consider is the classically conformal SM which is extended by a scalar doublet and a hidden SU(2) gauge group. First, we review the quantum effective action and the techniques of thermal field theory. We explain why usual perturbation theory breaks down at high temperatures and introduce a novel method to alleviate this problem by resumming diagrams with the so-called gap equation. By this approach, we restore the validity of perturbation theory at finite temperature and thus account for reliable results in the early universe. With such an improved potential at hand we study the thermal history of the universe within the context of the conformal extension of the SM and compare it with the SM results. We study the phase transitions of our model by three different approaches: Sequential symmetry breaking, Gildener-Weinberg method and the multi-field approach. In the last case, we obtain an improved effective potential dependent on two background fields which allows us to trace the global minimum in the two-dimensional field space with increasing temperature. We show that with the Gildener-Weinberg method and the multi-field approach, the conformal extension of the SM entails a strong first-order phase transition. Moreover, the multi-field approach indicates that the phase transitions in our model is a two-step transition. Using these results we analyze the process of bubble nucleation for the Gildener-Weinberg method and the multi-field approach. Finally, we estimate the stochastic gravitational wave backgrounds (SGWB) produced by the collision of bubble walls. Our estimates show that the conformal model in consideration leads to the production of a SGWB which could be detected by the prospective LISA gravitational wave detector.

Acknowledgments

I would like to thank my supervisor, Dr. Tomislav Prokopec for the opportunity to work on this interesting topic, his instructive guidance and the time he dedicated to supervise this project. I am grateful to my co-supervisor Dr. Bogumiła Świeżewska who has dedicated a lot of time to help me understanding the fundamental aspects of this project and in the writing process of this thesis. The valuable discussions in the weekly meetings with Tomislav and Bogumiła were indispensable for the development of this thesis. Furthermore, I would like to thank Sara and my parents for their support.

Contents

Notation and Conventions **4**

Introduction **5**

1 The Quantum Effective Action **8**
1.1 One-particle Irreducible Approach 8
1.1.1 Scalar Fields 12
1.1.2 Fermion Fields 14
1.1.3 Gauge Bosons 15
1.1.4 General One-Loop Corrections 16
1.2 Two-particle Irreducible Approach 16

2 Field Theory at Finite Temperature **20**
2.1 Grand-canonical Ensemble 20
2.2 The Kubo-Martin-Schwinger Relation 21
2.3 Generating Functionals 22
2.3.1 Feynman Propagator at Finite Temperature 22
2.4 Imaginary Time Formalism and Feynman Rules 25
2.5 The Effective Potential at Finite Temperature 26
2.5.1 Scalar Fields 27
2.5.2 Fermion Fields 29
2.5.3 Gauge Bosons 30
2.5.4 General Thermal Corrections 30

3 Improved Effective Potential **31**
3.1 Breakdown of Perturbation Theory at Finite Temperature 32
3.2 Resumming with the Gap Equation 34
3.2.1 Zero Temperature 37
3.2.2 Vanishing External Momentum 38
3.2.3 Hartree-Fock Approximation 38
3.2.4 High Temperature Expansion 38
3.3 Improved Effective Potentials from Gap Equations 39
3.4 Renormalization Group Improvement of the Gap Equation 41

4 Numerical Solutions of the Gap Equation **43**
4.1 Scalar Field with Vanishing External Momentum 43

5 Conformal Extensions of the Standard Model **48**
5.1 Introducing the SU(2)cSM 49

6 Phase Transition in the SU(2)cSM **53**
6.1 Setup . . . 53
6.1.1 Field Content . . . 53
6.1.2 Thermal Masses . . . 54
6.1.3 Benchmark Point . . . 55
6.1.4 Running of the SM Parameters . . . 56
6.2 Sequential Symmetry Breaking . . . 56
6.3 Gildener-Weinberg Method . . . 60
6.3.1 Revisiting the Improvement of the Effective potential . . . 65
6.4 Multi-Gap Equation Method . . . 66
6.4.1 Zero Temperature Results . . . 68
6.4.2 Turning on the Temperature . . . 69

7 Bubble Nucleation **73**
7.1 Overshooting-Undershooting Method . . . 77
7.2 Multi-Field Case . . . 77
7.3 Results for the Gildener-Weinberg Case . . . 79
7.4 Results for Multi-Gap Case . . . 80

8 Prediction of Stochastic Gravitational Wave Background **83**

Conclusions **87**

A High Temperature Expansion for J_B **90**

B Sunset Diagram in the Gap Equation **93**

C Gap Equation for the Higgs Boson in the SM **97**

Notation and Conventions

- We work in natural units, i.e. the speed of light c, the reduced Planck constant $\hbar$ and the Boltzmann constant k_B are set to one,

$$c = \hbar = k_B = 1.$$

- The Minkowski metric $\eta_{\mu\nu}$ has the signature $(+,-,-,-)$.
- Four-vectors are denoted by k and spatial vectors by $\mathbf{k}$.
- We will work in Landau gauge. This does not require ghost-compensating terms and the free propagator for gauge bosons reads

$$\Delta_{\mu\nu}(k) = \frac{-i}{k^2 + i\epsilon}\left(\eta_{\mu\nu} - \frac{k_\mu k_\nu}{k^2}\right).$$

- Divergent integrals are regulated by dimensional regularization $d = 4 - \epsilon$ and we use the $\overline{\text{MS}}$ renormalization scheme. The counter-terms are proportional to

$$\left(\frac{1}{\epsilon} - \frac{1}{2}\gamma_E - \frac{1}{2}\log(4\pi)\right).$$

Introduction

Since the discovery of the Higgs boson at the LHC in 2012, the Standard Model (SM) of particle physics is considered as an experimentally validated theory describing in one framework interactions of elementary particles. With that discovery the important complement of the SM with the Brout–Englert–Higgs mechanism was confirmed. The Brout–Englert–Higgs mechanism explains the generation of masses of gauge bosons and fermions in the SM. Despite this remarkable success, several issues like dark matter, baryogenesis, the hierarchy problem, inflation and ultimately the unification with gravity are not addressed by the SM and remain open problems of particle physics and cosmology. Supersymmetric versions of the SM are one widely studied proposal to extend the SM offering solutions to the aforementioned issues. However, the current lack of experimental evidence for superpartnes of the minimal supersymmetric SM, motivates to also take alternative extensions of the SM into account. Compared to supersymmetry these alternatives often offer more minimalistic approaches to extend the SM and it seems appealing to study them with regard to the open problems in high-energy physics.

Promising canditates are classically conformal extensions of the SM. The proposed conformal SM (cSM) has a classical scale invariance because the Higgs mass term in the calssical potential is omitted. Therefore, only dimensionless paramaters are present in the model. It was proposed first by W. Bardeen [1] to allievate the hierarchy problem of the SM. Due to the absence of the Higgs mass parameter, no fine-tuning between the tree-level mass of the Higgs boson and its quantum corrections is needed. In the cSM all masses are generated purely by quantum corrections. This generation of mass scales is based on radiative symmetry breaking (RSB) introduced in the seminal paper of S. Coleman and E. Weinberg [2]. To generate the Higgs mass in the cSM by RSB requires a rather large self-coupling of the Higgs field [3, 4]. This is considered to be problematic because it leads to Landau poles below the Planck scale [5]. This is a reason why reserach has propelled directed towards extended versions of the cSM where the experimentally measured mass of the Higgs can be generated via RSB. It was proposed to extend the cSM in various ways: a real scalar, a complex scalar, multiple scalars, gauge groups or fermions (see ref. [5] and references therein). A particular appeal of these models is that they can address problems like dark matter, neutrino masses and baryogenesis. We give a more thorough introduction to conformal extensions of the SM in the beginning of chapter 5 and introduce the model which we will study in this thesis: an extension with a scalar doublet and a hidden SU(2) gauge group (SU(2)cSM).

Conformal extensions of the SM have, among other SM extensions, the striking feature to potentially entail a strong first-order electroweak phase transition. Phase transitions are phenomena which can be observed at all scales. The boiling of water, the magnetization of ferromagnets and superconductivity are just a few examples of this phenomena. The phase

transition which we will study in this thesis are rooted in the theory of the electroweak interactions and might lead to cosmological remnants. The vacuum expectation value of the Higgs boson $\langle h \rangle$ consititutes the order paramter of this phase transition because it seperates the phase $\langle h \rangle = 0$ where electroweak symmetry is preserved and the phase $\langle h \rangle \neq 0$ where it is broken. We know that the electroweak symmetry is broken in the universe today, because the observed finite masses of the electroweak gauge bosons require a condensation of the Higgs field to $\langle h \rangle \neq 0$. It was D. Kirzhnits [6] who discovered first that the symmetry might be restored at high temperatures in the early universe. The phase transition is characterized by the critical temperature, above which electroweak symmetry is restored. This started research to study the cosmological consequences of the electroweak phase transition of the SM. However, it was shown that the transition in the SM is too smooth (i.e. a crossover) to lead to cosmological remnants [7]. However, this situation can be altered in various scenarios beyond the SM.

The cosmological implications of the electroweak phase transition are significant if it is a first-order phase transition. This can be characterized by a critical temperature where the free energy (i.e. the effective potential) has two local minima coexisting for some temperature range. If the temperatures drops below the critical temperature, the system can be trapped in a metastable state (false vacuum) because of the potential barrier between the two local minima. The system can transition from the false vacuum to the stable state (true vacuum) by quantum or thermal tunneling through the potential barrier. In this case the phase transition leads to bubble nucleation. This is a phenomenon, where bubbles of the true vacuum are formed in the sea of the old phase until the whole system is in the true vacuum. In cosmology, these bubbles can be formed in the early stages of the universe and expand until they fill the whole universe. Eventually the bubbles will collide and these events might trigger a production of a stochastic background of gravitational waves (SGWB). Furthermore, cosmological bubble nucleation from an electroweak phase transition offers the possibility of electroweak baryogenesis [8].

In this thesis, we will consider the SGWB from bubble collisions in a conformal extension of the SM. This is a promising research area due to recent developments in the possibility of gravitational wave detection. In 2016, the LIGO collaboration announced the successful detection of gravitational waves produced by a black hole merger. However, the sensitivity of the LIGO detector is not high enough to eventually measure SGWB from a first-order phase transition at the electroweak scale. The potential detection of a SGWB is therefore postponed to the LISA mission expected to launch in 2034. The LISA detector will be the first space-based gravitatioanl wave detector consisting of three spacecrafts seperated by 2.5 million km in a triangular formation following the Earth in its orbit around the Sun [9]. The vast length of the arms of this laser interferometer increases the sensitivity of gravitational wave detection in the low frequency band ($\sim$ mHz) and paves the road to measure SGWB from first-order phase transition. This has propelled research to study cosmological first-order phase transition in extension of the SM and estimate its SGWB (see e.g. refs. [10–16]).

The investigation of a thermal phase transition in the early universe is based on an effective potential which takes quantum and thermal effects into account. The effective potential can be computed perturbatively where the usual approach is an expansion in number of loops. This method is not valid at high temperatures due to infrared divergences of so-called hard thermal loops of bosonic fields. This issues is usually resolved by resumming so-called daisy diagrams yielding thermal masses for bosons [17–20]. This approach is the standard technique in the literate to restore perturbativity of the effective potential at high

temperatures and to study thermal phase transitions in the early universe. We propose a new method which is related to the method of ref. [21] in section 3.3, resumming a broader class of diagrams. The resummation technique we introduce is based on the self-consistent gap equation for the scalar fields in theory. This approach yields resummed masses for the scalar fields, which can be used to derive the improved effective potential directly. With this we hope to increase the accuracy compared to the daisy resummation and also give a formalism which is valid beyond the high temperature expansion. With our method we are able to restore perturbativity also at low temperatures at which the daisy resummation technique is not sufficient. Furthermore, this method is appealing since the gap equation can be derived from the two-particle-irreducible (2PI) effective action and allows to resum certain classes of higher-order diagrams. In the method we present, we use the resummed masses to obtain the effective potential directly which corresponds to the 1PI approach (see section 3.3 for more details). If the full 2PI approach is used, the computation of the 2PI effective action yields a resummation of a broader class of diagrams compared to our method. This approach is not studied in this thesis, but it should be compared to our method in the future. Moreover, the gap equation offers the possibility to include finite momentum corrections to the effective action which allows the inclusion of the gradient corrections to the effective action, but this is beyond the scope of this thesis and is left for future research.

This thesis is structured as follows. First, we will review in chapter 1 the quantum effective action which is a useful formalism to study phase transition of QFTs. The formalism is then generalized to field theories at finite temperature in chapter 2. The beginning of chapter 3 concerns the occurence of hard thermal loops at high temperatures and the method of daisy resummation. Subsequently, we introduce the aforementioned gap equation method to consistently resum diagrams and show how to obtain the improved effective potential. The numerical implementation of solving the gap equation is explaind in chapter 4, where we in particular analyze the impact of improving the effective potential by comparing it with standard one-loop results. The conformal extension of the SM which will be studied in this thesis is introduced in chapter 5. Chapter 6 contains the study of the thermal phase transition by three approaches: sequential symmetry breaking, Gildener-Weinberg method and the multi-gap equation approach. The results we find are re-investigated in chapter 7 regarding the details of bubble nucleation and finally in chapter 8 we estimate the power spectra of potential SGWB from bubble collisons.

Chapter 1

The Quantum Effective Action

To study phase transitions in the early universe, it is of significant importance to know the vacuum expectation value (VEV) of the quantum scalar field, since it constitutes the order parameter of phase transitions. The VEV itself can be treated as a classical field and it is possible to describe the dynamics of the VEV field by building a classical effective theory taking quantum effects to a certain loop order into account. This formalism is called the quantum effective action. We introduce the standard one-particle irreducible effective action in section 1.1 which is sufficient at one-loop order. This approach is generalized in section 1.2 to the two-particle irreducible approach, which encodes a resummation prescription for a certain class of diagrams and can improve the perturbative approach beyond the usual loop expansion.

1.1 One-particle Irreducible Approach

In this section we follow the references [2, 22–25]. To introduce the general concept of the effective action, we consider a theory of one scalar field described by the lagrangian $\mathcal{L}[\phi(x)]$ and an action functional

$$S[\phi] = \int d^4x \mathcal{L}[\phi(x)]. \tag{1.1}$$

We can introduce an external source $J(x)$ to the theory by coupling it linearly to the scalar field. The generating functional for this theory in the in-out formalism is denoted by the path integral

$$Z[J] = \langle 0_{\text{out}}|0_{\text{in}}\rangle_J = \int \mathcal{D}\phi \exp\left[i\left(S[\phi] + \phi \cdot J\right)\right], \tag{1.2}$$

where we used the shorthand notation

$$\phi \cdot J = \int d^4x \phi(x) J(x). \tag{1.3}$$

The physical meaning of the generating functional (1.2) is the transition amplitude between the two vacuum states $|0_{\text{in}}\rangle$ and $|0_{\text{out}}\rangle$ in presence of the source $J(x)$. In diagrammatic language, the generating functional is the sum of all connected an disconnected Feynman diagrams in the vacuum to vacuum amplitude, where the Feynman rules are defined by

the action $S[\phi]$ and the source term $\phi \cdot J$. The generating functional $Z[J]$ can be expanded in a series

$$Z[J] = 1 + \sum_{n=1}^{\infty} \int \mathrm{d}^4x_1 \ldots \mathrm{d}^4x_n \, G^{(n)}(x_1, \ldots, x_n) J(x_1) \ldots J(x_n), \tag{1.4}$$

which contains all connected and unconnected correlation functions (i.e. Green's functions) $G^{(n)}$. The time ordered n-point functions are obtained by functional differentiation with respect to the sources and setting the sources then to zero

$$G^{(n)}(x_1, \ldots, x_n) = \langle 0 | T\phi(x_1) \ldots \phi(x_n) | 0 \rangle = \frac{(-i)^n}{Z[0]} \frac{\delta^n Z[J]}{\delta J(x_1) \ldots \delta J(x_n)} \bigg|_{J=0}. \tag{1.5}$$

One can obtain a generating functional $W[J]$ for the connected Green's function by defining

$$Z[J] = \exp\left(iW[J]\right). \tag{1.6}$$

The expansion of the functional $W[J]$

$$W[J] = \sum_{n=1}^{\infty} \frac{i^{n-1}}{n!} \int \mathrm{d}^4x_1 \ldots \mathrm{d}^4x_n \, G_c^{(n)}(x_1, \ldots, x_n) J(x_1) \ldots J(x_n), \tag{1.7}$$

contains all connected Green's functions. They can be obtained by the formula

$$G_c^{(n)}(x_1, \ldots, x_n) = \langle 0 | T\phi(x_1) \ldots \phi(x_n) | 0 \rangle_c = (-i)^{n-1} \frac{\delta^n W[J]}{\delta J(x_1) \ldots \delta J(x_n)} \bigg|_{J=0}. \tag{1.8}$$

That this functional actually generates connected Green's functions, can be illustrated by considering for instance the connected two-point function

$$G_c^{(2)}(x_1, x_2) = \frac{1}{i} \frac{\delta^2 W[J]}{\delta J(x_1) \delta J(x_2)} \bigg|_{J=0} = \langle 0 | T\phi(x_1)\phi(x_2) | 0 \rangle - \left(\langle 0 | \phi(0) | 0 \rangle \right)^2, \tag{1.9}$$

where the disconnected diagrams in $G^{(2)}(x_1, x_2) = \langle 0 | T\phi(x_1)\phi(x_2) | 0$ are canceled by the second term. *. Therefore, the two-point function $G_c^{(2)}$ corresponds to connected Feynman diagrams. This generalizes for arbitrary n-point functions. In the presence of a source $J(x)$ we can obtain the vacuum expectation value of $\phi(x)$, which corresponds to the one point function, by

$$G_C^{(1)}(x) = \frac{\delta W[J]}{\delta J(x)} \bigg|_{J=0} = \frac{1}{iZ[J]} \frac{\delta Z[J]}{\delta J(x)} \bigg|_{J=0} = \left(\frac{\langle 0 | \phi(x) | 0 \rangle}{\langle 0 | 0 \rangle} \right)_J = \varphi(x)_J. \tag{1.10}$$

The subscript J is to indicate that the expectation value depends on the source term. To define the effective action, we will assume that eq. (1.10) is invertible. We define $J_\varphi(x)$ as the source term for which the field $\phi(x)_J$ has the prescribed value φ:

$$\varphi_J(x) = \varphi(x) \quad \text{if} \quad J(x) = J_\varphi(x). \tag{1.11}$$

The classical field $\varphi_J(x)$ (also called average or background field) reduces to the VEV v of the field ϕ for a vanishing source term

$$v = \varphi_J(x) \bigg|_{J=0}. \tag{1.12}$$

*We used a translational invariant vacuum state in eq. (1.9), i.e. $\langle 0 | \phi(x) | 0 \rangle = \langle 0 | \phi(0) | 0 \rangle$.

The effective action is defined as a functional Legendre transformation of $W[J]$

$$\Gamma[\varphi] = W[J_\varphi] - \int \mathrm{d}^4x\, \varphi(x) J_\varphi(x), \tag{1.13}$$

which is a functional of the classical field $\varphi(x)$. The dependence on the source term is eliminated by means of eqs. (1.10) and (1.11). A functional derivative of the effective action with respect to the classical field yields

$$\begin{aligned}\frac{\delta\Gamma[\varphi]}{\delta\varphi(x)} &= \frac{\delta W[J_\varphi]}{\delta\varphi(x)} - \int \mathrm{d}^4x' \left(\frac{\delta\varphi(x')}{\delta\varphi(x)} J_\varphi(x') + \varphi(x') \frac{\delta J_\varphi(x')}{\delta\varphi(x)} \right) \\ &= \int \mathrm{d}^4x' \left[\left(\frac{\delta W[J]}{\delta J(x')} \right) \Big|_{J=J_\varphi} \frac{\delta J_\varphi(x')}{\delta\varphi(x)} + \varphi(x') \frac{\delta J_\varphi(x')}{\delta\varphi(x)} \right] - J_\varphi(x),\end{aligned} \tag{1.14}$$

where we used $\delta\varphi(x)/\delta\varphi(x') = \delta^{(4)}(x - x')$ and the functional chain rule in the first term. By equation (1.10) with $\varphi_J(x) = \varphi(x)$ eq. (1.14) simplifies to

$$\frac{\delta\Gamma[\varphi]}{\delta\varphi(x)} = -J_\varphi(x) \tag{1.15}$$

and for a vanishing source term this reduces to

$$\frac{\delta\Gamma[\varphi]}{\delta\varphi(x)}\bigg|_{J=0} = 0. \tag{1.16}$$

Due to eq. (1.12) this is equivalent to requiring

$$\frac{\delta\Gamma[\varphi]}{\delta\varphi(x)}\bigg|_{\varphi=v} = 0. \tag{1.17}$$

This relation reveals that the vacuum expectation value of the quantum field ϕ in the absence of sources is a functional stationary point of the effective action Γ. In this way, it explains the terminology of the effective action: the VEV of a quantum field is obtained by a stationary principle of an action functional as in a classical theory with action $S[\varphi]$ but also taking quantum effects into account. These quantum effects can be accounted for by perturbation theory organized in an expansion in terms of loops.

The effective action has also a useful interpretation in terms of Feynman diagrams, which we discuss next. We will show that the effective action contains all correlation functions (also called proper vertices) of the quantum theory to a given loop order. To see this, we start by expanding the effective action in the classical field

$$\Gamma[\varphi] = \sum_{n=1}^{\infty} \frac{1}{n!} \int \mathrm{d}^4x_1 \ldots \mathrm{d}^4x_n \, \frac{\delta^n\Gamma[\varphi]}{\delta\varphi(x_1)\ldots\delta\varphi(x_n)} \varphi(x_1)\ldots\varphi(x_n) \tag{1.18}$$

and we will show that the coefficients defined by

$$\Gamma^{(n)}(x_1, \ldots, x_n) = \frac{\delta^n\Gamma[\varphi]}{\delta\varphi(x_1)\ldots\delta\varphi(x_n)} \tag{1.19}$$

correspond to the mentioned correlation functions. For $n = 1$ we directly find using eq. (1.15) that we obtain the one-point correlation function given by the source term. Going

one order higher, we need to exploit the relation

$$\begin{aligned}\delta^4(x-y) = \frac{\delta\varphi(x)}{\delta\varphi(y)} &= \frac{\delta}{\delta\varphi(y)}\left.\frac{\delta W[J]}{\delta J(x)}\right|_{J=J_\varphi} \\ &= \int \mathrm{d}^4 z\, \frac{\delta J_\varphi(z)}{\delta\varphi(y)}\left.\frac{\delta^2 W[J]}{\delta J(z)\delta J(x)}\right|_{J=J_\varphi} \\ &= \int \mathrm{d}^4 z\, \frac{\delta\Gamma[\varphi]}{\delta\varphi(y)\delta\varphi(z)}\left.\frac{\delta^2 W[J]}{\delta J(z)\delta J(x)}\right|_{J=J_\varphi}. \end{aligned} \tag{1.20}$$

For $J = 0$ and thus $\varphi = v$ this shows us that

$$\Gamma^{(2)}(x,y)\Big|_{\varphi=v} = \left(\left.\frac{\delta^2 W[J]}{\delta J(x)\delta J(y)}\right|_{J=0}\right)^{-1} = i\left(G_c^{(2)}\right)^{-1}(x,y). \tag{1.21}$$

In the light of eq. (1.8) we obtain the inverse of the connected two-point function. We car interpret $\Gamma^{(2)}$ as the one-particle irreducible (1PI) amputated two-point Green's function. By taking higher functional derivatives we obtain similar expressions to eq. (1.21) for proper n-point vertices.

It is convenient to write eq. (1.18) in momentum space. Therefore, we write the n-point functions in terms of their Fourier transforms

$$\Gamma^{(n)}(x_1,\ldots,x_n) = \prod_{i=1}^{n}\left[\int \frac{\mathrm{d}^4 p_i}{(2\pi)^4}\right](2\pi)^4\delta^{(4)}\left(\sum_{i=1}^{n} p_i\right)\tilde{\Gamma}^{(n)}(p_1,\ldots,p_n)\exp\left(i\sum_{i=1}^{n} x_i p_i\right). \tag{1.22}$$

Writing the delta function as integral, eq. (1.18) reads

$$\Gamma[\varphi] = \sum_{n=1}^{\infty}\frac{1}{n!}\prod_{i=1}^{n}\left[\int \mathrm{d}^4 x_i \int \frac{\mathrm{d}^4 p_i}{(2\pi)^4}\varphi(x_i)\right]\int \mathrm{d}^4 x\, \tilde{\Gamma}^{(n)}(p_1,\ldots,p_n)\exp\left(i\sum_{i=1}^{n}(x_i - x)p_i\right). \tag{1.23}$$

Furthermore, we expand $\tilde{\Gamma}^{(n)}$ around vanishing momenta

$$\tilde{\Gamma}^{(n)}(p_1,\ldots,p_n) = \Gamma^{(n)}(0,\ldots,0) + \sum_{i=1}^{n}\frac{\partial}{\partial p_i^\mu}\left.\tilde{\Gamma}^{(n)}(p_1,\ldots,p_n)\right|_{p_i=0} p_{i,\mu} + \ldots. \tag{1.24}$$

Substituting eq. (1.24) to eq. 1.23 we can cast the effective potential in the following form

$$\Gamma[\varphi] = \sum_{n=1}^{\infty}\frac{1}{n!}\int \mathrm{d}^4 x\, \tilde{\Gamma}^{(n)}(0,\ldots,0)\varphi(x)^n + \frac{1}{2}\int \mathrm{d}^4 x\, Z(\varphi)\partial_\mu\varphi\partial^\mu\varphi + \ldots. \tag{1.25}$$

Our formalism can be further simplified if the field is in the ground state $\varphi(x) = v_\varphi$ which is constant in space-time. In this case, we can work with an effective potential $V_{\text{eff}}(v_\varphi)$ instead of the effective action functional $\Gamma[\varphi]$. The effective potential is defined as the zero-momentum term of the effective action (cf. eq. (1.25))

$$V_{\text{eff}}(\varphi) = -\sum_{n=1}^{\infty}\frac{1}{n!}\tilde{\Gamma}^{(n)}(0,\ldots,0)\varphi(x)^n. \tag{1.26}$$

For a constant field $\varphi(x) = v_\varphi$ we have the relation

$$\Gamma[v_\varphi] = -V_{\text{eff}}(v_\varphi) \int \mathrm{d}^4x \,, \tag{1.27}$$

and thus the functional stationary condition of the effective action in eq. (1.17) reduces to a stationary point of the effective potential

$$\left.\frac{\partial V_{\text{eff}}}{\partial \varphi}\right|_{\varphi=v} = 0. \tag{1.28}$$

Note that the effective potential is a function of φ and not a functional of φ as the effective action $\Gamma[\varphi]$. The expansion of the effective potential in eq. (1.26) can be interpreted in a convenient diagrammatic way if the desired loop order of the effective potential is specified. In fact, this is the approach we will use to derive the effective potential for certain models.

The coefficients $\tilde{\Gamma}^{(n)}(0,\ldots,0)$ correspond to proper vertices in momentum space with vanishing external momenta. At zero loop order the proper vertex functions are given by the regular vertex functions defined by the classical potential $V^{(0)}(\varphi)$ in the lagrangian. So at zero loop order we find that the effective potential reduces to the tree level potential $V(\phi) = V_{\text{eff}}(\varphi)$, which is what we expect at this order in perturbation theory. However, at the one loop level the proper vertex function get modified by quantum corrections. We denote this part as

$$V^{(1)}(\varphi) = \sum_{n=1}^{\infty} \frac{\varphi^n}{n!} \tilde{\Gamma}^{(n)}_{(1)}(0,\ldots,0), \tag{1.29}$$

where $\tilde{\Gamma}^{(n)}_{(1)}$ are the 1PI irreducible Feynman diagrams at one-loop order and n external legs connected to the background field φ. Thus, eq. (1.29) corresponds to the sum of all one-loop diagrams with vanishing external momenta, with n external legs each contributing the factor φ. The one-loop part of the effective potential is also often called Coleman-Weinberg potential [2]. To render the final result finite, we have to add counter terms $\Delta V(\varphi)$ to the effective potential. To sum up, at one loop order the effective potential is

$$V_{\text{eff}}(\varphi) = V^{(0)}(\varphi) + V^{(1)}(\varphi) + \Delta V(\varphi). \tag{1.30}$$

In the following three subsections, we derive the one-loop corrections $V^{(1)}$ for scalar fields, fermion field and gauge boson fields by the aforementioned diagrammatic approach following refs. [26, 27]. Another diagrammatic approach to derive the one-loop corrections is given in ref. [25]. In this approach, one uses the Feynman rules for the shifted theory [†] and computes the loops without external legs.

1.1.1 Scalar Fields

Consider a massive scalar theory with the lagrangian

$$\mathcal{L}_\phi = \frac{1}{2}\partial_\mu\phi\partial^\mu\phi - V^{(0)}(\phi). \tag{1.31}$$

and classical potential

$$V^{(0)}(\varphi) = \frac{m^2}{2}\varphi^2 + \frac{\lambda}{4!}\varphi^4, \tag{1.32}$$

where φ is the background field. The Feynman rules for this theory are:

[†]The shifted theory is obtained by replacing $S[\phi] \to S[\varphi + \tilde{\phi}]$, where φ is the background field of ϕ.

- scalar propagator: $\frac{i}{k^2-m^2+i\epsilon}$,
- self-interaction vertex: $-i\lambda$.

At one-loop order $V_\varphi^{(1)}$ should be computed as the sum of all 1PI diagramms containing one loop and zero external momenta. Due to the structure of the classical potential (1.32) only diagrams with an even number of external legs contribute. In terms of Feynman diagrams, the sum follows the pattern

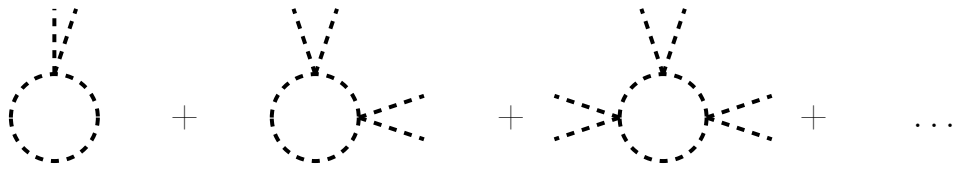

The n-th diagram of this infinite sum, consists of n propagators inside the loop, n vertices and $2n$ external legs. With the Feynman rules of lagrangian (1.31) the propagators give a factor $i^n(k^2-m^2+i\epsilon)^{-n}$, the vertices including the symmetry factor of exchanging the external legs give a factor $-i\lambda/2$ and the pairs of external legs contribute φ^{2n}. The overall symmetry factor is $n!/2n$ because the vertices can be positioned in $n!$ ways but there is a mirror symmetry rendering some of these diagrams equivalent, hence we need to divide by $2n$. Additionally, this coefficient is multiplied by $1/n!$ in the expression for $V^{(1)}$ (cf. eq. (1.29)). According to eq. (1.29) we obtain for the scalar field

$$V_\varphi^{(1)}(\varphi) = i\sum_{l=1}^{\infty}\frac{1}{2n}\int\frac{\mathrm{d}^4k}{(2\pi)^4}\left(\frac{\lambda\varphi^2/2}{k^2-m^2+i\epsilon}\right)^l. \tag{1.33}$$

The additional i is coming from the definition of the generating functional $W[J]$ (cf. eq. (1.6) and (1.27)). By performing the sum over l we obtain

$$V_\varphi^{(1)}(\varphi) = -\frac{i}{2}\int\frac{\mathrm{d}^4k}{(2\pi)^4}\log\left(1-\frac{\lambda\varphi^2/2}{k^2-m^2+i\epsilon}\right). \tag{1.34}$$

To compute this integral we perform a Wick rotation

$$k^0 = ik_E^0, \quad k_E = (-ik^0,\mathbf{k}), \quad k^2 = -k_E^2, \tag{1.35}$$

where the subscript E stands for Euclidean. Now we get

$$\begin{aligned} V_\varphi^{(1)}(\varphi) &= \frac{1}{2}\int\frac{\mathrm{d}^4k_E}{(2\pi)^4}\log\left(1+\frac{\lambda\varphi^2/2}{k_E^2+m^2}\right) \\ &= \frac{1}{2}\int\frac{\mathrm{d}^4k_E}{(2\pi)^4}\left[\log\left(k_E^2+m^2+\lambda\varphi^2/2\right)-\log\left(k_E^2+m^2\right)\right]. \end{aligned} \tag{1.36}$$

Both integrals are UV-divergent and require some regularization prescription. The second term is a field-independent infinite constant term and can be dropped from the effective potential. Using dimensional regularization and the $\overline{\mathrm{MS}}$ scheme the finite part of the first term in eq. (1.36) which is not canceled by counterterms is [2]

$$V_\varphi^{(1)}(\varphi) = \frac{m(\varphi)^4}{64\pi^2}\left[\log\left(\frac{m(\varphi)^2}{\mu^2}\right)-\frac{3}{2}\right]. \tag{1.37}$$

This is the result for dimensional regularization with $\overline{\mathrm{MS}}$ scheme, with renormalization scale μ whereas in ref. [2] a cutoff regularization scheme was used. The computation in

the $\overline{\text{MS}}$ scheme can be found in ref. [27]. The infinite part of the integral (1.36) will be canceled by a suitable choice of the counterterms ΔV in the effective potential. We have defined the so-called field-dependent mass of the scalar field

$$m(\varphi)^2 = m^2 + \frac{\lambda}{2}\varphi^2. \tag{1.38}$$

Eq. (1.37) is the usual one-loop term in the effective potential (or Coleman-Weinberg potential) for scalar fields with field dependent mass $m(\varphi)$.

1.1.2 Fermion Fields

We consider N fermionic fields $\psi^1, \ldots, \psi^N$ interacting with one scalar field with the lagrangian

$$\mathcal{L}_\psi = i\bar{\psi}_a \gamma^\mu \partial_\mu \psi^a + \bar{\psi}_a y_b^a \phi \psi_b, \tag{1.39}$$

where y_a^b is the Yukawa coupling matrix between two fermionic fields and one scalar field. The Feynman rules of this theory are

- fermion propagtor: $\frac{i}{\not{k}+i\epsilon}\delta_b^a$,
- Yukawa interaction vertex: $-iy_b^a\varphi = -i(M_\psi(\varphi))_b^a$,

where we already defined the field-dependent mass matrix $M_\psi(\varphi)$ of the fermions. We now need to sum all vacuum one-loop diagrams with fermion propagators in the loop. The contributing diagrams are depicted by

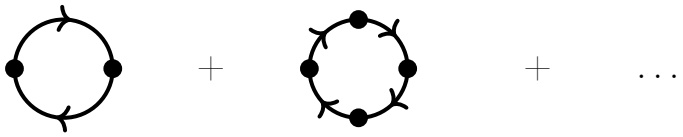

where the black dots denote the Yukawa vertex which in this case includes the external leg φ. Diagrams with an odd power of φ drop out, because the number of propagator is then also odd and the trace of an odd number of γ-matrices vanishes. For a diagram with $2l$ vertices the propagators contribute

$$\text{Tr}\Big[i^{2l}(\gamma\cdot k)^{2l}(k^2)^{-2l}\Big], \tag{1.40}$$

with a trace in the spinor space. We have dropped the ϵ terms for convenience. The vertices contribute

$$\text{Tr}_f[-iM_\psi(\varphi)^{2l}], \tag{1.41}$$

where the trace rungs over the different fermionic fields. If we combine these two, multiply by the appropriate symmetry factors and include a minus sign for the fermion loop, we obtain

$$-\frac{1}{2l}\frac{\text{Tr}_f[M_\psi(\varphi)^{2l}]}{k^{2l}}\,\text{Tr}[\mathbf{1}], \tag{1.42}$$

where we have used $(\gamma\cdot k)^2 = k^2$. The trace in spinor space $\sigma = \text{Tr}[\mathbf{1}]$ counts the degrees of freedom of the fermions. For Dirac fermions that is $\sigma = 4$ and for Weyl fermions $\sigma = 2$.

Including now the overall factor i and integration over the loop momentum we obtain for the one-loop term of the fermions

$$V_\psi^{(1)}(\varphi) = -i\sigma \sum_{l=1}^{\infty} \mathrm{Tr}_f \int \frac{\mathrm{d}^4k}{(2\pi)^4} \frac{1}{2l} \left[\frac{M_\psi^2}{k^2}\right]^{2l}$$
$$= i\frac{\sigma}{2} \sum_{l=1}^{\infty} \mathrm{Tr}_f \int \frac{\mathrm{d}^4k}{(2\pi)^4} \log\left(1 - \frac{M_\psi^2}{k^2}\right). \tag{1.43}$$

As in the previous section, the integral is solved after performing a Wick rotation for the momenta

$$V_\psi^{(1)}(\varphi) = -\sigma\, \mathrm{Tr}_f\, \frac{1}{2} \int \frac{\mathrm{d}^4k_E}{(2\pi)^2} \log\big(k_E^2 + M_\psi^2(\varphi)\big), \tag{1.44}$$

where we have omitted the field independent term. The integral which has to be solved in eq. (1.44) is the same as in the case of scalar fields. For a diagonal mass matrix $M_\psi(\varphi) = m_\psi(\varphi)\mathbf{1}$ the trace Tr_f reduces to a factor N and we obtain [27]

$$V_\psi^{(1)}(\varphi) = -\sigma N \frac{m_\psi(\varphi)^4}{64\pi^2} \left[\log\left(\frac{m_\psi(\varphi)^2}{\mu^2}\right) - \frac{3}{2}\right], \tag{1.45}$$

which differs by a factor of $(-\sigma N)$ compared to the scalar field (cf. (1.37)). For instance, a quark has the factors $\sigma = 4$ and $N = 3$ and thus eq. (1.45) counts correctly its twelve degrees of freedom (3 colors $\times$ 2 spins $\times$ 2 electric charges).

1.1.3 Gauge Bosons

Consider now a gauge boson interacting with a scalar field, described by the lagrangian

$$\mathcal{L}_A = -\frac{1}{4} F_{\mu\nu} F^{\mu\nu} + e^2 A_\mu A^\mu \phi^2. \tag{1.46}$$

The Feynman rules in Landau gauge read:

- gauge boson propagator: $\frac{-i}{k^2+i\epsilon}\Delta_{\mu\nu} = \frac{-i}{k^2+i\epsilon}\Big(\eta_{\mu\nu} - \frac{k_\mu k_\nu}{k^2}\Big)$,
- scalar-gauge-boson vertex: $2ie^2\eta_{\mu\nu}$.

To compute the one-loop term of the gauge boson $V_A^{(1)}$ we have to sum the diagrams depicted by

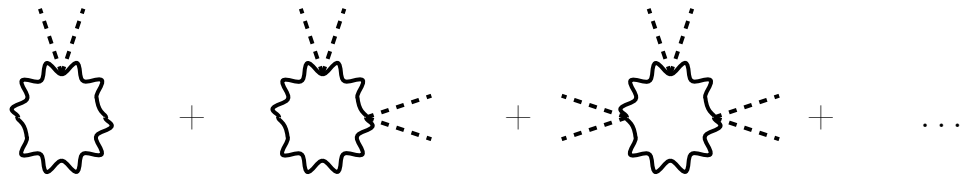

The derivation of $V_A^{(1)}$ is very similar to the scalar field case, but the trace of the projectors $\Delta_{\mu\nu}$ changes the final result. The projector has the property

$$\mathrm{Tr}[\Delta^n] = \mathrm{Tr}[\Delta] = d - 1, \tag{1.47}$$

where d counts space-time dimensions. With that in mind, the l-th diagram of the sum reads

$$\frac{1}{2l}\left(\frac{(e\varphi)^2}{k^2+i\epsilon}\right)^{2l}(d-1) \tag{1.48}$$

The one-loop term is obtained by including the overall i, summing over l and integrating over the loop momentum k. After performing the summation and omitting field independent terms, we obtain the Euclidean integral

$$V_A^{(1)}(\varphi) = \frac{1}{2}\int \frac{\mathrm{d}^4 k_E}{(2\pi)^4}(d-1)\log\big(k_E^2 + m_A^2(\varphi)\big), \tag{1.49}$$

where $m_A(\varphi) = e\varphi$ is the field dependent mass of the gauge boson. Using dimensional regularization when solving the integral, the factor $d-1 = 3-\epsilon$ causes a slight modification of the final result [27]

$$V_A^{(1)}(\varphi) = 3\frac{m_A^4(\varphi)}{64\pi^2}\left[\log\left(\frac{m_A^2(\varphi)}{\mu^2}\right) - \frac{5}{6}\right]. \tag{1.50}$$

The factor 3 counts the degrees of freedom of a massive gauge boson.

1.1.4 General One-Loop Corrections

To sum up the last three sections, we give the general one-loop term

$$V_i^{(1)}(\varphi) = n_i\frac{m_i^4(\varphi)}{64\pi^2}\left(\log\left(\frac{m_i^2(\varphi)}{\mu^2}\right) - C_i\right), \tag{1.51}$$

for a field with field dependent mass $m_i(\varphi)$. The coefficients n_i and C_i can be determined by

$$n_i = \begin{cases} 1 \text{ for scalar fields,} \\ -4 \text{ for Dirac fermions,} \\ 3 \text{ for gauge boson,} \end{cases} \tag{1.52}$$

$$C_i = \begin{cases} \frac{3}{2} \text{ for scalar fields and fermions,} \\ \frac{5}{6} \text{ for gauge bosons.} \end{cases} \tag{1.53}$$

If a model contains multiple particles, the total one-loop correction is given by the sum over all particles present in the theory

$$V^{(1)}(\varphi) = \sum_i V_i^{(1)}(\varphi). \tag{1.54}$$

1.2 Two-particle Irreducible Approach

Cornwall, Jackiw and Tomboulis generalized the 1PI effective action approach to a n-PI approach [28]. The n-PI effective action $\Gamma_n[\varphi, G^{(2)}, \ldots, G^{(n)}]$ has next to functional dependence on the one-point function $\varphi(x)$ also functional dependence on the n-point functions denoted by $G^{(2)}(x_1, x_2), \ldots, G^{(n)}(x_1, \ldots, x_n)$. Previously, we have seen that the

only functional dependence on the 1PI effective action is the one-point function, i.e. the classical background field $\varphi(x)$. We will discuss this generalization by the example of the 2PI effective action following ref. [29]. As the name suggests, the 2PI effective action contains 2PI diagrams. Since one-loop diagrams cannot be 2PI, this method is usually used if results beyond one-loop level are desired. In fact, at one-loop order, it is not necessary to go beyond the 1PI approach, since the 2PI effective action would simply reduce to the usual 1PI effective action. In contrast, for results at n-loop order it is necessary to use the m-PI effective action with $m \geq n$ to be self-consistent [29]. All descriptions with $m \geq n$ are then equivalent, so it is usually most convenient to choose $m = n$.

The 2PI effective action is a helpful formalism if the usual perturbative expansion in loops breaks down (e.g. at high temperatures) and a resummation technique alleviating this problem is needed. This method can be seen as a reorganization of perturbation theory where infinite number of diagrams belonging to a certain class is resummed into effective proper vertices encoded by the effective action. In this way, the perturbative approach to the effective potential can be improved significantly. We will elaborate on this resummation technique in more detail in chapter 3.

The generating functional $Z[J, R]$ in the 2PI description for a scalar field ϕ with action $S[\phi]$ is defined by

$$\begin{aligned} Z[J,R] &= \exp(iW[J,R]) \\ &= \int \mathcal{D}\phi \exp\left[i\left(S[\phi] + \int \mathrm{d}^4x\, \phi(x)J(x) + \frac{1}{2}\int \mathrm{d}^4x \int \mathrm{d}^4y\, \phi(x)R(x,y)\phi(y)\right)\right], \end{aligned} \tag{1.55}$$

where apart from the local source $J(x)$ a bilocal source $R(x, y)$ is introduced. As in the 1PI approach, the functional $W[J, R]$ generates connected Green's functions. The connected one- and two-point functions are defined by

$$\langle \phi(x) \rangle = \frac{\delta W[J,R]}{\delta J(x)} = \varphi(x), \tag{1.56}$$

$$\langle T\phi(x)\phi(y) \rangle = 2\frac{\delta W[J,R]}{\delta R(x,y)} \ = \left(G(x,y) + \varphi(x)\varphi(y)\right), \tag{1.57}$$

respectively. Eq. (1.57) is defined such that the contribution of the disconnected part drops out (cf. eq. (1.9)). The 2PI effective action is obtained by a double Legendre transformation of $W[J, R]$ with respect to both source terms,

$$\Gamma^{\mathrm{2PI}}[\phi, G] = W[J,R] - \int \mathrm{d}^4x\, \frac{\delta W[J,R]}{\delta J(x)} J(x) - \int \mathrm{d}^4x \int \mathrm{d}^4y\, \frac{\delta W[J,R]}{\delta R(x,y)} R(x,y). \tag{1.58}$$

Here we assumed that eqs. (1.56) and (1.57) can be inverted to get an expression for $J(x)$ and $R(x, y)$ for prescribed $\varphi(x)$ and $G(x, y)$ (according to eq. (1.11)). For simplicity, we do not denote this dependence in this section. Using eqs. (1.56) and (1.57) we get

$$\begin{aligned} \Gamma^{\mathrm{2PI}}[\phi, G] &= W[J,R] - \int \mathrm{d}^4x\, \varphi(x)J(x) - \frac{1}{2}\int \mathrm{d}^4x \int \mathrm{d}^4y\, G(x,y)R(x,y) \\ &\quad - \frac{1}{2}\int \mathrm{d}^4x \int \mathrm{d}^4y\, \varphi(x)\varphi(y)R(x,y) \\ &= W[J,R] - \varphi \cdot J - \frac{1}{2}\mathrm{Tr}(R \cdot G) - \frac{1}{2}\varphi \cdot R \cdot \varphi, \end{aligned} \tag{1.59}$$

where the functional dependence on J and R on the right hand side is removed by means of eqs. (1.56) and (1.57). We can take two different functional derivatives of the 2PI effective action

$$\frac{\delta\Gamma^{2\mathrm{PI}}[\phi,G]}{\delta\varphi(x)} = -J(x) - \int \mathrm{d}^4y\, R(x,y)\varphi(y), \tag{1.60}$$

$$\frac{\delta\Gamma^{2\mathrm{PI}}[\phi,G]}{\delta G(x,y)} = -\frac{1}{2}R(x,y), \tag{1.61}$$

In the case of vanishing sources, the 2PI effective action obeys two stationary conditions,

$$\left.\frac{\delta\Gamma^{2\mathrm{PI}}[\varphi,G]}{\delta\varphi}\right|_{J,R=0} = 0 \tag{1.62}$$

$$\left.\frac{\delta\Gamma^{2\mathrm{PI}}[\varphi,G]}{\delta G}\right|_{J,R=0} = 0. \tag{1.63}$$

Also in the 2PI formalism, the first condition (1.62) determines the VEV of the field. To relate the effective action to diagrams and interpret the second stationary condition (1.63), we write the classical action as

$$S[\phi] = \int \mathrm{d}^4x \int \mathrm{d}^4y\, \phi(x) iD_0(x-y)\phi(y) + S_{\mathrm{int}}[\phi], \tag{1.64}$$

where D_0 is the inverse of the free propagator and S_{int} includes cubic and higher interaction terms. Furthermore, we introduce the functional operator

$$D^{-1}(\varphi;x,y) = \frac{\delta S[\varphi]}{\delta\varphi(x)\delta\varphi(y)} = D_0^{-1}(x,y) + \frac{\delta S_{\mathrm{int}}[\varphi]}{\delta\varphi(x)\delta\varphi(y)}, \tag{1.65}$$

which is the propagator in the shifted theory at tree level. With these definitions the 2PI effective action can be written as [28]

$$\Gamma[\varphi,G]^{2\mathrm{PI}} = S[\varphi] + \frac{i}{2}\mathrm{Tr}\ \mathrm{Log}(G^{-1}) + \frac{i}{2}\mathrm{Tr}(D^{-1}G) + \Gamma_2[\phi,G] + \mathrm{const.} \tag{1.66}$$

The term Γ_2 contains all 2PI irreducible vacuum diagrams with vertices defined by S_{int} in the shifted theory and G used as propagator. Applying stationary condition (1.63) to (1.66) yields the so-called gap equation

$$G^{-1}(\varphi;x,y) = D^{-1}(x,y) - 2i\frac{\delta\Gamma_2[\varphi,G]}{\delta G(x,y)}. \tag{1.67}$$

The last term can be identified with a self energy

$$\Sigma(\varphi,G;x,y) = -2i\frac{\delta\Gamma_2[\varphi,G]}{\delta G(x,y)}, \tag{1.68}$$

because inverting the gap equation to get an expression for G gives a Dyson-Schwinger-like equation

$$G(\varphi;x,y) = D(x,y) - D(x,y)\cdot\Sigma(\varphi,G;x,y)\cdot D(x,y) + \ldots. \tag{1.69}$$

This infinite series resums the self-energies according to

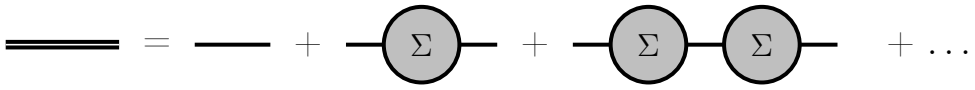

In this way, the resummed propagator G (double line) is obtained by iterating the self-energies Σ with the tree-level propoagator D (single line). It should be noted that the self-energies Σ are obtained self-consistently, i.e. the resummed propagator G is used. Hence, the iteration of the gap equation is more complicated than the diagrams suggest. We will clarify this method in chapter 3 with a concrete example and show which class of diagrams is resummed if Γ_2 is computed at the two-loop level. Solving the gap equation (1.67) is equivalent to resumming an infinite number diagrams to obtain the resummed propagator $G(\varphi)$. Once $G(\varphi)$ is found, it has to be plugged into eq. (1.66) to obtain the 2PI effective action. After the integrals in eq. (1.66) are solved, the 2PI effective action $\Gamma^{2\mathrm{PI}}[\phi, G(\phi] = \Gamma[\phi]$ reduces to a 1PI effective action Γ because it has only functional dependence on φ. The effective action Γ then generates the n-point functions in the resummed theory [30].

Chapter 2

Field Theory at Finite Temperature

All methods introduced in the last chapter where derived on the assumption of an empty space-time. This reflects for instance in the computation of the n-point functions $\langle T\phi_1(x_1)\dots\phi_n(x_n)\rangle$ where the expectation values are taken in the vacuum state denoted by $|0\rangle$ (cf. eq. (1.5)). This formalism is suitable for instance for particle interactions in collider experiments but not for particle interactions in the early universe. The early universe was hot and the matter and radiation densities were non-negligible. Hence, expectation values should not be taken with the vacuum state, but with a thermal state. This adaption of the field theoretic description introduced in chapter 1 will result in so-called field theory at finite temperature which is the suitable formalism for particle interactions in the early universe. The approach we use is based on the assumption that the typical timescale of particle interactions in the early universe were small compared to the Hubble time scale. Hence, particles interact many times during one Hubble time, keeping the universe in thermal equilibrium. In other words, the universe is expanding adiabatically and correlation functions can be computed in thermal equilibrium for the processes we are interested in in this thesis. This chapter is directed towards the derivation of the one-loop effective at finite temperature, allowing us to study thermal phase transitions in the early universe. We will follow closely the review [26]. In addition, we recommend the reviews [31, 32] and the textbook [33].

2.1 Grand-canonical Ensemble

First, we briefly introduce the grand-canonical ensemble, to show how expectation values are calculated in thermal equilibrium. The grand-canonical ensemble describes a system connected with a reservoir (or thermal bath) at temperature T. In this formalism energy and particles can be exchanged between the system and reservoir, but the temperature T, the chemical potentials μ_i and the volume are fixed. The canonical density operator for a system with Hamiltonian H reads

$$\rho = \frac{1}{Z}\exp\left(-\beta H - \beta\sum_i \mu_i Q_i\right), \tag{2.1}$$

where $\beta = 1/T$ is the inverse temperature and Q_i is a set of conserved charges. The partition function Z defined as

$$Z = \mathrm{Tr}\left[\exp\left(-\beta H - \beta \sum_i \mu_i Q_i\right)\right] \tag{2.2}$$

ensures the correct normalization of the density operator

$$\mathrm{Tr}(\rho) = 1. \tag{2.3}$$

The grand canonical average (or thermal average) of an operator $\hat{O}$ is computed by

$$\left\langle \hat{O} \right\rangle = \mathrm{Tr}\Big(\hat{O}\rho\Big), \tag{2.4}$$

which is the desired formula to compute expectation values in a thermal bath with temperature T and chemical potentials μ_i. In the following of this thesis we will consider only cases with zero chemical potentials.

2.2 The Kubo-Martin-Schwinger Relation

The Kubo-Martin-Schwinger (KMS) relation is a very powerful relation for field theory at finite temperature. To derive it, we start by considering the Feynman propagator of a scalar field

$$G(x, x') = \theta(t - t')G_+(x, x') + \theta(t' - t)G_-(x, x'), \tag{2.5}$$

where $G_\pm(x, x')$ are the positive and negative frequency Wightman functions defined by

$$G_+(x, x') = \left\langle \phi(x)\phi(x') \right\rangle, \quad G_-(x, x') = \left\langle \phi(x')\phi(x) \right\rangle. \tag{2.6}$$

For a field theory at finite temperature the expectation values are obtained by means of eq. (2.4), i.e.

$$iG_+(x, x') = \frac{1}{Z}\,\mathrm{Tr}\Big(e^{-\beta H}\phi(x)\phi(x')\Big). \tag{2.7}$$

For a time independent Hamiltonian H, we can write the scalar field as

$$\phi(t, \mathbf{x}) = e^{itH}\phi(0, \mathbf{x})e^{-itH}. \tag{2.8}$$

Using the cyclic property of the trace, we obtain

$$\begin{aligned} iG_+(x, x') &= \frac{1}{Z}\,\mathrm{Tr}\Big(e^{iH(t+i\beta)}\phi(0, \mathbf{x})e^{-iH(t+i\beta)}e^{-\beta H}\phi(t', \mathbf{x'})\Big) \\ &= \frac{1}{Z}\,\mathrm{Tr}\Big(e^{-\beta H}\phi(t', \mathbf{x'})\phi(t + i\beta, \mathbf{x})\Big), \end{aligned} \tag{2.9}$$

from which we can derive the KMS relation

$$iG_+(t, \mathbf{x}; t', \mathbf{x'}) = iG_-(t + i\beta, \mathbf{x}; t', \mathbf{x'}), \tag{2.10}$$

stating that the Wighman functions are periodic in imaginary time with period β. This motivates to analytically continue the time t to the complex plane and exploit the KMS relation (2.10) to derive the Feynman propagator for fields at finite temperature.

2.3 Generating Functionals

Since we want to analytically continue the time t, we have to adjust the definitions of the generating functional introduced in chapter 1. The Green's function contain a time-ordering operator T which has to be generalized to a time-ordering operator in the complex plane T_C. This time ordering means that the fields should be ordered along a contour C in the complex plane, which will be specified later. The Green's function read now

$$G^{C,(n)}(x_1,\ldots,x_n) = \langle T_C \phi(x_1)\ldots\phi(x_n)\rangle\,. \tag{2.11}$$

If we define a parametrization of C by $t = z(\tau)$, where τ is real, the time ordering T_C reduces to the usual time ordering T along τ. The step function is then simply given by $\theta_c(t-t') = \theta(\tau-\tau')$ and the delta function by $\delta_c(t) = (\partial z/\partial t)^{-1}\delta(\tau)$. Furthermore, functional derivatives obey

$$\frac{\delta f(x)}{\delta f(x')} = \delta_c(t-t')\delta^{(3)}(\mathbf{x}-\mathbf{x'}). \tag{2.12}$$

The generating functional for the Green's function (2.11) reads

$$\begin{aligned} Z^T[J] &= \sum_{n=0}^{\infty}\frac{i^n}{n!}\int_c \mathrm{d}^4x_1\ldots\mathrm{d}^4x_n\, J(x_1)\ldots J(x_n)G^{C,(n)}(x_1,\ldots,x_n) \\ &= \left\langle T_C \exp\left[i\int_C \mathrm{d}^4x\, J(x)\phi(x)\right]\right\rangle, \end{aligned} \tag{2.13}$$

where the time integral has to be computed along the contour C. Similarly to the $T=0$ case we can define $Z^T[J] = \exp\bigl(iW^T[J]\bigr)$ and obtain the effective action at finite temperature by

$$\Gamma^T[\varphi] = W^T[J] - \int_C \mathrm{d}^4x\,\varphi(x)J(x). \tag{2.14}$$

This effective action satisfies the stationary condition in eq. (1.17) and can be used to define an effective potential at finite temperature (cf. eq. (1.27)).

2.3.1 Feynman Propagator at Finite Temperature

Boson Fields

First, we want to determine which time contours C are allowed by requiring the Green's function to be analytic with respect to t. First, we need to define the Feynman propagator (2.5) with the correct step function along the contour C,

$$G^C(x-y) = \theta_C(x^0-y^0)G_+(x-y) + \theta_C(y^0-x^0)G_-(x-y). \tag{2.15}$$

We use a complete set of energy-eigenstates $|n\rangle$ with eigenvalues $H|n\rangle = E_n|n\rangle$ to write eq. (2.6) at the point $\mathbf{x}=\mathbf{y}=0$ in the spectral form

$$G_+(x^0-y^0) = Z^{-1}\sum_{m,n}|\langle m|\,\phi(0)\,|n\rangle|^2 e^{-itE_n(x^0-y^0)}e^{itE_m(x^0-y^0+i\beta)}. \tag{2.16}$$

We now require that the sum over m and n is convergent to ensure that $G_+(x^0 - y^0)$ is analytic where we assume that the exponential dominate this convergence. This implies that $-\beta \leq \mathrm{Im}(x^0 - y^0) \leq 0$ and hence requires $\theta_C(x^0 - y^0) = 0$ if $\mathrm{Im}(x^0 - y^0) > 0$. The convergence of $G_-(x^0 - y^0)$ is analyzed by using (2.6). It shows that $0 \leq \mathrm{Im}(x^0 - y^0) \leq \beta$ and hence $\theta_C(y^0 - x^0) = 0$ for $\mathrm{Im}(x^0 - y^0) < 0$ is required. The final requirement for the convergence of the Feynman propagator defined on the strip

$$-\beta \leq \mathrm{Im}(x^0 - y^0) \leq \beta, \tag{2.17}$$

is the definition $\theta_C(t) = 0$ for $\mathrm{Im}(t) > 0$. The latter condition implies that C must be chosen such that a point moving along it has monotonically decreasing or constant imaginary part [26]. By the KMS condition (2.10), it is sufficient to define the Green functions on the strip $-\beta \leq \mathrm{Im}(t) \leq 0$.

To derive the Feynman propagator for a free scalar field with mass m, it is useful to expand the field in creation and annihilation operators

$$\phi(x) = \int \frac{\mathrm{d}^3 p}{(2\pi)^3 2\omega_p} \left[a(p) e^{-ip\cdot x} + a^\dagger(p) e^{ip\cdot x} \right], \quad \omega_p = \sqrt{\mathbf{p}^2 + m^2}, \tag{2.18}$$

which obey the equal-time commutation relation

$$\left[a(p), a^\dagger(k) \right] = \delta^{(3)}(\mathbf{p} - \mathbf{k}). \tag{2.19}$$

Furthermore, it can be checked with eq. (2.18) that the Feynman propagator satisfies the Klein-Gorden propagator equation

$$-\big(\partial_\mu \partial^\mu + m^2\big) G^C(x - y) = i\delta_C(x^0 - y^0)\delta^{(3)}(\mathbf{x} - \mathbf{y}). \tag{2.20}$$

The Hamiltonian can be expressed in terms of the ladder operators as

$$H = \int \frac{\mathrm{d}^3 p}{(2\pi)^3} \omega_p a^\dagger(p) a(p). \tag{2.21}$$

Using eqs. (2.19) and (2.4) and the energy-eigenstate basis $|n\rangle$ to compute the trace, we obtain the thermal averages of the number operator and its hermitian conjugate

$$\left\langle a^\dagger(p) a(k) \right\rangle = n_{\mathrm{BE}}(\omega_p)\delta^{(3)}(\mathbf{p} - \mathbf{k}), \tag{2.22}$$

$$\left\langle a(p) a^\dagger(k) \right\rangle = [1 + n_{\mathrm{BE}}(\omega_p)]\delta^{(3)}(\mathbf{p} - \mathbf{k}), \tag{2.23}$$

where $n_{\mathrm{BE}}(\omega_p)$ is the Bose-Einstein distribution,

$$n_{\mathrm{BE}}(\omega) = \frac{1}{e^{\beta\omega} - 1}. \tag{2.24}$$

We take the Fourier tansform of the Wightman function

$$G_+(x - y) = \int \frac{\mathrm{d}^4 k}{(2\pi)^4} \tilde{G}_+(k) e^{-ik\cdot(x-y)}, \tag{2.25}$$

and use eqs. (2.18), (2.22) and (2.23) to obtain

$$G_+(x - y) = \int \frac{\mathrm{d}^4 p}{(2\pi)^4} \rho(k) \left[1 + n_{\mathrm{BE}}(k^0) \right] e^{-ik\cdot(x-y)}, \tag{2.26}$$

where we defined the so-called spectral density $\rho(k) = \pi\delta(k^2 - m^2)\left[\theta(k_0) - \theta(-k^0)\right]$. Using the KMS relation (2.10) in Fourier space

$$i\tilde{G}_-(k) = e^{-\beta k^0} i\tilde{G}_+(k), \tag{2.27}$$

we obtain for the Feynman propagator

$$G^C(x-y) = \int \frac{\mathrm{d}^4k}{(2\pi)^4}\rho(k)\left[\theta_C(x^0 - y^0) + n_{\mathrm{BE}}(k^0)\right] e^{-ik\cdot(x-y)}, \tag{2.28}$$

where we used $\theta_C(x) = 1 - \theta_c(-x)$. The particular representation of the Feynman propagator depends on the choice of the time contour C, which has to fulfill the conditions derived in this section. The common choices for C are the so-called imaginary time formalism and the real time formalism. We will elaborate on the imaginary time formalism in section 2.4 and for the real time formalism we refer to ref. [26]. Before that, we give the general form of the Feynman propagator for fermionic fields.

Fermion Fields

For fermion field eq. (2.15) gets replaced by

$$\begin{aligned} S^C_{\alpha\beta}(x-y) &= \left\langle T_C \psi_\alpha(x)\bar{\psi}_\beta(y)\right\rangle \\ &= \theta_C(x^0 - y^0)S^+_{\alpha\beta}(x-y) - \theta_C(y^0 - x^0)S^-_{\alpha\beta}(x-y), \end{aligned} \tag{2.29}$$

where α and β are spinor indices. The Wightman functions for fermions are

$$S^+_{\alpha\beta}(x-y) = \left\langle \psi_\alpha(x)\bar{\psi}(y)\right\rangle, \tag{2.30}$$

$$S^-_{\alpha\beta}(x-y) = \left\langle \bar{\psi}_\beta(y)\psi_\alpha(x)\right\rangle. \tag{2.31}$$

The KMS relation for fermions can be derived analogous to the scalar fields, but gets modified by a sign due to anti-commutation of fermion fields to

$$S^+_{\alpha\beta}(t, \mathbf{x}) = -S^-_{\alpha\beta}(t + i\beta, \mathbf{x}). \tag{2.32}$$

This shows that the fermionic Wightman functions are anti-periodic in imaginary time with period β. The Feynman propagator for fermions should satisfy the equation

$$(i\gamma\cdot\partial - m)_{\alpha\lambda} S^C_{\lambda\beta}(x-y) = i\delta_C(x^0 - y^0)\delta^{(3)}(\mathbf{x}-\mathbf{y})\delta_{\alpha\beta}. \tag{2.33}$$

It is possible to decompose the Feynman propagator according to

$$S^C_{\alpha\beta}(x-y) = (i\gamma\cdot\partial + m)_{\alpha\beta} S^C(x-y), \tag{2.34}$$

where $S^C(x-y)$ satisfies eq. (2.20). The further procedure is equivalent to the previous section: we expand the Fermion fields in creation operators $b^\dagger$ and annihilation operators b obeying the anti-commutation relation $\left\{b^\dagger, b\right\} = 1$. The thermal averages can then be computed with a complete set of eigenstates and using the Pauli exclusion principle,

$$\left\langle b^\dagger(p)b(k)\right\rangle = n_{\mathrm{FD}}(\omega)\delta^{(3)}(\mathbf{p}-\mathbf{k}), \tag{2.35}$$

$$\left\langle b(p)b^\dagger(k)\right\rangle = \left[1 - n_{\mathrm{FD}}(\omega)\right]\delta^{(3)}(\mathbf{p}-\mathbf{k}). \tag{2.36}$$

We obtain the Fermi-Dirac distribution

$$n_{FD}(\omega) = \frac{1}{e^{\beta\omega}+1} \tag{2.37}$$

as statistical weights. Finally, we obtain

$$S^C(x-y) = \int \frac{\mathrm{d}^4k}{(2\pi)^4}\rho(k)\left[\theta_C(x^0-y^0) - n_{\mathrm{FD}}(k^0)\right] e^{-ik\cdot(x-y)}. \tag{2.38}$$

The Feynman propagator for fermions is now determined by eqs. (2.38) and (2.34).

2.4 Imaginary Time Formalism and Feynman Rules

So far, the result for the Feynman propagators depend on the choice of the time contour C from an arbitrary time t down to $t - i\beta$. This is sufficient because the KMS relations (2.10) and (2.32) provide the (anti-) periodicity of the Wightman functions in imaginary time with period β. Different choices of the contour correspond to different formulations of quantum field theory at finite temperature. The most obvious choice for the contour is to consider a straight line along the imaginary axis connecting the two boundary points. This can be parameterized by $t = -i\tau$ with $0 \leq \tau \leq \beta$. This contour is also called Matsubara contour since Matsubara first set up this formalism. The main advantage of this formalism is that the quantum field theory is formulated very close the know formalism at $T = 0$. A perturbation theory based on the imaginary time formalism will resemble the $T = 0$ Feynman rules, as we will see later.

First, we introduce the convenient notation for the Feynman propagator

$$G(\tau, \mathbf{x}) = \int \frac{\mathrm{d}^4k}{(2\pi)^4}\rho(k)e^{i\mathbf{k}\cdot\mathbf{x}}e^{-\tau k^0}\left[\theta(\tau) + \eta n(k^0)\right] \tag{2.39}$$

where η is a symbol for either $\eta = \eta_b \equiv +1$ for bosons or $\eta = \eta_F \equiv -1$ for fermions. The Bose-Einstein and Fermi-Dirac distributions can be replaced by

$$n(\omega) = \frac{1}{e^{\beta\omega} - \eta}. \tag{2.40}$$

In this way, we can treat bosons and fermions within one framework. With the specified contour, the Feynman propagator reads

$$G(\tau, \mathbf{x}) = \theta(\tau)G_+(\tau, \mathbf{x}) + \theta(-\tau)G_-(\tau, \mathbf{x}) \tag{2.41}$$

The KMS relation can now be expressed by $G(\tau + \beta) = \eta G(\tau)$ for $-\beta \leq \tau \leq 0$ and $G(\tau - \beta) = \eta G(\tau)$ for $0 \leq \tau \leq \beta$. Eq. (2.39) can be Fourier transformed to

$$\tilde{G}(\omega_n, \mathbf{k}) = \int_{\alpha-\beta}^{\alpha} \mathrm{d}\tau \int \mathrm{d}^3x\, e^{i\omega_n\tau - i\mathbf{x}\cdot\mathbf{k}}G(\tau, \mathbf{x}), \tag{2.42}$$

where $0 \leq \alpha \leq \beta$. The Fourier transform in imaginary time is discrete due to the periodicity of $G(\tau)$. The discrete frequencies, also called Matsubara frequencies are given by

$$\omega_n = 2n\pi\beta^{-1}, \tag{2.43}$$

$$\omega_n = (2n+1)\pi\beta^{-1}, \tag{2.44}$$

for bosons and for fermions, respectively. After inserting eq. (2.39) into eq. (2.42), we obtain the Feynman propagator in momentum space

$$\tilde{G}(\omega_n, \mathbf{k}) = \int_{-\infty}^{\infty} \frac{\mathrm{d}k^0}{2\pi} \frac{\rho(k)}{k^0 - i\omega_n} = \frac{1}{\mathbf{k}^2 + m^2 + \omega_n^2}, \tag{2.45}$$

where the residue theorem was used in the derivation. To show the formal analogy to $T = 0$ QFT, we can define an Euclidean propagator by

$$i\Delta(-i\tau, \mathbf{x}) = G(\tau, \mathbf{x}). \tag{2.46}$$

With eq. (2.45) we obtain the the inverse Fourier transform

$$\begin{aligned} \Delta(\tau, \mathbf{x}) &= \frac{1}{\beta} \sum_{n=-\infty}^{\infty} \int \frac{\mathrm{d}^3 k}{(2\pi)^3} \frac{-i}{\omega_n^2 + \mathbf{k}^2 + m^2} e^{-i\omega_n \tau + i\mathbf{k}\cdot\mathbf{x}} \\ &= \frac{1}{\beta} \sum_{n=-\infty}^{\infty} \int \frac{\mathrm{d}^3 k}{(2\pi)^3} \frac{i}{k^2 - m^2} e^{-i\omega_n \tau + i\mathbf{k}\cdot\mathbf{x}}. \end{aligned} \tag{2.47}$$

In the last line, we introduced an Euclidean four momentum by $p^\mu = (p^0, \mathbf{p}) = (i\omega_n, \mathbf{p})$. From eq. (2.47) we can deduce Feynman rules for field theory at finite temperature in the imaginary time formalism:

$$\begin{aligned} \text{Boson propagator:} \quad & \frac{i}{k^2 - m^2}, \quad k^\mu = (i2\pi n\beta^{-1}, \mathbf{k}), \\ \text{Fermion propagator:} \quad & \frac{i}{\gamma \cdot k - m}, \quad k^\mu = (i\pi(2n+1)\beta^{-1}, \mathbf{k}), \\ \text{Loop integral:} \quad & \frac{i}{\beta} \sum_{n=-\infty}^{\infty} \int \frac{\mathrm{d}^3 k}{(2\pi)^3} \\ \text{Vertex function:} \quad & -i\beta(2\pi)^3 \delta\left(\sum_i \omega_i\right) \delta^{(3)}\left(\sum_i \mathbf{p}_i\right) \end{aligned} \tag{2.48}$$

Integrating over internal momenta translates to an integral over the spatial momenta and a summation over the Matsubara modes. For the limiting case $\beta \to \infty$ one can replace $\beta^{-1} \sum \to \int \mathrm{d}k_E^0 / (2\pi)$. In this limit, the imaganiray time formalism reduces to the Euclidean formulation of QFT at zero temperature.

2.5 The Effective Potential at Finite Temperature

In this section, we derive the effective potential at finite temperature in the one-loop approximation using the imaginary time formalism. Ultimately, the goal is to split the one-loop corrections in effective potential to a $T = 0$ contribution and $T > 0$ contribution * which allows us to clearly identify the temperatures dependence of the effective potential. In other words, we intend to write the effective potential as

$$V_{\text{eff}}(\varphi) = V^{(0)}(\varphi) + V^{(1)}(\varphi) + V^T(\varphi), \tag{2.49}$$

*In general, this is not possible at arbitrary loop order. However, it is possible for the one-loop correction.

where $V^{(0)}$ is the classical potential, $V^{(1)}$ are the one-loop contributions at $T = 0$ (derived in section 1.1) and V^T are the one-loop thermal corrections which vanish at $T = 0$. We will use the results from sections 1.1.1, 1.1.2 and 1.1.3 and translate them to the Feynman rules of the imaginary time formalism to derive the thermal corrections V^T. As before, we split this derivation to scalar fields, fermion fields and gauge bosons.

2.5.1 Scalar Fields

If we translate eq. (1.36) to the Feynman rules at finite temperature in eq. (2.48), we obtain

$$V_1(\varphi, T) = \frac{1}{2\beta} \sum_{n=-\infty}^{\infty} \int \frac{\mathrm{d}^3 k}{(2\pi)^3} \log\big(\omega_n^2 + \omega^2\big), \tag{2.50}$$

where

$$\omega^2 = \mathbf{k}^2 + m^2(\varphi). \tag{2.51}$$

The field dependent mass is defined in eq. (1.38). The one-loop correction $V_1(\varphi, T)$ in eq. (2.50) is temperature-dependent, but does not classify the temperature-dependent and temperature independent part separately as it was required in eq. (2.49). To achieve this, the first step is to perform the sum over Matsubara frequencies. We define,

$$v(\omega) = \sum_{n=-\infty}^{\infty} \log\big(\omega_n^2 + \omega^2\big) \tag{2.52}$$

such that,

$$\frac{\partial v}{\partial \omega} = \sum_{n=-\infty}^{\infty} \frac{2\omega}{\omega_n^2 + \omega^2}. \tag{2.53}$$

The identity

$$f(y) = \sum_{n=1}^{\infty} \frac{y}{y^2 + n^2} = -\frac{1}{2y} + \frac{\pi}{2} \coth(\pi y) = -\frac{1}{2y} + \frac{\pi}{2} + \pi \frac{e^{-2\pi y}}{1 - e^{-2\pi y}} \tag{2.54}$$

with $y = \beta\omega/2\pi$ gives

$$\frac{\partial v}{\partial \omega} = 2\beta \bigg(\frac{1}{2} + \frac{e^{-\beta\omega}}{1 - e^{-\beta\omega}} \bigg). \tag{2.55}$$

This can be integrated to

$$v(\omega) = 2\beta \bigg[\frac{\omega}{2} + \frac{1}{\beta} \log\Big(1 - e^{-\beta\omega}\Big) \bigg] + (\omega - \text{independent terms}) \tag{2.56}$$

Omitting the constant term, the final result of the summation is

$$V_1(\varphi; \beta) = \int \frac{\mathrm{d}^3 k}{(2\pi)^3} \bigg[\frac{\omega}{2} + \frac{1}{\beta} \log\Big(1 - e^{-\beta\omega}\Big) \bigg]. \tag{2.57}$$

The second term vanishes in the limit $T = 0$, hence it suggest that $\omega/2$ is the one-loop effective potential at zero temperature and the second term is the thermal correction. The

first term, can be cast into the known form of one-loop corrections for $T = 0$ by using the residue theorem for the integral

$$\omega \int_{-\infty}^{\infty} \frac{\mathrm{d}x}{2\pi i} \frac{1}{-x^2 + \omega^2 - i\epsilon} = \frac{1}{2}, \tag{2.58}$$

where the contour is closed anticlockwise below the real interval $(-\infty, \infty)$. In this way, we pick up the pole at $x = -\sqrt{\omega^2 - i\epsilon}$ giving the residue $1/2\omega$. Integration of eq (2.58) with respect to ω yields

$$-\frac{i}{2} \int_{-\infty}^{\infty} \frac{\mathrm{d}x}{2\pi} \frac{1}{-x^2 + \omega^2 - i\epsilon} = \frac{\omega}{2} + \text{const} \tag{2.59}$$

So we may rewrite up to constant

$$\int \frac{\mathrm{d}^3k}{(2\pi)^3} \frac{\omega}{2} = -\frac{i}{2} \int \frac{\mathrm{d}^4k}{(2\pi)^4} \log\bigl(-(k^0)^2 + \omega^2 - i\epsilon\bigr) \tag{2.60}$$

and, after performing a Wick rotation $k^0 = ik_E^0$, this reads

$$V_{T=0}^{(1)}(\varphi) = \int \frac{\mathrm{d}^3k}{(2\pi)^3} \frac{\omega}{2} = \frac{1}{2} \int \frac{\mathrm{d}^4k_E}{(2\pi)^4} \log\bigl(k_E^2 + m(\varphi)^2\bigr). \tag{2.61}$$

This is the expression we obtained in eq. (1.36) for $T = 0$ case. To sum up, we are able to write the one-loop correction according to

$$V_1(\varphi, T) = V^{(1)}(\varphi) + V^T(\varphi), \tag{2.62}$$

where $V^{(1)}$ is defined in eq. (1.37) and the thermal corrections are defined by

$$V^T(\varphi) = \frac{1}{2\pi^2\beta^4} J_B\left[\frac{m(\varphi)^2}{T^2}\right], \tag{2.63}$$

where J_B is the thermal function for boson fields,

$$J_B(y^2) = \int_0^{\infty} \mathrm{d}x\, x^2 \log\Bigl(1 - e^{\sqrt{x^2+y^2}}\Bigr). \tag{2.64}$$

The integral can be solved analytically if a high temperature expansion is performed,

$$\begin{aligned} J_B(y^2) =& -\frac{\pi^4}{45} + \frac{\pi^2}{12}y^2 - \frac{\pi}{6}\left(y^2\right)^{3/2} - \frac{1}{32}y^4 \log\frac{y^2}{a_B} \\ & - 2\pi^{7/8} \sum_{m=1}^{\infty} \frac{(-1)^m}{(m+2)!} \Gamma\left(m + \frac{1}{2}\right) \left(\frac{y^2}{4\pi^2}\right)^{m+2} \zeta(2m+1), \end{aligned} \tag{2.65}$$

$$a_B = 16\pi^2 \exp\left(\frac{3}{2} - 2\gamma_E\right), \tag{2.66}$$

which is valid for $y^2 = (m/T)^2 \ll 1$. The calculation of eq. (2.65) can be found in appendix A. The high temperature expansion (2.65) is widely used in the context of electroweak phase transition.

2.5.2 Fermion Fields

For fermions, we consider the theory defined in section 1.1.2 but assume for simplicity a diagonal mass matrix $M_f(\varphi)$ for the N fermions. We start from eq. (1.44) at finite temperature, i.e.

$$V_1^{\psi}(\varphi,T) = -\frac{\sigma N}{2\beta}\sum_{n=-\infty}^{\infty}\int\frac{\mathrm{d}^3k}{(2\pi)^3}\log\bigl(\omega_n^2+\omega^2\bigr), \tag{2.67}$$

where in this section $\omega^2 = \mathbf{k}^2 + M_f^2(\varphi)$. As in the previous section, we perform the Matsubara sum. It is helpful to denote first

$$\frac{1}{2}f\Bigl(\frac{y}{2}\Bigr) = \sum_{n=1}^{\infty}\frac{y}{y^2+4n^2}, \tag{2.68}$$

$$\begin{aligned}\sum_{n=0}^{\infty}\frac{y}{y^2+(2n+1)^2} &= f(y) - \frac{1}{2}f\Bigl(\frac{y}{2}\Bigr)\\ &= \frac{\pi}{4} - \frac{\pi}{2}\frac{1}{e^{\pi y}+1},\end{aligned} \tag{2.69}$$

where the function f is defined in eq. (2.54). The sum in eq. (2.67) reads

$$v(\omega) = 2\sum_{n=0}^{\infty}\log\biggl(\frac{\pi^2(2n+1)^2}{\beta^2}+\omega^2\biggr), \tag{2.70}$$

and its derivative is

$$\frac{\partial v}{\partial\omega} = \frac{4\beta}{\pi}\sum_{n=0}^{\infty}\frac{y}{y^2+(2n+1)^2}, \tag{2.71}$$

where we defined $y = \beta\omega/\pi$. We can sum this according to eq. (2.69), hence

$$\frac{\partial v}{\partial\omega} = 2\beta\biggl(\frac{1}{2}-\frac{1}{1+e^{\beta\omega}}\biggr). \tag{2.72}$$

After integration with respect to ω and omitting the ω independent terms we obtain

$$V_1^{\psi}(\varphi,T) = -\sigma N\int\frac{\mathrm{d}^3k}{(2\pi)^3}\biggl(\frac{\omega}{2}+\frac{1}{\beta}\log\Bigl(1+e^{-\beta\omega}\Bigr)\biggr) \tag{2.73}$$

As for scalar fields, the first term corresponds to the zero temperature one-loop correction and the second term corresponds to the one-loop thermal correction. The first term can be rewritten to the standard $T=0$ result in eq. (1.44) by the method showed in the previous section. To sum up, we obtain

$$V_1^{\psi}(\varphi,T) = V_{\psi}^{(1)}(\varphi) + V_{\psi}^{T}(\varphi), \tag{2.74}$$

where $V_{\psi}^{(1)}$ is defined in eq. (1.45) and the thermal correction is defined

$$V^{T}(\varphi) = -\frac{\sigma N}{2\pi^2\beta^4}J_F\bigl[M_f(\varphi)^2\beta^2\bigr], \tag{2.75}$$

containing the thermal function for fermions

$$J_F(y^2) = \int_0^\infty dx x^2 \log\Big(1 + e^{-\sqrt{x^2+y^2}}\Big). \tag{2.76}$$

The corresponding high temperature expansion is given by [26]

$$\begin{aligned} J_F(y^2) =& \frac{7\pi^4}{360} - \frac{\pi^2}{24}y^2 - \frac{1}{32}y^4 \log\frac{y^2}{a_f} \\ & - \frac{\pi^{7/2}}{4}\sum_{l=1}^{\infty}(-1)^l \frac{\zeta(2l+1)}{(l+1)!}(1-2^{-2l-1})\Gamma\left(l+\frac{1}{2}\right)\left(\frac{y^2}{\pi^2}\right)^{l+2}, \end{aligned} \tag{2.77}$$

$$a_f = \pi^2 \exp\left(\frac{3}{2} - 2\gamma_E\right). \tag{2.78}$$

2.5.3 Gauge Bosons

The derivation for thermal corretions of gauge bosons is closely related to the scalar field case. We consider the model specified in eq. (1.46) and start by translating eq. (1.49) to Feynman rules at finite temperature,

$$V_1^A(\varphi, T) = (d-1)\frac{1}{2\beta}\sum_{n=-\infty}^{\infty}\int \frac{\mathrm{d}^3k}{(2\pi)^3}\log\big(\omega_n^2 + \omega^2\big), \tag{2.79}$$

where here $\omega^2 = m_A(\varphi)^2 + \mathbf{k}^2$. The only difference to the scalar field case is the additional factor of $(d-1)$ counting the three degrees of freedom of the gauge boson. We can follow the derivation from the scalar field (starting at eq. (2.52)) to compute the one-loop corrections coming from a gauge boson. The result is

$$V_1^A(\varphi, T) = V_A^{(1)} + 3\frac{1}{2\pi^2\beta^4}J_B\left(\frac{m_A^2(\varphi)}{T^2}\right), \tag{2.80}$$

where the zero temperature part $V_A^{(1)}$ is defined in eq. (1.50).

2.5.4 General Thermal Corrections

To sum up the last three sections, we give the general one-loop thermal correction

$$V_i^T(\varphi) = \frac{T^4}{2\pi^2}n_i J_i\left(\frac{m_i^2(\varphi)}{T^2}\right), \tag{2.81}$$

where $m_i(\varphi)$ is the field dependent mass of particle species i and n_i is defined as in eq. (1.52). With the notation J_i we indicate that the function J_B is used for bosons and the function J_F for fermions. If a model contains multiple particles, the total one-loop correction at finite temperaturer reads (cf. eqs. (1.51) and (1.54))

$$V_1(\varphi, T) = \sum_i \Big(V_i^{(1)}(\varphi) + V_i^T(\varphi)\Big). \tag{2.82}$$

Chapter 3

Improved Effective Potential

In this chapter we argue why the one-loop effective potential at finite temperature derived in section 2.5 is not a good approximation for the processes we intend to study. The derivation of the 1PI effective potential is based on certain perturbative approach, the expansion in number of loops. This expansion converges badly if terms of higher-loop orders are of a similar magnitude as terms with lower loop order and the validity of the perturbative computation is jeopardized. To restore the validitiy of the perturbative approach, one has to use techniques which resum terms of all loop orders to new a expression (e.g. an effective mass). The aim of this resummation is to rearrange the perturbative expansion in such a way that perturbativity is restored and the perturbative result is a reasonable approximation to the problem. We call the effective potential improved by such a technique the improved effective potential.

One of these techniques is the renormalization group (RG) improvement, which can be used in case of large logarithms in the one-loop corrections. The large logarithms occur at all loop orders when a large hierarchy between the mass scale and the renormalization scale μ is present and might spoil the perturbative expansion although the coupling parameter λ is small ($\lambda < 4\pi$). By using the RG group equations one can change the renormalisation scale to a convenient field-dependent value, rendering the logarithm small enough such that the perturbative expansion can be trusted. This was studied by S. Coleman in E. Weinberg [2] in case of a massless ϕ^4 theory and scalar QED. They use the RG equation to resum the large logarithms into a running coupling constant. Using this method, one integrates the beta function to obtain the running coupling constant and this corresponds to summing a power series of the large logarithms. However, this technique is not straightforward when multiple scales are present in the case of multiple scalar fields. In this case, the field-dependent masses of the fields can have very different values and fixing the renormalisation scale such that all logarithms are rendered small is not possible. For this reason, multi-renormalisation scale methods have been introduced [34]. The authors of ref. [35] developed a formalism where the RG improvement of multiscale models can be handled with a single renormalization scale by solving the RG equations with suitably chosen boundary conditions.

In this thesis, we will not use the method of RG improvement. The main reason for improving the effective potential in this work is the breakdown of the loop expansion due to thermal effects. We will see in the following section, that thermal field theory contains so-called hard thermal loops for bosons. These are diagrams which contain infrared divergences at high temperatures and this class of diagrams will spoil the usual perturbative

approach. We will comment on a sub-class of diagrams which contain hard thermal loops and how this issue is usually resolved in the lituature by the so-called daisy resummation yielding thermal masses for the bosons. In section 3.2 we introduce a resummation technique by the gap equation which is encoded in the 2PI formalism. We show that by solving the gap equation a richer class of diagrams than the daisy diagrams can be resummed into an effective mass M. The gap equation we derive can be used beyond the high temperature expansion and also at $T = 0$. We will show that in certain limits this approach reduces to the computation of thermal masses following from the daisy resummation. The importance of the resummation we introduce in this chapter is anaylzed in chapter 4. Another advantage of the gap equation is that an eventual momentum dependence of the effective mass $M(k)$ can be taken into account. In this thesis, we derive the gap equation only for scalar fields, but the method can be in principle generalized to gauge bosons and fermions.

3.1 Breakdown of Perturbation Theory at Finite Temperature

It is a well-known problem in field theories at high temperatures, that the conventional perturbative expansion in number of loops breaks down. The root of this problem are infrared divergences of the loop integrals at finite temperature. The task is therefore to resum these diagrams into an effective theory, where perturbation theory is restored. E. Braaten and R. Pisarski [36] developed such an effective theory for the strong interactions. They resum the so-called hard thermal loops causing the infrarered divergences into effective propagator and vertices. If the effective propagator and vertices are used, the validity of perturbation theory as loop expansion is restored also at high temperatures.

A resummation method for a scalar field at finite temperature was first adressed by R. Parwani [17] in was generalized to the SM by P. Arnold and O. Espinosa [37]. In both works, the resummation techqniue is based on resumming so-called daisy diagrams. This procedure yields effective masses, also called thermal masses in the context of finite temperature field theory. This method is widely used in the literature to improve the effective potential in regard to the study of electroweak phase transitions (see e.g. refs. [18–20, 26]). We will follow the argumentation of ref. [26] to explain why the resummation of daisies is appropriate and constitutes the dominant part which causes the breakdown of perturbation theory.

Consider the Feynman diagram for a scalar field with tree-level mass m and self interaction λ:


$= A$

With Feynman rules at finite temperature T (cf. eq. (2.48)) the diagram corresponds to

$$A = \lambda T \sum_{n=\infty}^{\infty} \int \frac{\mathrm{d}^3 k}{(2\pi)^3} \frac{1}{\omega_n^2 + \mathbf{k}^2 + m^2}, \tag{3.1}$$

and is related to the integral we solved in eq. (2.50) by

$$A = \lambda T \frac{\partial}{\partial m^2} \sum_{n=\infty}^{\infty} \int \frac{\mathrm{d}^3 k}{(2\pi)^3} \log\big(\omega_n^2 + \mathbf{k}^2 + m^2\big). \tag{3.2}$$

The thermal part of this diagram, which vanishes if $T = 0$, is therefore given by

$$\begin{aligned} A_T &= \lambda \frac{T^4}{\pi^2} \frac{\partial}{\partial m^2} J_B\left(\frac{m^2}{T^2}\right) \\ &= \lambda \frac{T^2}{\pi^2} \frac{\partial}{\partial y^2} J_B(y)\Big|_{y=m/T} . \end{aligned} \tag{3.3}$$

In the high temperature limit $y \ll 1$ the leading term is $A_T \sim \lambda T^2$ (cf. eq. (2.65)). So at high temperatures the diagram A is $\mathcal{O}(\lambda T^2)$ and if $m \sim \lambda T^2$ the one loop expression A is of the same order as the tree-level contribution. A breakdown of loop expansion at high T can be expected. This is clarified for higher order diagrams if we consider the daisy diagrams

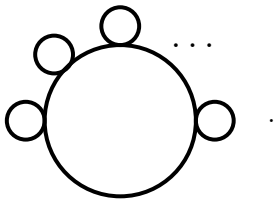

The dots are supposed to indicate that the diagrams has n petals, i.e. the loops which contain only one vertex. The daisy diagrams contain in total $n + 1$ loops and at leading order in temperature they scale as [26]

$$A_n = \lambda^{n+1} \frac{T^{2n+1}}{m^{2n-1}}. \tag{3.4}$$

The comparison of two consecutive orders

$$\alpha = \frac{A_{n+1}}{A_n} = \lambda \frac{T^2}{m^2}, \tag{3.5}$$

shows that α is the expansion parameter of the expansion in loops if we consider the daisy diagrams. If perturbation theory is valid, we should have $\alpha \ll 1$. The high temperature expansion which we introduced is based on $(m/T)^2 \ll 1$. Eq. (3.5) shows that even if $\lambda \ll 1$ is guaranteed, in the high temperature limit the expansion parameter α grows large and perturbation theory breaks down. The daisy resummation consists of resumming all orders of α. This is performed by computing the self-energies resembling diagram A of all bosons in the high temperature expansion and then solving the corresponding Dyson-Schwinger equation. This approach yields the so-called thermal masses $M^2 = m^2 + \Pi(T)$ which are then substituted in the usual one-loop effective potential for the tree-level masses (see e.g. ref. [20]). Of course more diagrams can be resummed, but the daisy diagrams are the leading contribution. We intend to resum a broader class of diagrams without using the high temperature expansion in the next section to improve the accuracy of our results. With that approach we can also ensure for reliable results in the intermediate stage between the low temperature limit and high temperature limit. In that stage, we expect that resummation of hard thermal loops should be taken into account but the high temperature expansion for the self-energies is a bad approximation. If the high temperature expansion is not reliable, the argument of only considering diagram A in the self-energies breaks down. Instead, at the one-loop level we should also take into account that the diagram

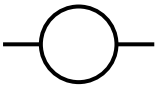

$= B,$

is of similar order as diagram A. That is why we intend to resum self-consistently diagrams belonging to class A and class B with the gap equation. Furthermore, we think it gives a theoretically more consistent framework to perform thermal resummation than ad hoc methods like daisy resummation. We compare the method introduced in the next section to the usual daisy resummation technique in chapter 4 for a scalar field.

3.2 Resumming with the Gap Equation

This section is dedicated to introduce the resummation procedure which is is encoded in the gap equation which was derived in section 1.2 from the 2PI effective action. We introduce this approach by studying a simple scalar theory with the tree-level potential defined in eq. (1.32) and field-dependent mass $m^2(\varphi)$ defined in eq. (1.38). The 2PI effective action of a scalar field at finite temperature was among others studied in refs. [21, 38]. The general form of the 2PI effective action (1.66) contains three different propagators. The tree-level propagator in the symmetric phase ($\varphi = 0$) is

$$D_0(k) = \frac{i}{k^2 - m^2}, \tag{3.6}$$

and the tree-level propagator in the shifted theory is

$$D(k) = \frac{i}{k^2 - m^2(\varphi)}. \tag{3.7}$$

The resummed propagator is denoted by $G(k)$ and has to be obtained form the gap equation (1.67). The term Γ_2 contains all vacuum 2PI diagrams in the theory with vertices defined in the shifted theory and using the resummed propagator $G(k)$. We will approximate this term up to two-loop order, which corresponds here to the lowest order. We will see that on the level of the gap equation this will yield an equation at one-loop level. The two diagrams contributing to Γ_2 are:

$\Gamma_2^{(a)} =$ 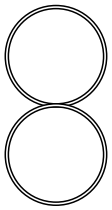 , $\Gamma_2^{(b)} =$ 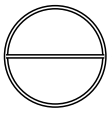 .

Double lines indicate that the resummed propagator G is used. We refer to diagram (a) as the double-bubble diagram and to diagram (b) as the sunset diagram. Including the overall factor $(-i)$ for the effective action (cf. eq. (1.6)), $(-i\lambda)$ for a vertex and the symmetry factors we obtain in position space

$$\Gamma_2^{(a)}[\phi, G] = -\frac{\lambda}{8} \int \mathrm{d}^4x\, \tilde{G}(x,x)\tilde{G}(x,x), \tag{3.8}$$

$$\Gamma_2^{(b)}[\phi, G] = i\frac{(\lambda\varphi)^2}{12} \int \mathrm{d}^4x\, \mathrm{d}^4y\, \tilde{G}(x-y)\tilde{G}(x-y)\tilde{G}(x-y), \tag{3.9}$$

where $\tilde{G}(x-y)$ is the propagator in position space. Using the Fourier transform

$$\tilde{G}(x-y) = \int \frac{\mathrm{d}^4k}{(2\pi)^4} G(k) e^{-ik(x-y)} \tag{3.10}$$

we can write Γ_2 as

$$\begin{aligned}\Gamma_2[\phi,G] =&\Gamma_2^{(a)}[\phi,G]+\Gamma_2^{(b)}[\phi,G]\\ &\int \mathrm{d}^4x\left(\frac{\lambda}{8}\int\frac{\mathrm{d}^4k}{(2\pi)^4}\int\frac{\mathrm{d}^4p}{(2\pi)^4}G(k)G(p)\right.\\ &\left.-i\frac{(\lambda\varphi)^2}{12}\int\frac{\mathrm{d}^4k}{(2\pi)^4}\int\frac{\mathrm{d}^4p}{(2\pi)^4}G(k)G(k-p)G(p)\right).\end{aligned}\tag{3.11}$$

The effective potential for the 2PI effective action is derived by factoring out the volume integral as it was done in eq. (1.27). Applying this to eq. (3.11) we get the expression

$$\begin{aligned}V_2(\phi,G)=-\frac{\Gamma_2[\phi,G]}{\int\mathrm{d}^4x}=&+\frac{\lambda}{8}\int\frac{\mathrm{d}^4k}{(2\pi)^4}\int\frac{\mathrm{d}^4p}{(2\pi)^4}G(k)G(p)\\ &-i\frac{(\lambda\varphi)^2}{12}\int\frac{\mathrm{d}^4k}{(2\pi)^4}\int\frac{\mathrm{d}^4p}{(2\pi)^4}G(k)G(k-p)G(p).\end{aligned}\tag{3.12}$$

The other terms in the 2PI effective action can be written as,

$$\mathrm{Tr}\big(D^{-1}G-1\big)=\int\mathrm{d}^4x\int\frac{\mathrm{d}^4k}{(2\pi)^4}\big(D^{-1}(k)G(k)-1\big),\tag{3.13}$$

$$\mathrm{Tr}\log\big(D_0G^{-1}\big)=\int\mathrm{d}^4x\int\frac{\mathrm{d}^4k}{(2\pi)^4}\log\big(D_0G^{-1}\big).\tag{3.14}$$

Thus, we can write the effective potential for the 2PI formalism as

$$\begin{aligned}V_{\text{eff}}(\varphi,G)=&-\frac{\Gamma^{2\text{PI}}[\phi,G]}{\int\mathrm{d}^4x}\\ =&V^{(0)}(\varphi)-\frac{i}{2}\int\frac{\mathrm{d}^4k}{(2\pi)^4}\log\big(D_0G^{-1}\big)-\frac{i}{2}\int\frac{\mathrm{d}^4k}{(2\pi)^4}\big(D^{-1}(k)G(k)-1\big)\\ &+V_2(\phi,G).\end{aligned}\tag{3.15}$$

The tree-level propagator D_0 is independent of φ and G (cf. (3.6)), so that term can be dropped and we obtain

$$\begin{aligned}V_{\text{eff}}(\varphi,G)=&V_{\text{tree}}(\varphi)-\frac{i}{2}\int\frac{\mathrm{d}^4k}{(2\pi)^4}\log\big(G^{-1}\big)-\frac{i}{2}\int\frac{\mathrm{d}^4k}{(2\pi)^4}\big(D(k)^{-1}G(k)-1\big)\\ &+V_2(\varphi,G).\end{aligned}\tag{3.16}$$

Exploiting the second stationary condition of the 2PI effective potential, we will obtain the gap equation for this model. After picking a certain ansatz for the resummed propagator G we obtain an equation which prescribes a resummation of infinite diagrams into an effective mass M of the scalar field. The functional stationary condition in eq. (1.63) reduces to a partial derivative with respect to the resummed propagator if we use the effective potential $V_{\text{eff}}(\varphi,G)$ instead of the effective action $\Gamma^{2\text{PI}}(\varphi,G)$,

$$\frac{\partial V_{\text{eff}}}{\partial G(k)}=\frac{i}{2}\big(G^{-1}(k)-D^{-1}(k)\big)+\frac{\partial V_2}{\partial G(k)}=0,\tag{3.17}$$

where the last term can be interpreted as the self-energy

$$\Sigma(\varphi,G,k)=\frac{\partial V_2}{\partial G(k)}=\frac{\lambda}{4}\int\frac{\mathrm{d}^4p}{(2\pi)^4}G(p)-i\frac{(\lambda\varphi)^2}{4}\int\frac{\mathrm{d}^4p}{(2\pi)^4}G(k-p)G(p).\tag{3.18}$$

To proceed it is necessary to pick an ansatz for the form of the resummed propagator. We will use the standard form for a scalar field,

$$G(k) = \frac{i}{k^2 - M^2(\varphi, k)}, \tag{3.19}$$

but with a momentum-dependent resummed mass M. In this notation the gap equation is an self-consistent equation to determine the resummed mass,

$$M^2(\varphi, k) = m^2(\varphi) + \Sigma(\varphi, M, k). \tag{3.20}$$

The self-energies in eq. (3.21) are 1PI diagramms containing one loop. Hence, the two loop 2PI diagrams in Γ_2 generate one loop 1PI diagrams in the gap equation. The gap equation for the scalar field can be represented by

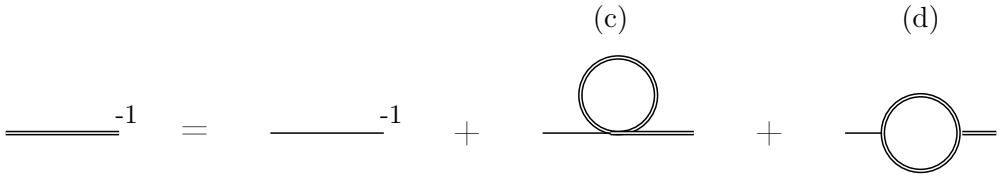

Note, that the the diagrams (c) and (d) are amputated so no propagators are used for the external legs. Since the self-energies are obtained self-consistently, the gap equation can be read as an iterative resummation prescription. Moreover, it is evident from eq. (3.18) that the sunset diagram (diagram (d)) introduces a momentum dependence to the resummed mass. If we consider only the bubble diagram (c) in the gap equation, the iteration will generate the daisy diagrams as a subclass. The full class of resummed diagrams will contain infinitely many iterations of diagram A and B from the last section and combinations of both. Note, that the gap equation is iterated in the loops of diagrams (c) and (d) and in the external legs facilitating a resummation of a broad class of diagrams. This class can be extended further, if diagrams beyond two-loop order are considered in Γ_2.

Translating eq. (3.18) with the help of Feynman rules at finite temperature and using the Feynman trick for the second integral (cf. appendix B) we obtain for the full temperature-dependent self-energy

$$\begin{aligned}\Sigma(\varphi, k, T) = &- \frac{\lambda}{4\beta} \sum_{n=\infty}^{\infty} \int \frac{\mathrm{d}^3 p}{(2\pi)^3} \frac{1}{\omega_n^2 + \mathbf{p}^2 + m^2(\varphi)} \\ &+ \frac{(\lambda\varphi)^2}{4\beta} \sum_{n=\infty}^{\infty} \int_0^1 \mathrm{d}x \int \frac{\mathrm{d}^3 p}{(2\pi)^3} \frac{1}{(\omega_n^2 + \mathbf{p}^2 + a(k,x)^2)^2},\end{aligned} \tag{3.21}$$

where we defined

$$a(k, x)^2 = k^2 x(1 - x) - M^2. \tag{3.22}$$

In order to solve the integrals in eq. (3.18), we introduce

$$I_0(m^2) = \frac{1}{2\beta} \sum_{n=\infty}^{\infty} \int \frac{\mathrm{d}^3 k}{(2\pi)^3} \log\big(\omega_n^2 + k^2 + m^2\big), \tag{3.23}$$

$$I_a(m^2) = \frac{1}{2\beta} \sum_{n=\infty}^{\infty} \int \frac{\mathrm{d}^3 k}{(2\pi)^3} \frac{1}{(\omega_n^2 + k^2 + m^2)^a}. \tag{3.24}$$

The first integral I_0 was computed in the derivation of the effective potential at finite temperature (see section 2.5.1). Therefore, it is helpful to introduce the relation

$$I_{j+1}(m^2) = \frac{(-1)^j}{j!}\frac{\partial^j}{\partial(m^2)^j} I_1(m^2). \tag{3.25}$$

In this notation, the gap equation (3.20) reads

$$M(\varphi,T,k)^2 = m(\varphi)^2 + \lambda I_1(M^2) - (\lambda\varphi)^2 \int_0^1 \mathrm{d}x\, I_2(a(k,x)^2). \tag{3.26}$$

The two integrals can be solved by using eq. (3.25) and using the result for eq. (2.62), (2.63) and (1.37). If dimensional regularization is used, the results before renormalization is

$$\begin{aligned} I_1(M^2) =& \frac{M^2}{32\pi^2}\left(-\frac{2}{\epsilon} + \gamma_E + \log(4\pi)\right) \\ &+ \frac{M^2}{32\pi^2}\left[\log\left(\frac{M^2}{\mu^2}\right) - 1\right] + \frac{1}{2\pi^2\beta^2}\left(\frac{\partial J_B(y^2)}{\partial y^2}\right)\Big|_{y=M/T}, \end{aligned} \tag{3.27}$$

$$\begin{aligned} \int_0^1 \mathrm{d}x\, I_2(a(k,x)^2) =& \frac{1}{32\pi^2}\left(\frac{2}{\epsilon} - \gamma_E - \log(4\pi)\right) \\ &- \frac{1}{32\pi^2}\int_0^1 \mathrm{d}x \left[\log\left(\frac{a(k,x)^2}{\mu^2}\right) + 16\left(\frac{\partial^2 J_B(y^2)}{\partial(y^2)^2}\right)\Big|_{y=a(k,x)/T}\right]. \end{aligned} \tag{3.28}$$

The first terms in eqs. (3.27) and (3.28) should be canceled by counter-terms in the $\overline{\mathrm{MS}}$ scheme. In fact, to renormalize the gap equation it is necessary to renormalize the 2PI effective action first and then derive the gap equation. This is indicated by the fact that the divergent terms in eqs. (3.27) and (3.28) depend on the resummed mass M which cannot be included in the counter-terms of the lagrangian since M is not a parameter of the original theory. The renormalization of the 2PI effective action is compared to the 1PI approach rather involved since it contains diagrams to all loop orders. For a detailed treatment of this procedure we refer to ref. [30]. After renormalization the divergent terms in eqs. (3.27) and (3.28) will be canceled an we obtain the renormalized gap equation [38]

$$\begin{aligned} M_R(\varphi,k)^2 =& m_R(\varphi)^2 + \lambda_R\left\{\frac{M_R^2}{32\pi^2}\left[\log\left(\frac{M_R^2}{\mu^2}\right) - 1\right] + \frac{1}{2\pi^2\beta^2}\left(\frac{\partial J_B(y^2)}{\partial y^2}\right)\Big|_{y=M_R/T}\right\} \\ &- \frac{(\lambda_R\varphi)^2}{\pi^2}\int_0^1 \mathrm{d}x\left[\frac{1}{32}\log\left(\frac{a_R(k,x)^2}{\mu^2}\right) + \frac{1}{2}\left(\frac{\partial^2 J_B(y^2)}{\partial(y^2)^2}\right)\Big|_{y=a(x)/T}\right] \end{aligned} \tag{3.29}$$

In the further, we will drop the subscript R again. In the next subsections we give the gap equation in various limits. We derive the gap equation for the Higgs boson in the SM in appendix C for vanishing external momentum. We drop the dependence of M on φ, T and k from now on.

3.2.1 Zero Temperature

In this limit the terms involving the thermal functions vanish and the gap equation simplifies to

$$M^2 = m^2(\varphi) + \frac{\lambda M^2}{32\pi^2}\left[\log\left(\frac{M^2}{\mu^2}\right) - 1\right] + \frac{(\lambda\varphi)^2}{32\pi^2}\int_0^1 \mathrm{d}x \log\left(\frac{a(k,x)^2}{\mu^2}\right). \tag{3.30}$$

The remaining x-integral is solved in appendix B.

3.2.2 Vanishing External Momentum

For vanishing external momentum we have $a(k,x)^2 = M^2$ and the x-integral is solved trivially. The gap equation reads in this limit

$$M^2 = m^2(\varphi) + \lambda I_1(M^2) - (\lambda\varphi)^2 I_2(M^2). \tag{3.31}$$

We can substitute eqs. (3.27) and (3.28) and we get

$$\begin{aligned} M^2 =& m^2(\varphi) + \lambda\left(\frac{M^2}{32\pi^2}\left[\log\left(\frac{M^2}{\mu^2}\right) - 1\right] + \frac{1}{2\pi^2\beta^2}\left(\frac{\partial J_B(y^2)}{\partial y^2}\right)\Big|_{y=M/T}\right) \\ &+ (\lambda\varphi)^2\left(\frac{1}{32\pi^2}\log\left(\frac{M^2}{\mu^2}\right) + \frac{1}{2\pi^2}\left(\frac{\partial^2 J_B(y^2)}{\partial (y^2)^2}\right)\Big|_{y=M/T}\right). \end{aligned} \tag{3.32}$$

We will use this gap equation for vanishing external momentum to obtain an improved effective potential. We elaborate on this method in section 3.3. To handle the derivatives of the thermal function one can either use the high temperature expansion (see section 3.2.4) or use the integral representation (cf. eq. (2.64)). The second option will be valid for any temperature but requires numerical solutions to the integrals J_B' and J_B''. To study the electroweak phase transition it can be important to compute the effective potential beyond the high temperature expansion, since bubble nucleation might begin at low temperatures where this approximation is not justified.

3.2.3 Hartree-Fock Approximation

In this approximation the sunset diagram is neglected over the double-bubble diagram. In a scalar theory with O(N) symmetry this can be justified because double-bubble diagram is $\mathcal{O}(N^2)$ and the sunset diagram is $\mathcal{O}(N)$ [39]. The gap equation simplifies to

$$M^2 = m^2(\varphi) + \lambda\left(\frac{M^2}{32\pi^2}\left[\log\left(\frac{M^2}{\mu^2}\right) - 1\right] + \frac{1}{2\pi^2\beta^2}\left(\frac{\partial J_B(y^2)}{\partial y^2}\right)\Big|_{y=M/T}\right). \tag{3.33}$$

3.2.4 High Temperature Expansion

To approximate the gap equation at high temperatures, we will use the high temperature expansion of the thermal function for bosons (cf. eq. (2.64)) and apply the derivatives,

$$\begin{aligned} \frac{\partial J_B}{\partial (y^2)} =& \frac{\pi^2}{12} - \frac{\pi}{4}(y^2)^{1/2} - \frac{1}{16}y^2\log\left(\frac{y^2}{a_B}\right) - \frac{1}{32}y^2 \\ &- \frac{\pi^{-9/8}}{2}\sum_{m=1}^{\infty}\frac{(-1)^m}{(m+1)!}\Gamma\left(m+\frac{1}{2}\right)\zeta(2m+1)\left(\frac{y^2}{4\pi^2}\right)^{m+1}, \end{aligned} \tag{3.34}$$

$$\begin{aligned} \frac{\partial^2 J_B}{\partial (y^2)^2} =& -\frac{\pi}{8}(y^2)^{-1/2} - \frac{1}{16}\log\left(\frac{y^2}{a_B}\right) - \frac{3}{32} \\ &- \frac{\pi^{-25/8}}{8}\sum_{m=1}^{\infty}\frac{(-1)^m}{m!}\Gamma\left(m+\frac{1}{2}\right)\zeta(2m+1)\left(\frac{y^2}{4\pi^2}\right)^{m}. \end{aligned} \tag{3.35}$$

When we substitute these expansions into the general gap equation (3.29) we observe that the $\log\big(M^2\big)$ of the $T = 0$ part and in the high temperature expansion cancel. In the further

we will truncate the high temperature expansions in eqs. (3.34) and (3.35) at the infinite sums with index m. The contribution to gap equation coming from the bubble diagram (c) reads

$$\Delta M_1 = \lambda\left(\frac{M^2}{32\pi^2}\log\left(\frac{a_B T^2}{4\pi\mu^2}\right) - \frac{3M^2}{64\pi^2} + \frac{T^2}{24} - \frac{MT}{8\pi}\right) \tag{3.36}$$

and the contribution from the sunset diagram (d) reads

$$\Delta M_2 = (\lambda\varphi)^2 \int_0^1 \mathrm{d}x \left[-\frac{1}{32\pi^2}\log\left(\frac{a_B T^2}{4\pi\mu^2}\right) + \frac{1}{16\pi}\left(\frac{a(k,x)^2}{T^2}\right)^{-1/2} + \frac{3}{64\pi^2}\right]. \tag{3.37}$$

In this notation the gap equation can be written as

$$M^2 = m(\varphi)^2 + \Delta M_1 + \Delta M_2. \tag{3.38}$$

Interestingly, at leading order in temperature the gap equation is approximated by

$$M^2 \approx m(\varphi)^2 + \frac{\lambda T^2}{24}, \tag{3.39}$$

which is automatically solved. This is the correct thermal mass M for a scalar field if the daisy resummation technique is used (e.g. refs. [17, 18]).

3.3 Improved Effective Potentials from Gap Equations

To obtain an effective potential in the 2PI formalism, it is necessary to first solve the gap equation. This yields the resummed propagator $G(\varphi)$ as a function of the background field. The resummed propagator is then substituted in the 2PI effective action (cf. eq. (1.66)),

$$\Gamma^{\mathrm{2PI}}[\varphi, G(\varphi)] = \Gamma[\varphi]. \tag{3.40}$$

This gives a an effective action which was improved by resummation of higher loop order diagrams and has φ as only functional dependence. The 1PI effective action Γ encodes all information of a quantum field theory, since it is the generating functional for all n-point functions [30]. The 2PI formalism resummed certain classes of diagrams and and should be seen as a consistent resummation method.

The expression for $\Gamma^{\mathrm{2PI}}[\varphi, G(\varphi)]$ contains integrals which have to be solved before generating n-point functions. The computation of the integrals amounts to a second stage of diagram resummation on top of the gap equation. We will skip this step in this thesis and use the solution of the gap equation to directly obtain the improved effective potential. The method presented here, only uses the gap equation to resum diagrams. This should be seen as an approximation to the full 2PI formalism which can be only applied in this form in the limit of vanishing external momentum for the gap equation. The approximation is based on the fact that the effective action generates the propagator by

$$\frac{\delta^2\Gamma}{\delta\varphi(x)\delta\varphi(y)} = i\Big(\tilde{G}(x,y)\Big)^{-1}, \tag{3.41}$$

and identifying $\tilde{G}(x,y)$ with the resummed propagator in the gap equation. We will now use the ansatz (3.19) for $G(k)$. In the limit of vanishing momenta that propagator is

$$i\,\tilde{G}(k)^{-1}\Big|_{k=0} = -M^2, \tag{3.42}$$

where M is momentum independent. So we find in position space

$$i\Big(\tilde{G}(x,y)\Big)^{-1}\Big|_{k=0} = -M^2 \int \frac{\mathrm{d}^4p}{(2\pi)^4} e^{ip\cdot(x-y)} = -M^2\delta^{(4)}(x-y). \tag{3.43}$$

The left hand side of eq. (3.41) can be computed in the vanishing momentum limit by using the expansion around zero momentum (cf. eq. (1.25)),

$$\begin{aligned}\frac{\delta^2\Gamma}{\delta\varphi(x)\delta\varphi(y)}\Big|_{k=0} &= \sum_{n=\infty}^{\infty} \frac{1}{(n-2)!}\tilde{\Gamma}^{(n)}(0,\ldots,0)\varphi(x)^{n-2}\delta^{(4)}(x-y) \\ &= -\frac{\partial^2 V_{\text{eff}}(\varphi)}{\partial\varphi^2}\delta^{(4)}(x-y),\end{aligned} \tag{3.44}$$

where in the second line we used the definition of the effective potential (cf. eq. (1.26)). Using eqs. (3.41), (3.42) and (3.44) we find for vanishing momentum that

$$M^2(\varphi) = \frac{\partial^2 V_{\text{eff}}(\varphi)}{\partial\varphi^2}. \tag{3.45}$$

We will use this relation to directly obtain the effective potential by integration after M was computed,

$$V^I_{\text{eff}}(\varphi) = \int_0^{\varphi} \mathrm{d}\varphi' \int_0^{\varphi'} \mathrm{d}\varphi''\, M^2(\varphi''). \tag{3.46}$$

If the gap equation is solved for finite external momenta k, the resummed mass acquires a momentum dependence $M^2(\varphi,k)$. In that case the expansion in eq. (3.44) is not valid and one has to use the full momentum expansion of the effective action (cf. eq. (1.24)). The solution of $M^2(\varphi,k)$ should then be also expanded in powers of momenta and thus one can obtain the coefficients of the finite momentum corrections (for instance $Z(\varphi)$ in eq. (1.25)).

In addition, this method can be used to obtain the self-energy from the usual one-loop terms in the effective potential at finite temperature $V^{(1)}_{\text{eff}}(\varphi,T)$. According to eq. (3.45) we can write this in terms of the field-dependent tree-level mass and the second derivative of the one-loop corrections,

$$\Big(M^{(1)}\Big)^2(\varphi) = \frac{\partial^2 V^{(1)}_{\text{eff}}(\varphi,T)}{\partial\varphi^2} = m^2(\varphi) + \frac{\partial^2 V^{(1)}(\varphi)}{\partial\varphi^2} + \frac{\partial^2 V^T(\varphi)}{\partial\varphi^2}. \tag{3.47}$$

The gap equation at zero external momentum is

$$M^2(\varphi) = m^2(\varphi) + \Sigma(\varphi,M)\Big|_{k=0}. \tag{3.48}$$

If we now set the tree-level mass to the resummed mass $m(\varphi)\to M$ in eq. (3.47) we can match the second derivative of the one-loop effective potential (3.47) to second derivative of the improved effective potential (3.48), i.e. $M^{(1)}(\varphi) = M(\varphi)$. In this way we can compute the self-energies by

$$-2\,\Sigma(\varphi)\Big|_{k=0} = \left(\frac{\partial^2 V^{(1)}(\varphi)}{\partial\varphi^2} + \frac{\partial^2 V^T(\varphi)}{\partial\varphi^2}\right)\Big|_{m^2=M^2}, \tag{3.49}$$

i.e. by taking two derivatives with respect to the background field, and then replacing the field-dependent mass with the resummed mass M. This formulates a self-consistent equation equivalent to the gap equation. We checked this explicitly for the gap equation of the Higgs boson in the SM (see appendix C).

To apply the derivatives in eq. (3.49), it is convenient for future reference to rewrite them according to the chain rule to

$$\begin{aligned}\frac{\partial^2}{\partial h^2} &= 2\frac{\partial}{\partial(h^2)} + 4h^2\frac{\partial^2}{\partial(h^2)^2} \\ &= \left[2\frac{\partial(m_i^2)}{\partial(h^2)} + 4h^2\frac{\partial^2(m_i^2)}{\partial(h^2)^2}\right]\frac{\partial}{\partial(m_i^2)} + 4h^2\left[\frac{\partial(m_i^2)}{\partial(h^2)}\right]^2\frac{\partial^2}{\partial(m_i^2)^2}.\end{aligned} \tag{3.50}$$

If the derivative acts on the thermal correction V^T we use

$$\frac{\partial^2}{\partial h^2} = \frac{1}{T^2}\left[2\frac{\partial(m_i^2)}{\partial(h^2)} + 4h^2\frac{\partial^2(m_i^2)}{\partial(h^2)^2}\right]\frac{\partial}{\partial(y_i^2)} + \frac{4h^2}{T^4}\left[\frac{\partial(m_i^2)}{\partial(h^2)}\right]^2\frac{\partial^2}{\partial(y_i^2)^2}, \tag{3.51}$$

where $y_i^2 = m_i^2/T^2$. In this way, the first and second derivatives of the thermal function J_B are generated in the gap equation (cf. eq. (3.29)). In the multi-field case we also need the derivative with respect to two different background fields,

$$\frac{\partial^2}{\partial\varphi_1\partial\varphi_2} = \frac{\partial^2(m_i^2)}{\partial\varphi_1\partial\varphi_2}\frac{\partial}{\partial m_i^2} + \frac{\partial(m_i^2)}{\partial\varphi_1}\frac{\partial(m_i^2)}{\partial\varphi_2}\frac{\partial^2}{\partial(m_i^2)^2}. \tag{3.52}$$

3.4 Renormalization Group Improvement of the Gap Equation

In this section we show how the gap equation improvement introduced in the previous section can be combined with RG improvement. We use the fact that the physical information of the theory is independent of the choice of the renormalization scale μ. Hence, the quantum effective action cannot depend on μ and should satisfy

$$\mu\frac{\mathrm{d}}{\mathrm{d}\mu}\Gamma[\varphi] = \left(\mu\frac{\partial}{\partial\mu} + \sum_{i=1}^{N_\lambda}\beta_i\frac{\partial}{\partial\lambda_i} - \frac{1}{2}\sum_{j=1}^{N_\varphi}\gamma_j\int\mathrm{d}^4x\,\varphi_j(x)\frac{\delta}{\delta\varphi_j(x)}\right)\Gamma[\varphi] = 0, \tag{3.53}$$

which is called the RG (Callan-Symanzik) equation. We wrote eq. (3.53) for a model with N_φ scalar fields and parametrized by the couplings $\lambda_1 \ldots \lambda_{N_\lambda}$ couplings. Furthermore, we defined the standard β function and anomalous dimensions

$$\beta_i = \mu\frac{\partial\lambda_i}{\partial\mu}, \tag{3.54}$$

$$\gamma_j = \mu\frac{\partial\log Z_j}{\partial\mu}, \tag{3.55}$$

respectively. The β functions take the running of the coupling constants with μ into account and the anomalous dimensions γ the runnning with μ of the field normalisations Z_j. Eq.

(3.53) can be used to derive a RG equation for the effective potential *

$$\mu \frac{\mathrm{d}V_{\text{eff}}}{\mathrm{d}\mu} = \left(\mu \frac{\partial}{\partial \mu} + \sum_{i=1}^{N_\lambda} \beta_i \frac{\partial}{\partial \lambda_i} - \frac{1}{2} \sum_{j=1}^{N_\varphi} \gamma_j \varphi_j \frac{\partial}{\partial \varphi_j} \right) V_{\text{eff}} = 0. \tag{3.56}$$

In the light of eq. (3.45) we find that the resummed mass is also scale independent,

$$\mu \frac{\mathrm{d}}{\mathrm{d}\mu} M^2 = \left(\mu \frac{\partial}{\partial \mu} + \sum_{i=1}^{N_\lambda} \beta_i \frac{\partial}{\partial \lambda_i} - \frac{1}{2} \sum_{j=1}^{N_\varphi} \gamma_j \varphi_j \frac{\partial}{\partial \varphi_j} \right) M^2 = 0. \tag{3.57}$$

The scale invariance of the resummed mass M shows that the RG improvement technique can also be applied on the level of the resummed mass M. Eq. (3.57) allows us to evaluate M at a certain renormalisation scale by using the running coupling constant $\lambda_i(\mu)$ and running field normalization $Z_j(\mu)$. For that one has to determine the β and γ functions to a certain loop order. In this way, large logarithms in the $T = 0$ corrections can be rendered small by choosing a conveninent renormalization scale and the perturbative approach is improved. If it is necessary to do both, gap equation improvement to handle hard thermal loops and RG improvement to handle large logarithms, then one has to solve the gap equation to obtain M^2 and subsequently perform the RG improvement of M^2. Finally, one obtains the improved effective potential by integration (cf. eq. (3.46)).

*In general the vacuum energy $V_{\text{eff}}(0)$ is not scale invariant and contributes to the RG equation of the effective potential. However, for classically conformal model this term is zero. Since we are interested in classically conformal models in thesis, we neglect this contribution in our discussion.

Chapter 4

Numerical Solutions of the Gap Equation

This chapter serves as an introduction to the numerical method we will use to improve the effective potential in the proceeding chapters. We analyze the dependence of the resummed mass on parameters of a simple scalar theory. These methods will be used to compute the effective potential for the SU(2)cSM which is introduced in the next chapter. Finally, we conclude with a discussion of the significance on improving the effective potential for this example and give an outlook why this improvement is important for studying phase transitions of more complicated models. In addition, we compare the gap equation approach to the daisy resummation approach.

4.1 Scalar Field with Vanishing External Momentum

We solve the gap equation at finite temperature and at zero momentum for the scalar theory studied in the previous chapter with the tree-level potential defined in eq. (1.32). The gap equation in that limit reads

$$\begin{aligned} M(\varphi)^2 =& m(\varphi)^2 + \lambda\left(\frac{M^2}{32\pi^2}\left[\log\left(\frac{M^2}{\mu^2}\right) - 1\right] + \frac{1}{2\pi^2\beta^2}\left(\frac{\partial J_B(y^2)}{\partial y^2}\right)\Big|_{y=M/T}\right) \\ &+ (\lambda\varphi)^2\left(\frac{1}{32\pi^2}\log\left(\frac{M^2}{\mu^2}\right) + \frac{1}{2\pi^2}\left(\frac{\partial^2 J_B(y^2)}{\partial (y^2)^2}\right)\Big|_{y=M/T}\right), \end{aligned} \tag{4.1}$$

with the tree-level mass

$$m^2(\varphi) = m_0^2 + \frac{\lambda}{2}\varphi^2. \tag{4.2}$$

The dimension-full parameters of this theory are the mass parameter m_0 and the temperature T. We will quantify these parameters in this chapters in units of the renormalisation scale μ, in practice setting μ to one in our computations. Since eq. (4.1) contains derivatives of the thermal function J_B, one either can use the high temperature expansion if $y \ll 1$ or the low temperature expansion $y \gg 1$. In the intermediate case $y \sim 1$ one should use numerical solution to the integral in $J_B(y)$. To account for correct results in all cases and an efficient numerical implementation we use the code of [40]. With that code at hand, we

are able to obtain reliable numerical solutions to the gap equation for any temperatures. The numerical solutions are obtained by starting with an arbitrary initial value for M^2 and plugging it in the right hand side of eq. (4.1). The numerical result is plugged back in that expression and iterated until M^2 converges. In a diagrammatic view on this procedure, each iteration corresponds to iterating the gap equation. Figure 4.1 shows the solution for an increasing number of iterations. For this model we find that the solution converges to a value with a precision of 10^{-4} for M^2 after four to five iterations.

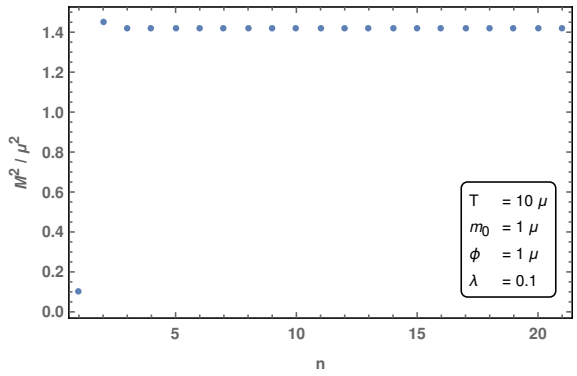

Figure 4.1: Value of M^2 after n iterations for the parameters specified in the box.

Figure 4.2 shows the dependence of the resummed mass on the parameters present in this model. We plot the corrections to the field-dependent mass defined as

$$\delta M^2(\varphi) = \frac{M^2(\varphi) - m^2(\varphi)}{m^2(\varphi)}. \tag{4.3}$$

For increasing temperature (cf. Fig. 4.2a) the correction to the field-dependent mass grows significantly. This provides evidence that the inclusion of diagrams with higher loop order is important at high temperature since they are of equal magnitude as the tree-level expression $m^2(\varphi)$. Furthermore, this signals the breakdown of perturbation theory induced by hard thermal loops as pointed out for instance in ref. [36]. Compared to that, the corrections at low temperature are very small even if $\varphi \gg \mu$ (cf. Fig. 4.2b). However, we know from Fig. 4.2b that the corrections for $\varphi/\mu \lesssim 5$ are larger for finite temperature than for vanishing temperature. At large field values $\varphi \gg \mu$ the correction does not depend significantly on the temperature, since the dominant contribution is expected to be due to the large logarithm in eq. (4.1). From the plot with increasing coupling (cf. Fig. 4.2c) we deduce that at finite temperature the corrections grow faster than at zero temperature. The increasing mass parameter (cf. Fig. 4.2d) shows that the corrections are most significant if the mass parameter is small compared to the temperature, i.e. in the high temperature limit. Hence, these corrections are most important in conformal models where $m_0 = 0$. Next, we compare our resummation techqniue not only with the usual one-loop results, but also with the inclusion of thermal masses. We do this on the level of the effective potential.

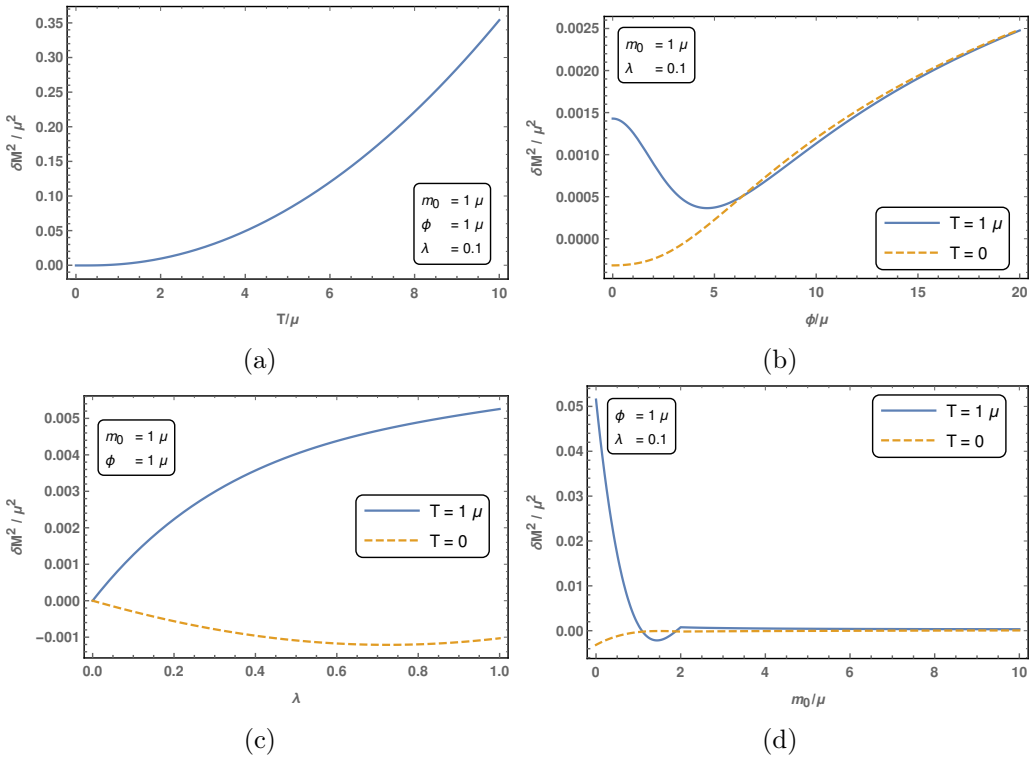

Figure 4.2: The dependence of $\delta M^2/\mu^2$ on (a) T/μ, (b) φ/μ, (c) λ and (d) m_0/μ. For panels (b),(c) and (d) the plots are shown for $T = 0$ and $T = 1\mu$.

The improved effective potential $V^I_{\text{eff}}(\varphi, T)$ for this theory is obtained by eq. (3.46). The standard one-loop effective potential at finite temperature for the scalar theory reads

$$V_{\text{eff}}(\varphi, T) = V^{(0)}(\varphi) + \frac{m^4(\varphi)}{64\pi^2}\left[\log\left(\frac{m^2(\varphi)}{\mu^2}\right) - \frac{3}{2}\right] + \frac{T^4}{2\pi^2} J_B\left(\frac{m^2(\varphi)}{T^2}\right). \tag{4.4}$$

The thermal mass $M_T(\varphi)$ of the scalar field is defined in eq. (3.39). Daisy resummation corresponds to replacing the tree-level mass $m(\varphi)$ in eq. (4.4) with $M_T(\varphi)$

$$V^{\text{daisy}}_{\text{eff}}(\varphi, T) = V_{\text{eff}}(\varphi, T)\Big|_{m(\varphi)=M_T(\varphi)}. \tag{4.5}$$

Fig. 4.3 shows the comparison of $V^I_{\text{eff}}(\varphi)$ and $V_{\text{eff}}(\varphi)$ at zero temperature and indicates that the two potentials are in accordance. Note, $V^{\text{daisy}}_{\text{eff}}(\varphi)$ reduces to $V_{\text{eff}}(\varphi)$ at $T = 0$. This shows that the conventional perturbative approach at zero temperature is valid and the resumming of higher-order diagrams has no significant effect on the effective potential. Fig. 4.3b shows the effective potentials in the vicinity of the minimum and illustrates that the location of the minimum and the second derivative at the minimum of both approach match to a high precision. We might also interpret this accordance of both effective potentials as a validation of the prescription for improving the effective potential introduced in chapter 3, since we do not expect a large effect of resummation at zero temperature.

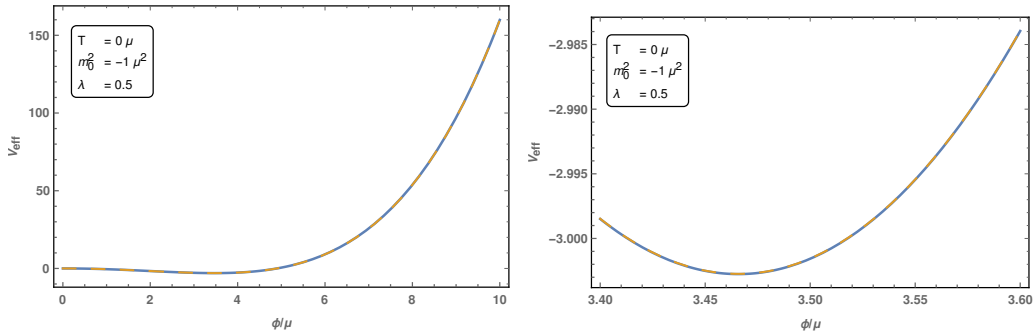

(a) (b)

Figure 4.3: The improved effective potential V_{eff}^{I} (solid blue line) versus the conventional one-loop effective potential V_{eff} (dashed yellow line) at zero temperature. The right plot shows the global minimum in higher resolution. In both panels the two plots are overlapping.

At finite temperature (cf. Fig. 4.4) the impact of the improvement of the effective potential is especially visible, if the VEV is not located at the origin. At low temperatures $T < \mu$ (cf. Fig. 4.4a) the three approaches to the effective potential do not show a significant difference as in the $T = 0$ case (cf. Fig. 4.3). We expect that this case is in the low temperature limit and thermal resummation is not necessary at this temperature. In contrast, Fig. 4.4b shows that V_{eff} and $V_{\text{eff}}^{\text{daisy}}$ coincide, but V_{eff}^{I} differs. These plots are generated for $T = 2.5\mu$ and we find for the ratio $m(\varphi)/T \sim 0.5$ at the VEV. This results suggests that this is the intermediate stage between high temperature and low temperature limit, where the daisy resummation technique asses thermal corrections wrongly. We conclude that the gap equation method is capable to improve the effective potential correctly at the intermediate stage, too. At $T = 5\mu$ (cf. Fig. 4.4c V_{eff} and $V_{\text{eff}}^{\text{daisy}}$ coincide less but the difference to V_{eff}^{I} is still significant. The two VEVs computed from V_{eff} and V_{eff}^{I} in Fig.4.4c vary approximately by $\Delta v \approx 0.25\mu$ and the two second derivatives evaluated at the VEV vary by about $\sqrt{V_{\text{eff}}''(v)} = \Delta M \approx 0.58\mu$. At even higher temperature $T = 10\mu$ (cf. Fig. 4.4d), when the VEV is located at the origin, the improvement of resummation by the gap equation approach compared to the daisy resummation approach is less significant. For this case the high temperature expansion is valid and the daisy resummation technique assess thermal corrections correctly. We can interpret this accordance at high temperatures again as a validation of the gap equation method. Although we find for V_{eff} and V_{eff}^{I} that the VEV is located at the origin, the second derivatives at the VEV vary by about $\Delta M \approx 0.41\mu^2$.

Furthermore, the overall shape of the potential plays an important role for models with a first-order phase transition. In that case the effective potential exhibits two local minima seperated by a potential barrier. The shape of this bump is crucial for the tunneling rate and hence for the correct description of bubble nucleation. We revisit this discussion in section 6.3.1 where a first-order phase transition is present.

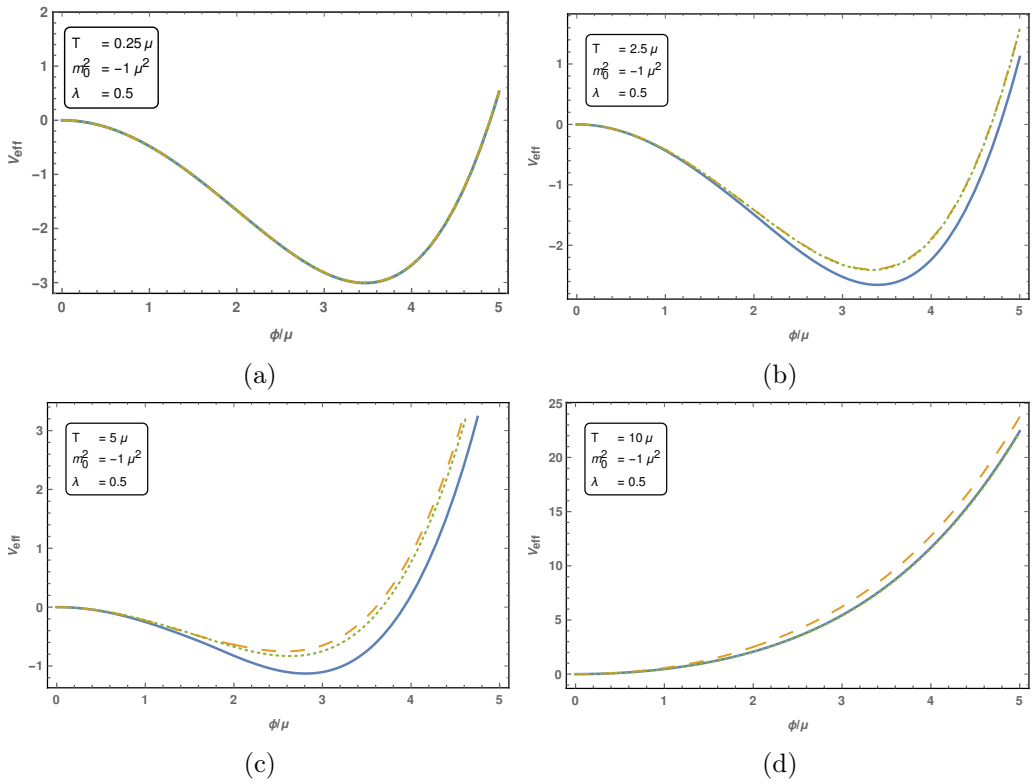

Figure 4.4: The improved effective potential V_{eff}^{I} (solid blue line) versus the conventional one-loop effective potential V_{eff} (dashed yellow line) and the daisy resummed effective potential $V_{\text{eff}}^{\text{daisy}}$ (dotted green line) at different temperatures.

Chapter 5

Conformal Extensions of the Standard Model

In this chapter we introduce conformal extensions of the standard model (SM) and discuss how they remedy some shortcomings of the SM. Since the discovery of the Higgs boson at the LHC, we know that the masses of the electroweak gauge bosons are generated by the Brout–Englert–Higgs mechanism. In this mechanism, the condensation of the Higgs boson spontaneously breaks the electroweak symmetry and generates the masses of the W and Z gauge bosons. Moreover, the masses of the fermions in the SM are generated through Yukawa couplings to the Higgs boson. The only mass parameter, hence the only dimensionfull parameter, which is present in the SM lagrangian is the tree-level mass term of the Higgs boson. In fact, a negative mass-squared term in the potential is needed to explain the non-zero VEV of the Higgs boson which is necessary for the Brout–Englert–Higgs mechanism.

The existence of this term is responsible for the so-called hierarchy problem of the SM. In the SM the Higgs boson receives quadratic divergent corrections form new heavy degrees of freedom to the mass, if a cut-off regularization scheme is used. One has to rely on unnatural fine-tuning for the cancelation of these terms [41]. It has been proposed that this can be resolved if the tree-level mass term of the Higgs boson is forbidden [1]. If the mass term is omitted, all parameters of the theory are dimensionless and the classical potential is scale invariant (conformal). A conformal SM (cSM) was first proposed in [1] and has also been studied in refs. with enlarged scalar sectors [41–45].

We do not observe conformal symmetry in nature at accessible energies and are led to the conclusion that conformal symmetry is radiatively (by quantum effects) broken at these energy scales and the Higgs boson acquires a finite mass. It is clear from the fact that the Higgs has no mass term in the classical potential of the cSM, this symmetry breakdown cannot be explained with the Brout–Englert–Higgs mechanism. It is necessary to invoke other mechanisms of symmetry breaking to open the window to conformal theories describing nature. The seminal paper of S. Coleman and E. Weinberg [2] proposes such a mechanism called radiative symmetry breaking (RSB). They have shown that a classically conformal symmetry of a theory can be broken by including quantum corrections. This means that the consideration of the the effective potential at one-loop level rather than only the classical potential is necessary. The interplay of the classical potential and one-loop terms in the effective potential might induce a non-zero VEVs of scalar fields. This

radiatively breaks the conformal symmetry since the vacuum condensate of a scalar field $\langle\phi\rangle$ introduces a dimensionful quantity into the lagrangian. It is conceivable that applying RSB mechanism in the cSM might be responsible for the non-zero VEV of the Higgs doublet and thereby a dynamical generation of all masses in the cSM by quantum effects. In other words, the SM could be interpreted as an effective field theory of the cSM at energies below some cutoff scale Λ below the Planck scale.

In ref. [2] it was argued that the cSM with dynamical generation of all masses by RSB is not realised in nature. The argument the authors give is a too small mass of the Higgs boson. However, the contribution from the top quark was not included since it was not yet discovered. With the inclusion of the top quark it is possible to generate the right Higgs mass via RSB with rather large self-coupling [3, 4]. This can lead to Landau poles of the running coupling constant before the Planck scale and is therefore conisdered as problematic [5]. For this reason, it was proposed to extend the cSM with an additional scalar field such that the electroweak vacuum can be generated via RSB. Such an extension can be achieved with so-called Higgs-portal models. In these models the additional scalar field only couples to Higgs boson with a dimensionless coupling constant and does not couple to other SM fields. In this way, there exists a portal between the hidden sector consisting of the additional scalar and possibly other matter fields and the cSM consisting of the SM fields. The process of spontaneous symmetry breaking in this model is particularly insightful if we consider a sequential approach. In this approach it is expected that the additional scalar acquires a VEV via RSB. The vacuum condensates of the additional scalar then consitutes a tree-level mass term for the Higgs boson and the spotaneous symmetry breaking in the SM sector looks like the Brout–Englert-Higgs mechanism. The actually realized process of symmetry breaking can be more complicated and will be discussed in chapter 6. Numerous extension with multiple real or complex scalar fields, additional gauge groups and additional fermions have been studied in the literature. The appeal to study these models is that they can address problems like dark matter, neutrino masses, inflation and electroweak baryogenesis (see ref. [5] and references therein). In particular, promising for this work, these models can entail a strong first-order phase transition in the electroweak or hidden sector. The absence of the negative m^2 in the tree-level potential of the cSM makes the potential flat around the origin and naturally supports the occurrence of a first-order phase transition if thermal corrections are included [5].

As already mentioned, in the simplest extension with one singlet scalar field the masses of the SM particles can be generated, but this recquires a large coupling between the Higgs doublet and the singlet. Consequently, this leads to a Landau pole close the the electroweak scale [5]. Hence, we will consider other extensions of the cSM in this thesis. The extension consists of an hidden $\mathrm{SU}(2)_X$ gauge group and a scalar forming a doublet under $\mathrm{SU}(2)_X$. The additional doublet is a singlet under the full $\mathrm{SU}(3)\times\mathrm{SU}(2)\times\mathrm{U}(1)$ SM gauge group and all SM fields are singlets unter the additional $\mathrm{SU}(2)_X$ gauge group. This model was proposed in [46] with a hidden $\mathrm{U}(1)_X$ gauge group and has generated a lot of research to accommodate dark matter in the models [47–51]. We refer to this model as SU(2)cSM.

5.1 Introducing the SU(2)cSM

In this section we introduce a Higgs-portal model with the aforementioned additional scalar doublet and a hidden gauge group $\mathrm{SU}(2)_X$. The tree-level potential includes self interaction

of both scalar doublets and a portal interaction between them. It reads

$$V^{(0)}(\mathbf{H},\mathbf{\Phi}) = \lambda_1(\mathbf{H}^\dagger\mathbf{H})^2 + \lambda_2(\mathbf{H}^\dagger\mathbf{H})(\mathbf{\Phi}^\dagger\mathbf{\Phi}) + \lambda_3(\mathbf{\Phi}^\dagger\mathbf{\Phi})^2, \tag{5.1}$$

where the Higgs doublet $\mathbf{H}$ and the additional scalar doublet $\mathbf{\Phi}$ can be written in terms of real scalar field as

$$\mathbf{H} = \frac{1}{\sqrt{2}}\begin{pmatrix} h_1 + ih_2 \\ h_3 + ih_4 \end{pmatrix}, \quad \mathbf{\Phi} = \frac{1}{\sqrt{2}}\begin{pmatrix} \varphi_1 + i\varphi_2 \\ \varphi_3 + i\varphi_4 \end{pmatrix}. \tag{5.2}$$

We demand that the effective potential is stable in the UV. Hence, the running coupling constants should satisfy at the Planck scale the stability conditions [52]

$$\lambda_1 \geq 0, \quad \lambda_3 \geq 0, \quad \lambda_2 \geq -2\sqrt{\lambda_1\lambda_2}. \tag{5.3}$$

The Lagrangian consisting of the hidden sector and the scalar fields reads

$$\mathcal{L}_X = -\frac{1}{4}F^X_{\mu\nu} - \frac{1}{2}(D_\mu\mathbf{H})^\dagger D^\mu\mathbf{H} - \frac{1}{2}(D_\mu\mathbf{\Phi})^\dagger D^\mu\mathbf{\Phi} - V^{(0)}(\mathbf{H},\mathbf{\Phi}), \tag{5.4}$$

where $F^X_{\mu\nu}$ is the field strength of the $\mathrm{SU}(2)_X$ gauge group and D_μ are the covariant derivatives, which can be written as

$$D_\mu\mathbf{H} = \big(\partial_\mu - igW^a_\mu t^a - ig'B_\mu y\big)\mathbf{H}, \tag{5.5}$$

$$D_\mu\mathbf{\Phi} = \big(\partial_\mu - ig_X X^a_\mu s^a\big)\mathbf{\Phi}, \tag{5.6}$$

where W^a_μ and B_μ are the SM $\mathrm{SU}(2)\times\mathrm{U}(1)$ gauge bosons before electroweak symmetry breaking with generators t^a and y. The X_μ gauge bosons correspond to the hidden $\mathrm{SU}(2)_X$ gauge group with generators s^a. Eqs. (5.5) and (5.6) show that $\mathbf{H}$ transforms as a singlet and $\mathbf{\Phi}$ as a doublet under the $\mathrm{SU}(2)_X$ gauge group. Due to the gauge symmetries the tree-level potential only depends on the radial fields defined by

$$h^2 = 2(\mathbf{H}^\dagger\mathbf{H}) = \sum_{i=1}^{4} h_i^2, \quad \varphi^2 = 2(\mathbf{\Phi}^\dagger\mathbf{\Phi}) = \sum_{i=1}^{4}\varphi_i^2. \tag{5.7}$$

Hence, the tree-level potential can be written as

$$V^{(0)}(h,\varphi) = \frac{1}{4}\big(\lambda_1 h^4 + \lambda_2 h^2\varphi^2 + \lambda_3\varphi^4\big). \tag{5.8}$$

The effective potential is given as a function of the two corresponding background fields h_J and φ_J, defined in eq. (1.10) as the expectation values in the presence of a source term J,

$$h_J = \left(\frac{\langle 0|h|0\rangle}{\langle 0|0\rangle}\right)_J, \quad \varphi_J = \left(\frac{\langle 0|\varphi|0\rangle}{\langle 0|0\rangle}\right)_J. \tag{5.9}$$

For a vanishing source term these fields correspond to the real VEVs of these quantum fields, i.e. the stationary points of the effective potential. We define these VEVs as

$$h_{J=0} = v, \quad \varphi_{J=0} = w. \tag{5.10}$$

From now on we will drop the subscript J of the background fields in eqs. (5.9). The scalar tree-level masses can be obtained from the Hessian of the tree-level potential. By using the gauge symmetries we can align the field basis such that the multiple of the background

fields $\vec{h} = (h_1, h_2, h_3, h_4)$ points along the fourth direction $\vec{h}_0 = (0, 0, 0, h)$ and similarly we define for $\vec{\varphi} = (\varphi_1, \varphi_2, \varphi_3, \varphi_4)$ this direction as $\vec{\varphi}_0 = (0, 0, 0, \varphi)$. In general, the field-dependent masses are obtained by evaluating the Hessian of the tree-level potential at the background fields. For our choice this means

$$m_{ij}^2(h, \varphi) = \left. \frac{\partial^2 V^{(0)}}{\partial \psi_i \partial \psi_j} \right|_{\vec{h}=\vec{h}_0, \vec{\varphi}=\vec{\varphi}_0}, \tag{5.11}$$

where $\vec{\psi} = (\vec{h}, \vec{\varphi})$. With these definitions we obtain the components

$$\left. \frac{\partial^2 V^{(0)}}{\partial h_i \partial h_j} \right|_{\vec{h}=\vec{h}_0, \vec{\varphi}=\vec{\varphi}_0} = \delta_{ij} \left(\lambda_1 h^2 + \frac{\lambda_2}{2} \varphi^2 + \delta_{i4} 2\lambda_1 h^2 \right), \tag{5.12}$$

$$\left. \frac{\partial^2 V^{(0)}}{\partial \varphi_i \partial \varphi_j} \right|_{\vec{h}=\vec{h}_0, \vec{\varphi}=\vec{\varphi}_0} = \delta_{ij} \left(\lambda_3 \varphi^2 + \frac{\lambda_2}{2} h^2 + \delta_{i4} 2\lambda_1 \varphi^2 \right), \tag{5.13}$$

$$\left. \frac{\partial^2 V^{(0)}}{\partial \varphi_i \partial h_j} \right|_{\vec{h}=\vec{h}_0, \vec{\varphi}=\vec{\varphi}_0} = \delta_{i4} \delta_{j4} \lambda_2 h \varphi. \tag{5.14}$$

The masses which follow from eqs. (5.12) and (5.13) for $i = 1, 2, 3$ correspond to the Goldstone fields of the Higgs doublet and the other scalar doublet, respectively. Their masses vanish at the stationary points of $V^{(0)}$. From eq. (5.14) it is clear that due to the Higgs portal coupling λ_2 the Hessian has off-diagonal components. To find the remaining two eigenvalues it is sufficient to diagonalize the matrix

$$\begin{pmatrix} m_{hh}^2 & m_{h\varphi}^2 \\ m_{\varphi h}^2 & m_{\varphi\varphi}^2 \end{pmatrix} = \begin{pmatrix} 3\lambda_1 h^2 + \frac{\lambda_2}{2}\varphi^2 & \lambda_2 h \varphi \\ \lambda_2 h \varphi & 3\lambda_3 \varphi^2 + \frac{\lambda_2}{2} h^2 \end{pmatrix}, \tag{5.15}$$

which yields

$$\begin{aligned} m_\pm^2(h, \varphi) =& \frac{1}{2} h^2 \left(3\lambda_1 + \frac{\lambda_2}{2} \right) + \frac{1}{2} \varphi^2 \left(\frac{\lambda_2}{2} + 3\lambda_3 \right) \\ & \pm \frac{1}{2} \sqrt{\left(h^2 \left(3\lambda_1 - \frac{\lambda_2}{2} \right) - \varphi^2 \left(3\lambda_3 - \frac{\lambda_2}{2} \right) \right)^2 + 4\lambda_2^2 h^2 \phi^2}. \end{aligned} \tag{5.16}$$

Together with the six Goldstone fields with masses

$$m_1^2(h, \varphi) = m_2^2(h, \varphi) = m_3^2(h, \varphi) = \lambda_1 h^2 + \frac{\lambda_2}{2} \varphi^2 \tag{5.17}$$

$$m_5^2(h, \varphi) = m_6^2(h, \varphi) = m_7^2(h, \varphi) = \lambda_3 \varphi^2 + \frac{\lambda_2}{2} h^2 \tag{5.18}$$

this defines the eight mass eigenvalues of the scalar sector. To obtain the mass eigenstates $\phi_\pm$ corresponding to mass eigenvalues $m_\pm$ we have to perform an orthogonal transformation on the gauge eigenstates h and φ according to

$$\begin{pmatrix} \phi_- \\ \phi_+ \end{pmatrix} = \begin{pmatrix} \cos\theta & -\sin\theta \\ \sin\theta & \cos\theta \end{pmatrix} \begin{pmatrix} h \\ \varphi \end{pmatrix}. \tag{5.19}$$

It should be noted, that these masess do not correspond to physical masses unless quantum corrections are included. Nevertheless, we stress that one of the mass eigenstates ϕ_- and ϕ_+ once quantum corrections are included is identified with the physical Higgs field. Which

one is the Higgs field is determined by matching one of the two mass eigenvalues to the experimental value of 125 GeV. In general it is possible that the Higgs boson is either the lighter or heavier scalar field. The mixing angle θ (cf. eq. (5.19)) is constrained by experimental results from LHC and LEP. The bounds are $|\cos\theta| \geq 0.93$ in case the Higgs boson is the lighter field and $|\sin\theta| \geq 0.87$ in the other case [53–55] *. The authors of ref. [56] show how Higgs portal models can be explored at the LHC. To obtain the correct Feynman rules for this model in the basis of the mass eigenstates one has to invert eq. (5.19) and express the Lagrangian in terms of ϕ_+ and ϕ_-, which will modify the couplings. In some cases (see section 6.3), it is more convenient to work in the basis of the gauge eigenstates (h, φ) and with an off-diagonal tree-level mass matrix as in (5.15).

The squared masses of the gauge bosons in the SM sector are

$$m^2_{W^+}(h) = m^2_{W^-}(h) = \frac{g^2 h^2}{4}, \tag{5.20}$$

$$m^2_Z(h) = \frac{h^2}{4}(g^2 + g'^2), \tag{5.21}$$

$$m^2_A = 0. \tag{5.22}$$

The massless photon field follows from the residual gauge symmetry $\mathrm{U}(1)_{\mathrm{EM}}$ of the SM. The hidden sector $\mathrm{SU}(2)_X$ contains three gauge bosons with masses squared given by

$$m^2_X(\phi) = \frac{g^2_X \varphi^2}{4}. \tag{5.23}$$

We introduced three dimensionless gauge coupling constants g, g' and g_X. The coupling g and g' are the SM SU(2) and U(1) gauge couplings which are related by the weak mixing angle

$$\tan(\theta_W) = \frac{g'}{g}. \tag{5.24}$$

The hidden gauge group $\mathrm{SU}(2)_X$ has the coupling g_X. The top quark acquires its mass by the Yukawa coupling to the Higgs field. The field-dependent top quark mass squared is

$$m_t(h)^2 = \frac{y_t^2}{2} h^2, \tag{5.25}$$

where y_t is the dimensionless Yukawa coupling of the top quark. We refrain from introducing other quark flavors or leptons to the analysis due their small masses at the electroweak scale.

The model we introduced has indeed a classical conformal symmetry since the stationary point of a stable classical potential is located at the origin ($h = 0, \varphi = 0$) and there all fields are massless. Furthermore, all couplings in the model $(\lambda_1, \lambda_2, \lambda_3, g, g', g_X, y_t)$ are dimensionless in four space-time dimensions. The SU(2)cSM contains two parameters more to the SM with parameters $(m_h, \lambda_h, g, g', y_t)$ Including quantum and thermal corrections to the effective potential might induce VEVs for the background fields and thus generate masses. In this case, the classical conformal symmetry is spontaneously broken.

*In these references the bounds were obtained for different models. We expect that these bounds also applies for the SU(2)cSM since the scalar sectors is similiar to the models in the ref. [53–55].

Chapter 6

Phase Transition in the SU(2)cSM

In this chapter we study the effectve potential of the SU(2)cSM at finite temperature. We are in particular interested in describing first-order phase transition and the corresponding critical temperature. To do that, we compute the improved effective potential with the methods introduced in chapter 3. We tackle this task by three approaches starting from appoximative methods. Firstly, we introduce the so-called sequential approach to the symmetry breaking in the SU(2)cSM which is valid for small portal couplings. This method is used for instance in refs. [47, 49]. Secondly, we use the Gildener-Weinberg (GW) method which is based on the assumption that the tree-level potential has a flat direction at some renormalisation scale in the field space. Also this method is used broadly in the literature (e.g. [50, 51]) and in particular to study phase transitions of Higgs portal models (e.g. [13, 14]). Both mentioned methods ultimately allow us to reduce the effective potential of the SU(2)cSM with multi-field dependence to a single-field dependence, which simplifies the improvement of the effective potential and the analysis of the phase transition significantly. Finally, we derive the improved effective potential with its full two-field dependence and show that GW method is not always a good approximation to study first-order phase transition with multiple fields. Moreover, it shows that the sequential approach is not applicable to study the phase transition of this model. Before that, we comment in section 6.1 on the methods we will use for the three cases.

6.1 Setup

6.1.1 Field Content

The field content of the SU(2)cSM which we will consider in our computations for the effective potential are the W,Z and X gauge bosons, the top quark and the two scalar fields with masses defined in eq. (5.16). All other tree-level masses can be found in section 5.1. The six Goldstone modes of this model (eqs. (5.17) and (5.18)) will be neglected in the one-loop term in the effective potential and thermal corrections. This is a common procedure in the literature since the effect of the Goldstone modes on the phase transitions is small [5, 57, 58]. This is based on the fact that these contribution scale as λ^2 so they are negligible compared to λ and g^4 contributions. Furthermore, the Goldstone bosons cause infrared divergences in the effective potential due to their vanishing masses at the stationary point. Resummation techniques exist to tame these divergences [59, 60], but we

choose a simple path by omitting the Goldstone bosons in the one-loop corrections.

6.1.2 Thermal Masses

Although we introduced the gap equation resummation technique to take care of the hard thermal loops, we will only apply this method to the two scalars in the model. This approach can be also applied to derive corrections to the gauge bosons masses. We refrain from deriving gap equations for the gauge bosons and use the results for the thermal masses from the literature. We do so since that will allow us to explicitly study the role of the gap equation resummation in the scalar sector of this multi-scalar model. From the gap equation perspective, the thermal masses are obtained by taking the leading order terms of the high temperature expansion of the gap equation (see section 3.2.4). For the derivation and discussion for a scalar field see ref. [18] and for the extension to gauge bosons see refs. [19, 20]. Corrections to the top quark mass are not necessary since fermions do not suffer from IR divergences due to their finite zero Matsubara mode [19]. At leading order in the high-temperature expansion only the longitudinal gauge bosons acquire a thermal mass. In the gauge field basis (A^a_μ and B_μ) before electroweak symmetry breaking the longitudinal thermal masses read [13, 20]

$$M_L^2(h,T) = \frac{h^2}{4}\begin{pmatrix} g^2 & 0 & 0 & 0 \\ 0 & g^2 & 0 & 0 \\ 0 & 0 & g^2 & -gg' \\ 0 & 0 & -gg' & g'^2 \end{pmatrix} + \frac{11}{6}T^2\begin{pmatrix} g^2 & 0 & 0 & 0 \\ 0 & g^2 & 0 & 0 \\ 0 & 0 & g^2 & 0 \\ 0 & 0 & 0 & g'^2 \end{pmatrix}. \quad (6.1)$$

Transforming the above matrix to the W^+_μ, W^-_μ, Z_μ and A_μ basis, we obtain the thermal masses of the longitudinal W, Z and photon [61]

$$M^2_{W_L} = m^2_W(h) + \frac{11}{6}g^2T^2, \quad (6.2)$$

$$M^2_{Z_L} = \frac{1}{2}m^2_Z(h) + \frac{11}{12}\frac{g^2}{\cos^2(\theta_W)}T^2 + \frac{\Delta}{2}, \quad (6.3)$$

$$M^2_{\gamma_L} = \frac{1}{2}m^2_Z(h) + \frac{11}{12}\frac{g^2}{\cos^2(\theta_W)}T^2 - \frac{\Delta}{2}, \quad (6.4)$$

$$\Delta^2 = m^4_Z(h) + \frac{11}{3}\frac{g^2\cos^2(2\theta_W)}{\cos^2(\theta_W)}\left[m^2_Z(h) + \frac{11}{12}\frac{g^2}{\cos^2(\theta_W)}T^2\right]T^2. \quad (6.5)$$

For the gauge bosons of the hidden gauge group, the thermal masses resemble the ones for the W bosons but with the gauge coupling g_X. This is in agreement with the general formula for thermal masses in extensions of the SM presented in ref. [62]. For the benchmark point (6.9) we will study in this thesis, the X gauge boson have a relatively high tree-level mass $m_X \approx 1$ TeV at the VEV. In the vicinity of this point, i.e. for large values of φ, the ratio $m^2_X/T^2 > 1$ shows that the high temperature limit is not valid for the X gauge bosons for temperatures at the electroweak scale $T \sim \mathcal{O}(100\text{ GeV})$. For this case, the daisy resummation is not valid since the high temperature expansion does not apply and one should rather use the tree-level mass. However, at lower values for φ, the high temperature limit is valid $m^2_X/T^2 < 1$ and the thermal mass gives the better estimate to the physical mass. To account for good accuracy in both cases, we use for the longitudinal mass of the

X gauge boson the expression

$$M_{X_L} = \begin{cases} m_X^2(\varphi) + \frac{11}{6} g_X^2 T^2 & \text{for } \frac{m_X^2}{T^2} < 1 \\ m_X^2(\varphi) & \text{for } \frac{m_X^2}{T^2} > 1. \end{cases} \tag{6.6}$$

This is crude approximation to the mass of the X gauge boson and can lead to discontinuities of our results at the point where $m_X(\varphi) = T$. To account for better accuracy in the range $m_X(\varphi) \sim T$ and a smooth transition between the high temperature and low temperatures phase, one should generalize the gap equation approach to gauge bosons. In that formalism, which is not presented in this thesis and left for future research, the thermal mass of the X gauge boson can be computed for any temperature and without reliance on the high temperature expansion.

All transverse gauge boson masses are to the leading order in the high temperature expansion given by their tree-level masses. The degrees of freedom $n = 3$ of a massive gauge boson at $T = 0$ are converted to one longitudinal degree of freedom $n_L = 1$ and two transverse degrees of freedom $n_T = 2$ at $T > 0$.

6.1.3 Benchmark Point

We closely follow ref. [5] in this section. The SU(2)cSM has four free parameters: three scalar couplings $\lambda_{1,2,3}$ and the hidden gauge coupling g_X. With knowledge of experimental data (Higgs VEV and mass) at $T \approx 0$ on can reduce the number of free parameters. The two stationary conditions for this model at $T = 0$,

$$\left.\frac{\partial V_{\text{eff}}(h,\varphi)}{\partial h}\right|_{h=v,\varphi=w} = 0, \tag{6.7}$$

$$\left.\frac{\partial V_{\text{eff}}(h,\varphi)}{\partial \varphi}\right|_{h=v\varphi=w} = 0. \tag{6.8}$$

can be used to replace the λ_1 and λ_3 in favor of λ_2, g_X and the VEVs v and w. The VEV of the Higgs doublet is known experimentally and will be fixed to its value $v \approx 246$ GeV, so the free paramaters left are λ_2, g_X and w. One can express w as a function of λ_2 and g_X requiring that $m_H = 125$ GeV. Thus, the SU(2)cSM can be parametrized by two parameters λ_2 and g_X. Furthermore, points in parameter space which entail a Landau pole below the Planck scale and which violate the bounds on the mixing angle θ are excluded. For a precise description of this anaylises we refer to ref. [5].

To study the phase transition, we will use one benchmark point found in ref. [5] which fulfill all aforementioned constraints. In sections 6.2 and 6.4 we will use the set of parameters given by

$$\begin{aligned} \mu &= v, \\ \lambda_1 &= 0.1236, \\ \lambda_2 &= -0.0030, \\ \lambda_3 &= -0.0047, \\ g_X &= 0.8500, \\ w &= 2411\text{GeV}, \end{aligned} \tag{6.9}$$

where all parameters are given at the scale μ of the Higgs VEV v . For the Gildener-Weinberg case in section 6.3, we use

$$\begin{aligned} \mu_{GW} &= 940\text{GeV}, \\ \lambda_1 &= 0.1055, \\ \lambda_2 &= -0.0030, \\ \lambda_3 &= 2 \cdot 10^{-5}, \\ g_X &= 0.8141, \\ w &= 2722\text{GeV}, \end{aligned} \tag{6.10}$$

where a flat direction was found at the renormalisatoin scale μ_{GW} in [5]. All parameters in (6.10) parameters are given at this scale at are related to the values in eq. (6.9) by the running of the coupling constants. More points in the parameter space fulfill all mentioned constraints and should by considered in a systematic study of phase transitions of the SU(2)cSM but this is beyond the scope of this thesis and is left for future research.

6.1.4 Running of the SM Parameters

To ensure correct numerical results, we need to use the running coupling constants of the SM evaluated at the renormalisation scales used in (6.9) and (6.10). We will use the one-loop beta functions of the weak couplings g and g' and the Yukawa top coupling y_t. They read [63, 64]

$$\beta_g = \mu \frac{\partial g}{\partial \mu} = -\frac{19 g^3}{96\pi^2}, \tag{6.11}$$

$$\beta_{g'} = \mu \frac{\partial g'}{\partial \mu} = -\frac{41 g'^3}{96\pi^2}, \tag{6.12}$$

$$\beta_{y_t} = \mu \frac{\partial y_t}{\partial \mu} = \frac{y_t}{16\pi^2}\left[\frac{9}{2} y_t^2 - 8 g_s^2 - \frac{9}{4} g^2 - \frac{17}{12} g'^2\right], \tag{6.13}$$

$$\beta_{g_s} = \mu \frac{\partial g_s}{\partial \mu} = -\frac{7 g_s^3}{16\pi^2}, \tag{6.14}$$

where g_s is the QCD coupling constant. The solution of these differential equations are obtained with the use of the initial values determined by their experimental values.

6.2 Sequential Symmetry Breaking

We start with the simplest approach to the electroweak phase transition of the SU(2)cSM. So-called sequential symmetry breaking gives an insightful intuition of the electroweak symmetry breaking pattern of the SU(2)cSM and how the usual Higgs mechanism is restored. The sequential approach to symmetry breaking is based on the assumption of a small portal coupling λ_2. In this limit the additional scalar decouples from the SM sector and acquires a VEV through RSB caused by loop corrections from the $\mathrm{SU}(2)_X$ gauge fields. This VEV generates an effective mass term for the Higgs boson and the symmetry breaking proceeds in the SM sector as usual. We discuss the validity of the sequential approach in

more detail since not only the value of the portal coupling is important, but also the ratio of the two VEVs. The effective potential has two stationary conditions

$$\left.\frac{\partial V_{\text{eff}}}{\partial h}\right|_{h=v,\varphi=w} = \lambda_1 v^3 + \frac{1}{2}\lambda_2 v w^2 + \left.\frac{\partial V^{(1)}}{\partial h}\right|_{h=v,\varphi=w} = 0, \tag{6.15}$$

$$\left.\frac{\partial V_{\text{eff}}}{\partial \varphi}\right|_{h=v,\varphi=w} = \lambda_3 w^3 + \frac{1}{2}\lambda_2 v^2 w + \left.\frac{\partial V^{(1)}}{\partial \varphi}\right|_{h=v,\varphi=w} = 0, \tag{6.16}$$

which are formulated at zero temperature. If scalar contributions to the one-loop term $V^{(1)}$ are dropped, then the last term in eq. (6.15) only contains contribution from the SM sector and the last term in eq. (6.16) contains only contribution form the hidden sector. This is a reasonable approximation if $\lambda_i \gg \lambda_i^2$ and thus tree-level terms dominate over scalar loop terms. The only terms which couple both equations are the ones proportional to λ_2. If we divide eq. (6.15) by v^3 and eq. (6.16) by w^3 we obtain

$$\lambda_1 + \frac{1}{2}\lambda_2 \frac{w^2}{v^2} + \frac{1}{v^3}\left.\frac{\partial V^{(1)}}{\partial h}\right|_{h=v,\varphi=w} = 0, \tag{6.17}$$

$$\lambda_3 + \frac{1}{2}\lambda_2 \frac{v^2}{w^2} + \frac{1}{w^3}\left.\frac{\partial V^{(1)}}{\partial \varphi}\right|_{h=v,\varphi=w} = 0. \tag{6.18}$$

If $\lambda_2 \ll \lambda_1, \lambda_3$ and $w \gg v$ then the second term in eq. (6.18) is negligible which means that the stationary condition for the VEV of φ is decoupled from the SM sector. In that case, φ can acquire a VEV through RSB if the hierarchy $\mathcal{O}(\lambda_3) \sim \mathcal{O}(g_X^4)$ applies (see ref. [5]). Furthermore, one can drop the one-loop contribution in eq. (6.17) since RSB is not effective in the SM sector [2] and the tree-level part dominates over the one-loop terms. In these approximations, the stationary conditions read

$$\lambda_1 + \frac{1}{2}\lambda_2 \frac{w^2}{v^2} = 0, \tag{6.19}$$

$$\lambda_3 + \frac{1}{w^3}\left.\frac{\partial V^{(1)}}{\partial \varphi}\right|_{h=v,\varphi=w} = 0. \tag{6.20}$$

Due to the assumption $w \gg v$ the λ_2 term in eq. (6.19) is not negligible. The above equations clarify the sequential symmetry breaking pattern. The scalar field φ decouples from the SM sector and might acquire a non-zero VEV w through RSB. If the hierarchies $w \gg v$ and $\lambda_2 < 0$ are true, the VEV w triggers the condensation of the Higgs doublet to its VEV $v^2 = -\frac{\lambda_2}{2\lambda_1} w^2$ by eq. (6.19). A further condition for that is $\lambda_2 < 0$.

The objective is now to study the symmetry breaking in the SM sector. In this approach the additional scalar field will be fixed to its vev $\langle\varphi\rangle = w$ at $T = 0$ and it becomes just a parameters of the model. To put it differently, the two-dimensional effective potential at finite temperature will be studied only along the constant $\varphi = w$ directions. This is of course a strong approximation, since thermal effects might change the true location of the minimum to regions where $\varphi \neq w$. We do not expect any interesting results here since it has been shown with non-perturbativ methods [7] that the electroweak phase transition in the SM is a crossover. The present approach reduces to the SM case and hence no first-order phase transition along the h direction should be expected.

As mentioned, the effective potential becomes a function of only h rather than a function of than h and φ,

$$V^{(0)}(h) = \frac{1}{4}(\lambda_1 h^4 + \lambda_2 w^2 h^2) + \text{const}, \tag{6.21}$$

where $\lambda_2 w^2$ can now be thought of as a mass term for the Higgs field. The field-dependent mass eigenvalue which correspond to the Higgs field is

$$m^2(h) = 3\lambda_1 h^2 + \frac{\lambda_2 w^2}{2}. \tag{6.22}$$

We use the set of parameters given in eqs. (6.9) use the method of section 3.3 to derive the gap equation and obtain the improved effective potential. For that we need the standard one-loop effective potential with thermal corrections,

$$V_{\text{eff}}(h,T) = V^{(0)}(h) + V^{(1)}(h) + V^{\text{T}}(h,T). \tag{6.23}$$

We use the general formulas provided in eqs. (1.51) and (2.81) for $V^{(1)}$ and V^{T} and then sum according to eq. (2.82) over the fields. This sum runs over transverse W and Z gauge bosons, longitudinal W,Z and γ gauge bosons, top quark and the scalar field with mass $m(h)$. With that at hand, the gap equation at zero external momentum can be written as

$$M^2(h,T) = m^2(h) + \frac{\partial^2}{\partial h^2}\Big(V^{(1)} + V^{\text{T}}\Big)\Big|_{m^2=M^2}. \tag{6.24}$$

Once this equation is solved for M^2 we can obtained the improved effective potential by two integrations with respect to h (cf. eq. (3.46)).

We show the results for $V_{\text{eff}}(h)$, $V'_{\text{eff}}(h)$ and $M^2 = V''_{\text{eff}}(h)$ in Fig. 6.1 for $T = 0$ and a high $T = 200$ GeV temperature where electroweak symmetry is restored (left column). Furthermore, we found a critical temperature $T_c \approx 180.843$ GeV where the effective potential has two degenerate minima. We also show the results for T_c and a temperature slightly above it to show that then the true VEV is located at the origin (right column). The physical information in Fig. 6.1 can be summarized by the following table:

Table 6.1: VEVs and masses for the SM case

T [GeV]	$v(T)$ [GeV]	M [GeV]
0	246.6	126.6
180.843 ($= T_c$)	0/20.0	4.7/4.8
180.850	0	4.7
200	0	44.5

The slashes in the second row indicate the degeneracy of the global minimum at $T = T_c$. It is surprising that our results point to a first-order phase transition which is excluded for the SM scenario in ref. [7], where non-perturbative methods were used. We expect that the barrier between the two degenerate minima in Fig. 6.1f is an artifact of the perturbative approach to the problem. Additionally, we can point out that the observed phase transition is extremely weak. The height of the barrier in Fig. 6.1f is small if we compare it to the energy density of a radiation bath which scales as T^4. This is also the reason why we normalize the plot of the effective potential as V_{eff}/T^4 . Then the height of the barrier is

$\mathcal{O}(10^{-7})$. Furthermore, the condition for a strong first-order electroweak transition in the literature is often stated by $v/T > 1$ * while in our case $v/T \sim \mathcal{O}(10^{-1})$. Therefore the first-order phase transition predicted by our model is extremely weak.

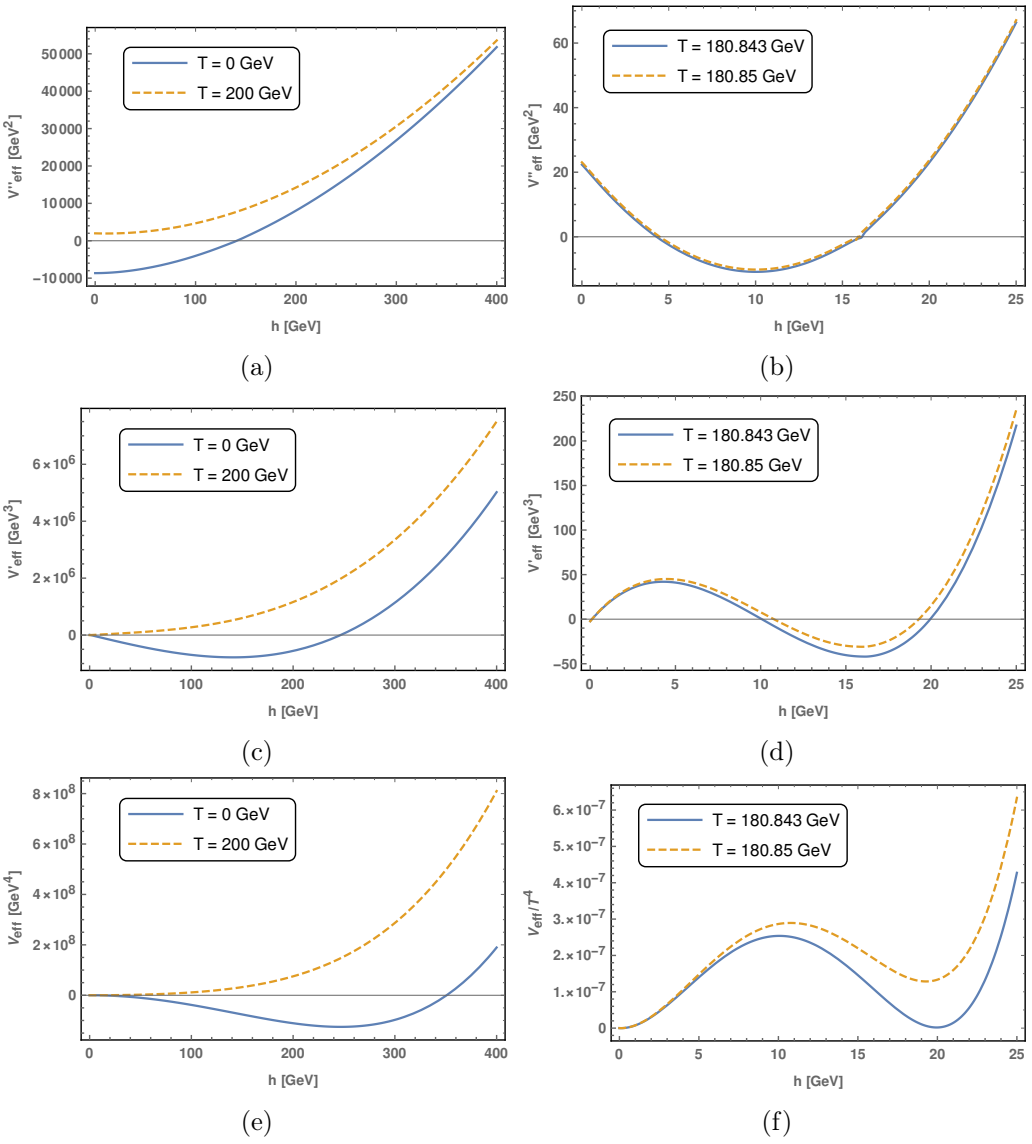

Figure 6.1: Improved effective potential $V_{\text{eff}}(h)$ (bottom panel), its first derivative $V'_{\text{eff}}(h)$ (middle panel) and second derivative $M^2 = V''_{\text{eff}}(h)$ (upper panel) for different temperatures derived from the sequential approach. Left column: $T = 0$ result and a high temperature result, where $V_{\text{eff}}(h)$ has only one local minimum. Right colum: the results at the critical temperature $T_c = 180.643$ GeV and a temperature slightly above it. Note that in the bottom right plot the effective potential is normalized by T^4. The VEVs and the values of running physical mass of the Higgs boson for these temperatures are given in table 6.1. The kink in panel (b) is a numerical artefact due to divergences in the gap equation at $h = 0$ and is smoothed by numerical integrations in the plots in panel (d) and (f).

*For reasons which will be clarified in chapter 8.

6.3 Gildener-Weinberg Method

The Gildener-Weinberg method [65] allows to study RSB for the case of multiple scalar fields, i.e. for an effective potential with multidimensional domain. In the absence of large logarithms and for a perturbative theory, the tree-level term in the effective potential is dominant over the one-loop scalar contribution. In case of a scalar theory with self interactions proportional to λ, the tree-level term is $\mathcal{O}(\lambda)$ and the one-loop term is $\mathcal{O}(\lambda^2)$. Hence, the quantum corrections are too small to modify the tree-level potential significantly and no minimum away from the origin can be generated through RSB. [†] However, in the multidimensional case, it is conceivable that the tree-level potential at some renormalisation scale is flat along a certain direction (see Fig. 6.2 for an illustration). We call that renormalisation scale the Gildener-Weinberg scale μ_{GW}. In this approach one has to use the running coupling constants of the model and search for this scale at which the tree tree-level potential exhibits a flat direction. Since the tree-level potential vanishes along the flat direction, the subleading one-loop terms can change the structure of the effective potential along that direction and induce a non-zero VEV located at the flat direction. In general, the condition for applicability is that away from the flat direction the tree-level potential dominates, i.e. $V^{(0)} > V^{(1)}$. If instead in the whole field space $V^{(0)} \sim V^{(1)}$ applies, then one should check whether the minimum found along the flat direction is the global minimum [5].

We will use this approach as a next approximate method since it will allow us to reduce the two-dimensional case of the SU(2)cSM to a one dimensional case. We will use the zero-temperature effective potential to determine the polar angle of the flat direction where the VEV is located. Subsequently, we will formulate the gap equation along that direction and study the effective potential on that ray in field space for finite temperature. This is possible because the polar angle of the flat direction (i.e. direction to the minimum) is equal to the angle of the orthogonal transformation which diagonalizes the mass matrix at tree-level. We show this in more detail below.

As in the previous case, this approach is a rough approximation to study thermal phase transition with multiple scalar fields with a one-dimensional effective potential. It is not guaranteed, that thermal correction will shift the VEV only along the flat direction towards the origin. In fact, the trajectory of the VEV with increasing temperature might be more complicated or a multi-step phase transition might occur. To take account of all that one has to use the full two-dimensional effective potential of this model as we do in the next section. However, with the Gildener-Weinberg approach the situation is somewhat altered with respect to the sequential approach since the interplay of the hidden sector and the SM sector is taken into account and more interesting results can be expected.

[†] If gauge fields with gauge coupling g and fermions with Yukawa coupling y are included, one has to ensure for the hierarchy $y^4, g^4 \ll \lambda$, such that the tree-level contribution is dominant over one-loop contributions in the effective potential.

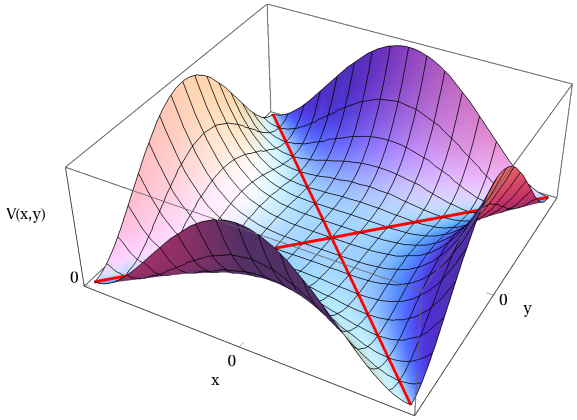

Figure 6.2: Example of a two-dimensional potential with flat directions (red lines).

Using the Gildener-Weinberg approach, we assume that the tree-level potential is dominant over the one-loop-term at the scale μ_{GW}. Hence, the stationary conditions for the SU(2)cSM at that scale can be approximated by (cf. eqs. (6.15) and (6.16))

$$\left.\frac{\partial V_{\text{eff}}}{\partial h}\right|_{h=v,\varphi=w} \approx \left.\frac{\partial V^{(0)}}{\partial h}\right|_{h=v,\varphi=w} = \lambda_1 v^3 + \frac{1}{2}\lambda_2 v w^2 = 0, \tag{6.25}$$

$$\left.\frac{\partial V_{\text{eff}}}{\partial \varphi}\right|_{h=v,\varphi=w} \approx \left.\frac{\partial V^{(0)}}{\partial \varphi}\right|_{h=v,\varphi=w} = \lambda_3 w^3 + \frac{1}{2}\lambda_2 w v^2 = 0, \tag{6.26}$$

which lead to

$$\begin{aligned} 4\lambda_1\lambda_3 - \lambda_2^2 &= 0, \\ w^2 &= -\frac{2\lambda_1}{\lambda_2} v^2. \end{aligned} \tag{6.27}$$

These equations can be seen as the conditions existence of a flat direction, because substitung them into the tree-levle potential shows that $V^{(0)}(v,w) = 0$. Subleading quantum contributions might change the location of the true minimum. For this reason, the flat direction determined by eqs. (6.27) should be seen as an approximation to the angle pointing to the true global minimum. Moreover, we can us eqs. (6.27) to simplify the tree-level mass matrix (cf. eq. (5.15)) of the two scalars fields h and φ evaluated at the VEVs

$$M^2 = \begin{pmatrix} 3\lambda_1 v^2 + \frac{\lambda_2}{2} w^2 & \lambda_2 v w \\ \lambda_2 v w & 3\lambda_3 w^2 + \frac{\lambda_2}{2} v^2 \end{pmatrix} = \begin{pmatrix} 2\lambda_1 v^2 & \sqrt{-2\lambda_1\lambda_2}\, v^2 \\ \sqrt{-2\lambda_1\lambda_2}\, v^2 & -\lambda_2 v^2 \end{pmatrix}. \tag{6.28}$$

This matrix has two mass eigenvalues

$$M_1^2 = (2\lambda_1 - \lambda_2) v^2, \tag{6.29}$$

$$M_2^2 = 0. \tag{6.30}$$

The second one corresponds to the flat direction since the second derivative along that directions should vanish. In the basis of the mass eigenstates one direction is given along the flat direction (corresponding to eigenvalue M_2^2) and one perpendicular to it. The two mass eigenstates can be written as

$$H = h\cos(\theta^*) + \varphi\sin(\theta^*), \tag{6.31}$$

$$S = \varphi\cos(\theta^*) - h\sin(\theta^*). \tag{6.32}$$

In the benchmark point we study (cf. eq. (6.10)) the physical Higgs field H is fixed to the field with tree-level mass M_2 and the other scalar S to the field with level-mass M_1, but in general the other choice is also valid. In our case this Higgs tree-level mass vanishes and this means that the Higgs mass will be purely generated by quantum effects. The polar angle of the flat direction is denoted by θ^*. It is convenient to work in polar coordinates for the gauge eigenstates,

$$\begin{aligned} h &= \rho\cos(\theta), \\ \varphi &= \rho\sin(\theta), \end{aligned} \tag{6.33}$$

where we introduce a radial field ρ and an angular field θ. For the VEVs we write this as

$$\begin{aligned} v &= v_\rho\cos(\theta^*), \\ w &= v_\rho\sin(\theta^*), \end{aligned} \tag{6.34}$$

where $v_\rho^2 = v^2 + w^2$. From eq. (6.31) it is clear that the Higgs mass eigenstate H reduces the radial field ρ on the flat direction where $\theta = \theta^*$. To determine the value of θ^*, we give the tree-level potential in polar coordinates (eq. (6.33))

$$V^{(0)}(\rho,\theta) = \frac{\rho^4}{4}\big(\lambda_1\cos^4(\theta) + \lambda_2\cos^2(\theta)\sin^2(\theta) + \lambda_3\sin^4(\theta)\big) \tag{6.35}$$

The polar angle of the flat direction can be determined by eqs. (6.27)

$$\theta^* = \arctan\left(\sqrt{\frac{-2\lambda_1}{\lambda_2}}\right) = \arctan\left(\sqrt{\frac{-\lambda_2}{2\lambda_3}}\right), \tag{6.36}$$

which is also the angle which diagonalizes the mass matrix in eq. (6.28). The non-zero tree level mass can be casted to

$$M_1^2 = (2\lambda_1 - \lambda_2)v^2 = -\lambda_2 v_\rho^2. \tag{6.37}$$

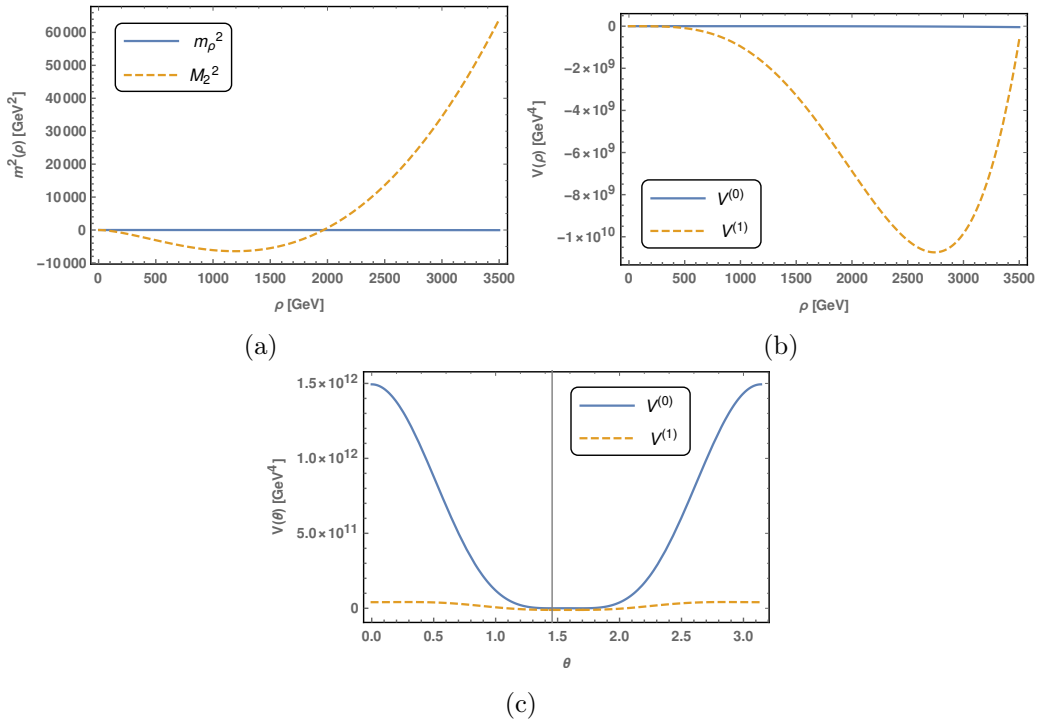

Figure 6.3: Panel (a): tree-level mass of the radial field vs the mass of the radial field obtained as second derivative of the one-loop effective potential along the flat direction $\theta = \theta^*$. Panel (b): tree-level part $V^{(0)}$ and one-loop part $V^{(1)}$ of the potential along the flat direction. In contrast, panel (c) shows the angular dependence of $V^{(0)}$ and $V^{(1)}$ if the radial field is fixed to the VEV v_ρ. The vertical grey line marks the flat direction θ^*. All plots are generated at $T = 0$.

We use now the benchmark point (6.10) to obtain results with the Gildener-Weinberg method. Fig. 6.3 illustrates that the aforementioned conditions for the validity of the Gildener-Weinberg approach are fulfilled. Fig. 6.3a and 6.3b exemplify that along the flat direction the effective potential is dominated by the one-loop contributions. In contrast, figure 6.3c shows that along the angular direction, the effective potential is dominated by the tree-level part thus justifying the classical approximation in eqs. (6.25) and (6.26). This means that along the perpendicular direction the tree-level potential is dominant over the one-loop term. Therefore we can approximate the mass of the perpendicular field by its tree-level mass in eq.(6.37). However, if quantum corrections are included in the mass matrix, the angle of the flat direction θ^* estimates the mixing angle θ in eq. (5.19) badly. See ref. [5] for a detailed discussion.

The Gildener-Weinberg method effectively reduces the two-dimensional problem to a one-dimensional problem. In other words, if the effective potential is written in polar coordiantes (as in eq. (6.35)), the only variable is ρ since θ is fixed to θ^*. For our approach to improve the effective potential this means to formulate the gap equation only along the flat direction. In this way, we obtain the mass of the Higgs boson by solving

$$M_2^2(\rho, T) = m_\rho^2 + \frac{\partial^2}{\partial \rho^2}\Big(V^{(1)}(\rho) + V^{\mathrm{T}}(\rho)\Big)\Big|_{m^2 = M^2, \theta = \theta^*} \tag{6.38}$$

The tree-level mass is $m_\rho = 0$ since it is the second derivative of the classical potential along the flat direction. To derive the gap equation (6.38) one has to derive $V^{(1)} + V^{\mathrm{T}}$

in coordinates (θ, ρ) with the help of eqs. (6.33). The field content is W,Z and X gauge bosons, the top quark and the radial scalar field ρ. The flat direction is determined by

$$\theta^* \approx 84^\circ.$$

To discuss the results, we show the effective potential and its first and second derivatives as in the previous section for the temperatures $T = 0$, a high temperature (here $T = 600$ GeV), the critical temperature T_c and a temperature slightly above it in Fig. 6.4 and summarize the physical information in table 6.2. Note that the phsyical mass and the VEV of the Higgs boson do not match their experimental values since in ref. [5] (reference for the benchmark point) the parameters are fixed to give correct results at the electroweak scale $\mu = v$. The results presented here are obtained at the Gildener-Weinberg scale $\mu_{\rm GW}$.

We can identify a first-order phase transition at the critical temperature $T_c \approx 360$ GeV. In this case the phase transition can be classified as strong since $v_\rho/T_c > 1$. The barrier seperating the two degenerate minima has the height of order $\mathcal{O}(10^{-1})$ if it is normalized by T^4. The results obtained from the GW method show that SU(2)cSM can entail a thermal strong-first order phase transition leading to bubble nucleation of the new phase. We investigate these issues further in chapter 7 and 8.

Table 6.2: VEVs and masses for the Gildener-Weinberg case

T [GeV]	v_ρ [GeV]	v [GeV]	M_2 [GeV]
0	2742	315	151
360	0/2582	0/296	110/122
380	2515	289	111
600	0	0	186

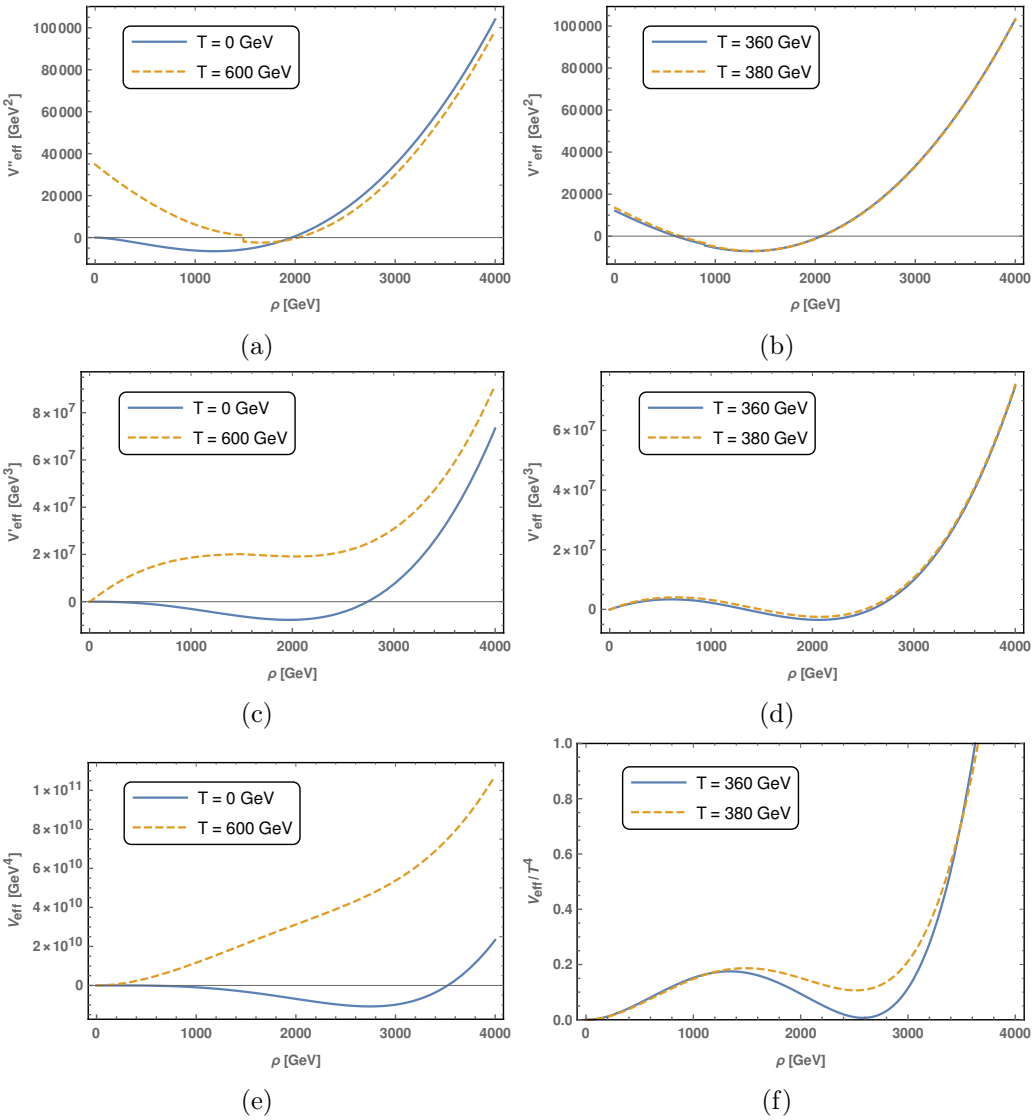

Figure 6.4: Improved potential (bottom panels) and the first two derivative (middle and upper panels) are shown for different temperatures derived in the Gildener-Weinberg approach. The left column show the zero temperature result and a high temperature result, where only one minimum exist. The right column shows the results at the critical temperature $T_c = 360$ GeV and a temperature slightly above it. Note that in the bottom right plot the effective potential is normalized by T^4. The VEVs and the values of the physical mass of the Higgs boson for these temperatures are shown in table 6.2.

6.3.1 Revisiting the Improvement of the Effective potential

In this section we discuss the effect of the improvement of the potential by the gap equation. The discussion in chapter 4 was applied to a simple toy model. Here we would like to see how the improvement affects physical quantities like the critical temperature of a more realistic model. As in chapter 4, we compare the improvement of the effective potential by the gap equation to the one-loop results and to the results of the daisy resummation method. For the latter, we use the thermal masses of the gauge bosons (see section 6.1.2) in the usual one-loop effective potential at finite temperature.

The deviation of the critical temperatures derived from the gap equation approach and the daisy resummation approach is (cf. Fig. 6.5b)

$$\Delta T_c \approx 360 - 343 \approx 17 \text{ GeV},$$

which shows that for this case at relatively high temperatures the gap equation improvement is more accurate than the daisy resummation approach. At lower temperature $T = 40$ GeV (cf. Fig. 6.5a), which will turn out to be approximately the nucleation temperature in section 7.3 for this case, the difference around false vacuum is considerable. The shape of the effective potential in the vicinity of the false vacuum is important for the details of bubble nucleation. We think that with the gap equation approach the accuracy of the determination of nucleation temperature, duration of the transition and latent heat [‡] for cosmological first-order phase transitions is improved. The discontinuities visible in Fig. 6.5 for the daisy approach are due the step-wise definition of the thermal mass of the X gauge bosons (cf. eq. (6.6)). In the gap equation results this jump is smoothed out due to interpolation and the two integrations to obtain the effective potential from M^2.

On the other hand, we compare in Fig. 6.5 the usual one-loop potential at finite temperature without thermal masses to the improved potential for $T = T_c$ and $T = 40$ GeV. The deviation is significant for both temperatures and the error in the critical temperature is

$$\Delta T_C \approx 360 - 334 \approx 26 \text{ GeV}.$$

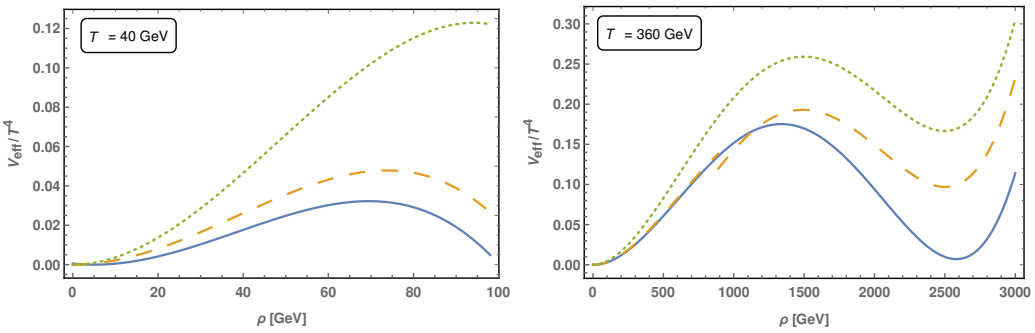

(a) (b)

Figure 6.5: Improved effective potential (blue solid line), the one-loop effective potential with thermal masses (yellow dashed line) and the one-loop effective potential with tree level masses (green dotted line) at the approximately the nucleation temperature (a) and at critical temperature (b). Note that panel (a) shows only the vicinity of the false vacuum at $\rho = 0$. The discontinuity of the result with thermal masses in panel (b) is due to the definition of the thermal mass for the X gauge bosons (cf. eq. (6.6)).

6.4 Multi-Gap Equation Method

As a final approach to the analysis of the phase transition in the SU(2)cSM we aim to study the effective potential in its full two-dimensional domain. This allows to examine the phase transition not solely along one direction (as in the Gildener-Weinberg approach) but to generate the two-dimensional effective potential at the critical temperature. Hence, one

[‡]These quantities will be defined in chapter 7.

can determine the true direction to the global minimum, search for a potential multi-step transition and study bubble nucleation in multi-dimensional field space. However, the disadvantage of this approach is the high computation time of the numerical implementation of the improved effective potential. Therefore, the resolution of the results in this section is lower than in the previous two sections and the results are afflicted with higher numerical errors. In the next paragraph we introduce the concept of the improvement for effective potentials with multiple scalar fields, which we refer to as the multi-gap equation method.

The SU(2)cSM contains two background fields h and φ. If we consider the effective potential in the (h, φ) basis, its Hessian M^2 is non-diagonal due to the portal coupling λ_2 (cf. eq. (5.15)). This shows that three gap equations need to be considered for obtaining the two dimensional improved effective potential. Therefore, we consider the non-diagonal tree-level matrix with the components given by eq. (5.15). We derive the gap equation by the approach of section 3.3 and therefore we need the one-loop terms of the effective potential at finite temperature. The field content is the W, Z and X gauge bosons, the top quark and the two scalar fields with masses $m_\pm$. The scalar field masses $m_\pm$ in the one-loop terms can be written in terms of the masses m_h, m_φ and $m_{h\varphi}$ in the off-diagonal basis,

$$m_\pm^2(h,\varphi) = \frac{1}{2}\left(m_h^2(h,\varphi) + m_\varphi^2(h,\varphi) \pm \sqrt{\left(m_h^2(h,\varphi)^2 - m_\varphi^2(h,\varphi)\right)^2 + 4m_{h\varphi}^4}\right). \tag{6.39}$$

With that at hand, we can formulate three gap equations for the three components of the off-diagonal mass matrix. We obtain the three resummed masses by

$$\begin{aligned} M_h^2(h,\varphi,T) =& m_h^2(h,\varphi) \\ &+ \frac{\partial^2}{\partial h^2}\Big(V^{(1)}(h,\varphi) + V^{\mathrm{T}}(h,\varphi)\Big)\Big|_{m_h=M_h, m_\varphi=M_\varphi, m_{h\varphi}=M_{h\varphi}}, \end{aligned} \tag{6.40}$$

$$\begin{aligned} M_\varphi^2(h,\varphi,T) =& m_\varphi^2(h,\varphi) \\ &+ \frac{\partial^2}{\partial \varphi^2}\Big(V^{(1)}(h,\varphi) + V^{\mathrm{T}}(h,\varphi)\Big)\Big|_{m_h=M_h, m_\varphi=M_\varphi, m_{h\varphi}=M_{h\varphi}}, \end{aligned} \tag{6.41}$$

$$\begin{aligned} M_{h\varphi}^2(h,\varphi,T) =& m_{h\varphi}^2(h,\varphi) \\ &+ \frac{\partial^2}{\partial h \partial \varphi}\Big(V^{(1)}(h,\varphi) + V^{\mathrm{T}}(h,\varphi)\Big)\Big|_{m_h=M_h, m_\varphi=M_\varphi, m_{h\varphi}=M_{h\varphi}}. \end{aligned} \tag{6.42}$$

Solving eqs.(6.40)-(6.42) by iterations yields the improved mass matrix

$$M^2(h,\varphi,T) = \begin{pmatrix} M_h^2 & M_{h\varphi}^2 \\ M_{h\varphi}^2 & M_\varphi^2 \end{pmatrix}. \tag{6.43}$$

In our considerations we use benchmark point (6.9) and are restricted to the case where the field with the lower mass of 125 GeV is the Higgs boson. We can integrate the components in the matrix (6.43) to obtain the two first derivatives of the effective potential

$$\frac{\partial V_{\mathrm{eff}}}{\partial h}(h,\varphi) = \int_0^h \mathrm{d}h'\, M_h^2(h',\varphi) + \int_0^\varphi \mathrm{d}\varphi'\, M_{h\varphi'}^2(0,y), \tag{6.44}$$

$$\frac{\partial V_{\mathrm{eff}}}{\partial \varphi}(h,\varphi) = \int_0^\varphi \mathrm{d}\varphi'\, M_\varphi^2(h,\varphi') + \int_0^h \mathrm{d}h'\, M_{h\varphi}^2(h',0), \tag{6.45}$$

where the off-diagonal component of the mass matrix (6.43) are used to fix the integration constants. Finally, we obtain the improved effective potential by

$$V_{\mathrm{eff}}(h,\varphi,T) = \int_0^h \mathrm{d}h'\, \frac{\partial V_{\mathrm{eff}}}{\partial x}(x,\varphi)\Big|_{x=h'} + \int_0^\varphi \mathrm{d}\varphi'\, \frac{\partial V_{\mathrm{eff}}}{\partial y}(0,y)\Big|_{y=\varphi'}, \tag{6.46}$$

carrying the full dependence on h and φ.

6.4.1 Zero Temperature Results

At zero temperature we find the global minimum of the improved potential to be located at

$$v \approx 250 \text{ GeV}, \quad w \approx 2431 \text{ GeV}. \tag{6.47}$$

In Fig. 6.6 we illustrate the improved effective potential by contour plots. The stationary points of the effective potential are found by the intersection of the zero contours of $\partial V_{\text{eff}}/\partial h$ and $\partial V_{\text{eff}}/\partial \varphi$ (cf. Fig. 6.7a and 6.7b). We then evaluate the effective potential at these points and the VEV is then defined as the values of the fields for which the minimum of that set is acquired. Further physical information is encoded in the resummed mass matrix (6.43). The two eigenvalues of that matrix can be computed at any point in the field space spanned by (h, φ). The two eigevalues $M_1(v, w)$ and $M_2(v, w)$ at the VEV (cf. Fig. 6.7c and 6.7d) are the masses of the Higgs boson and the additional scalar, respectively. The two eigenvalues are complex at some points in field space, since the second derivative of the effective potential is negative in some regions (white regions in Fig. 6.7c and 6.7d). Evaluating the mass eigenvalues at the VEVs (6.47) we find the physical masses

$$M_1 \approx 124 \text{ GeV}, \quad M_2 \approx 148 \text{ GeV}. \tag{6.48}$$

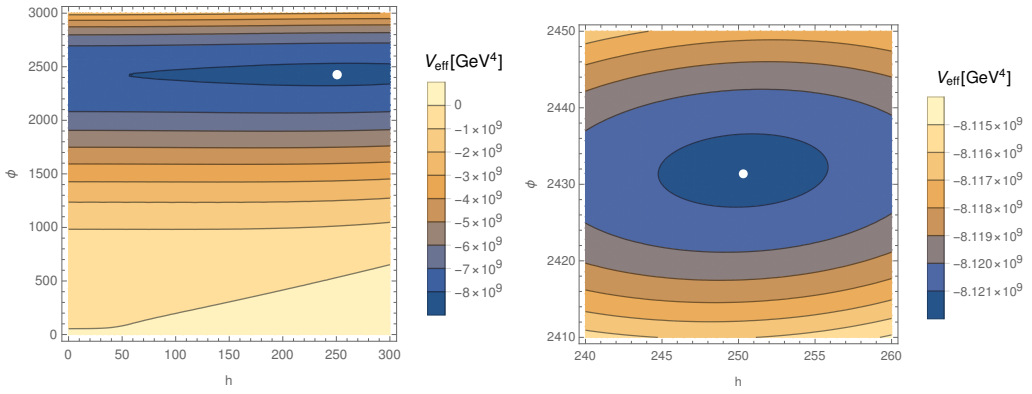

(a) (b)

Figure 6.6: Improved effective potential at $T = 0$. The white points represent the global minimum of the potential.

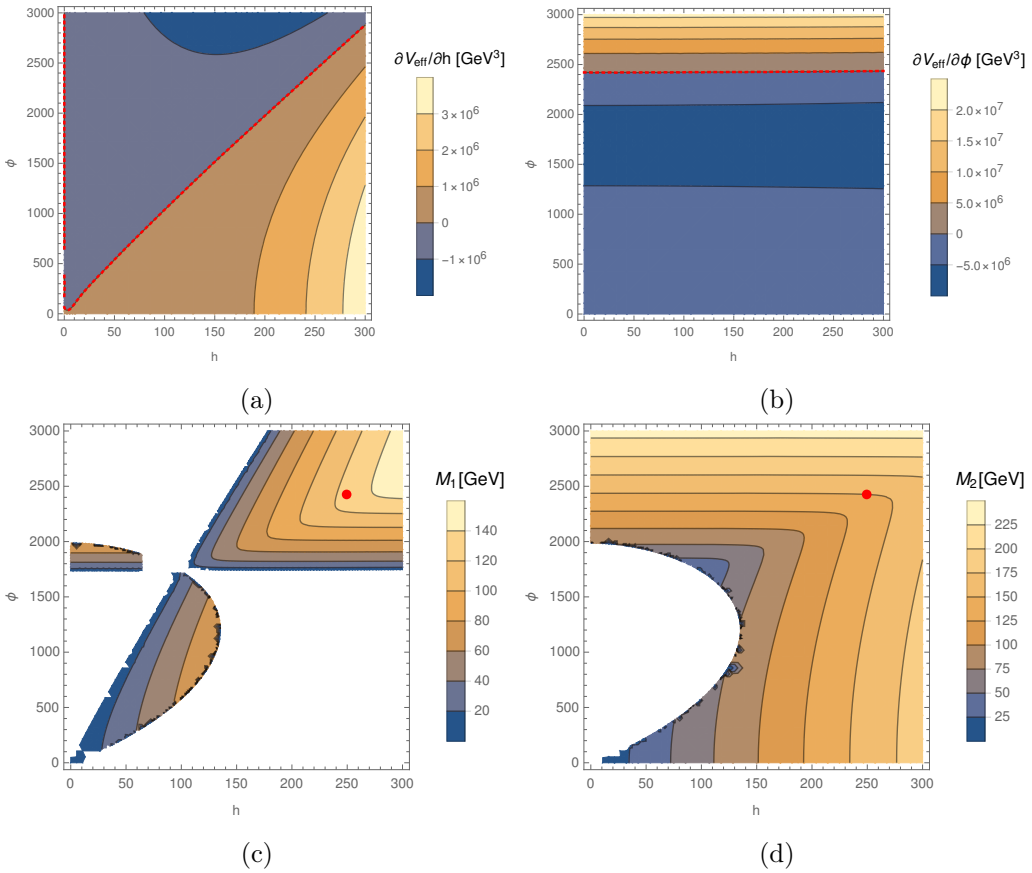

Figure 6.7: Upper panels: the two derivatives of the effective potential at $T = 0$, the red dotted lines correspond to the zero contours. Bottom panels: the eigenvalues of the resummed mass matrix (6.43) and the red dots indicate the location of the global minimum of the potential. At this point the eigenvalues are given by eqs. (6.48). The white regions correspond to imaginary masses M_1 or M_2.

6.4.2 Turning on the Temperature

To study the improved effective potential at finite temperature systematically, we look numerically for the VEV as we did for zero temperature in the previous section. To do that, we discretize the temperature to steps of $\delta T = 5$ GeV and scan in the interval $0 \leq T \leq 330$ GeV. The resulting locations of the minima for various temperatures are visualized in Fig. 6.8. This intermediate result hints to the possibility of a multi-step phase transition. For $T > 327$ GeV the VEV is located at the origin. At $T_1 \approx 327$ GeV we register a jump in the φ direction of about 2316 GeV which could correspond to a first-order phase transition. We refer to this event as critical point I and discuss it in the next subsection. For temperatures in the range $179 < T < 327$ GeV, the VEV is located approximately at $h \approx 0$ and $\varphi \sim 2300$ GeV and no phase transition is observed. At $T_2 \approx 179$ GeV the VEV jumps again about 40 GeV in the h direction (see figure 6.8b) and refer to this as critical point II. For low temperatures $O < T < 179$ GeV the VEV seems to continuously shift to the $T = 0$ VEV at $h = v$ and $\varphi = w$.

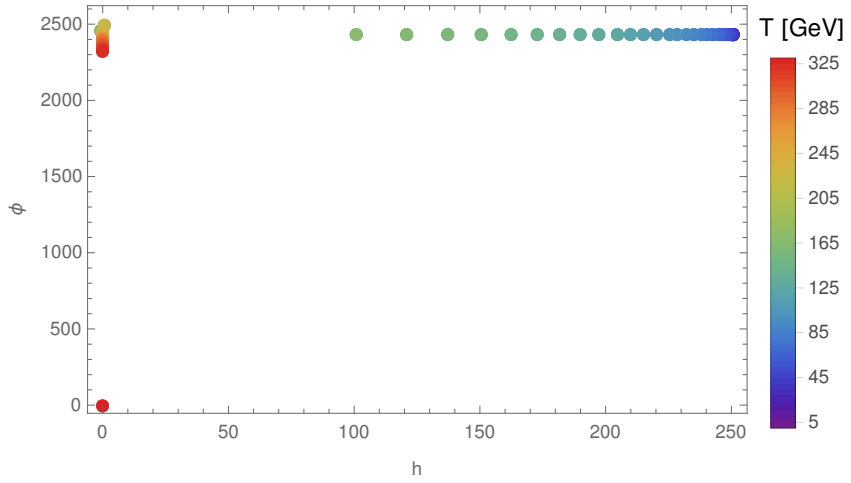

(a)

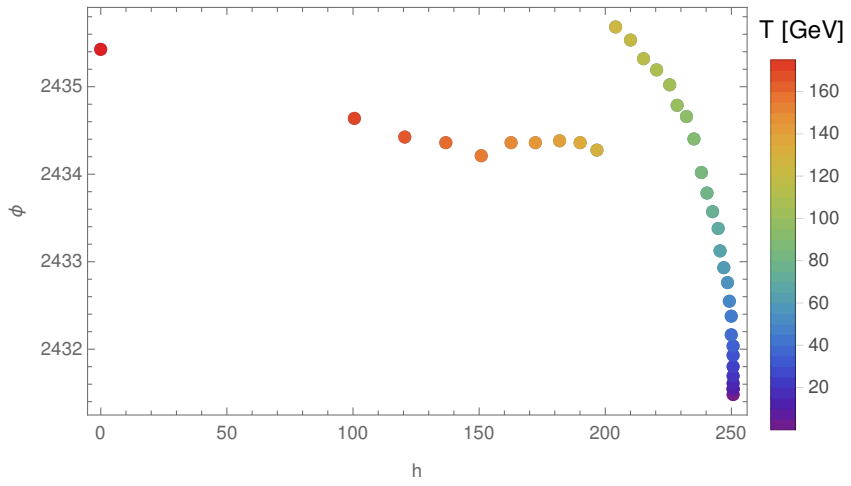

(b)

Figure 6.8: The dots indicate the location of the VEVs with varying temperature in steps of $\delta T = 5$ GeV. The top panel covers the the temperature range $0 \leq T \leq 330$ GeV and thus showing both phase transitions. The bottom panel covers for the temperature range $0 \leq T \leq 180$ GeV, thus giving a more detailed picture on the first phase transition. The jump in the φ direction at $h \approx 200$ GeV is solely due to the definition of the thermal mass of the X gauge bosons in eq. (6.6).

Critical Point I

The critical point I might lead to a first-order transition since two degenerate minima were found in Fig. 6.9b. The transition is aligned approximately at the $h = 0$ line. The critical values

$$w_c \approx 2316 \text{ GeV}, \quad T_1 \approx 327 \text{ GeV}, \tag{6.49}$$

are obtained from the improved effective potential in Fig. 6.9. If the transition proceeds between the two generated minima in Fig. 6.9a then it can be classified as strong first-order phase transition with a relatively high potential barrier. In that case it can be considered as a phase transition solely in the hidden sector, since the VEV of the Higgs doublet v does not jump, whereby the VEV of the additional scalar field w does.

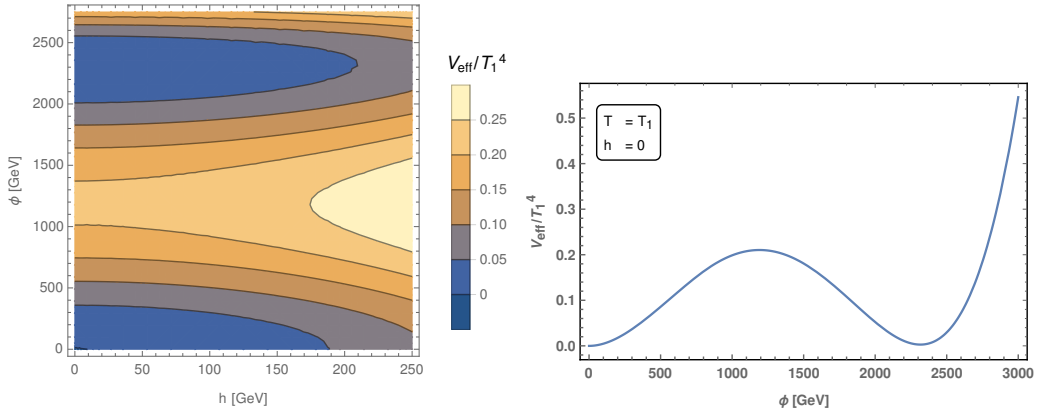

(a) (b)

Figure 6.9: Left panel: the improved effective potential at the critical temperature T_1. The degenerate minima are both located at $h = 0$ and the φ-coordinates are $\varphi = 0$ and $\varphi = w_c$. The right panel indicates the φ dependence of the improved effective potential for the constant $h = 0$.

Critical point II

We analyze the jump in the h direction of the global minimum which can be best seen in figure 6.8b in more detail. At the temperature T_2 the effective potential is exhibiting two degenerate minima and the corresponding critical values are

$$v_c \approx 40 \text{ GeV}, \quad T_2 \approx 179 \text{ GeV}. \tag{6.50}$$

The line connecting the degenerate minima is given approximately by the constant $\phi \approx 2437$ GeV line and v_c is the distance of the degenerate minima in that direction. The barrier is relatively small since at this point $V_{\text{eff}}/T_2^4 \sim \mathcal{O}(10^{-5})$. Although $v_c/T_2 \ll 1$ at this critical point, the phase transition might start at lower temperatures (i.e. the nucleation temperature) where the phase transition can be classified as strong $v/T > 1$. Furthermore, to discuss the phase transition for this effective potential with two critical points, one has to scrutinize the process of bubble nucleation in the multi-field case. Two scenarios are in general possible for the case with two critical points. On the one hand, the field can first transition from the origin to the critical point I and subsequently from this point to the critical point II. On the other hand, the field can transition directly from the origin to the critical point II if the nucleation temperature is very small. To take account of all that, we introduce the theory of bubble nucleation in the next chapter and study the phase transition of the multi-gap results in section 7.4.

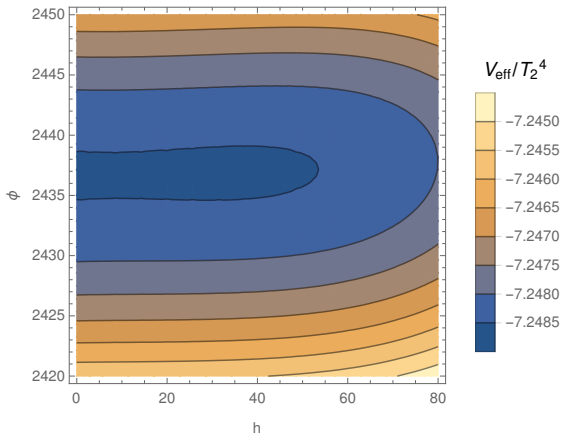

Figure 6.10: Improved effective potential at the critical temperature T_2. The two degnerate minima are both located at $\varphi = 2437$ GeV and the h-values are $h = 0$ and $h = v_c$. The barrier between the two degenertate minima is very small compared to the depth of the effective potential, hence it is not visible in this contour plot.

Chapter 7

Bubble Nucleation

In the last chapter we have shown that the SU(2)cSM can entail a first-order phase transition. In this chapter we would like to study the cosmological implications of this phase transition, in particular the process of bubble nucleation. A first-order phase transition is characterized by the coexistence of two degenerate minima at a critical temperature T_c. These two minima are seperated by a potential barrier which prevents the background field to directly jump from the false vacuum (global minimum for $T < T_c$) to the true vacuum (global minimum for $T > T_c$). Hence, the metastable phase might be present in the system up to some lower temperature which is called nucleation temperature T_n. At finite temperature the transition between the two vacua proceeds via thermal tunneling. This process is called bubble nucleation because the true vacuum is generated by formation of bubbles in which the field is in the true vacuum. The bubbles then expand in the sea of the false vacuum and in this way the false vacuum in the universe is converted to the true vacuum [26]. This process is particularly interesting to study in the context of cosmology, since we know that the universe is cooling down adiabatically with $T \sim a^{-1}(t)$ were $a(t)$ is the scale factor in the FLRW metric. In the case where the potential barrier between the minima is sufficiently high and broad to suppress the tunneling rate on Hubble time scales, the true vacuum is supercooled by the expansion of the universe *. Once the tunneling rate is efficient enough to nucleate at least one bubble in the Hubble volume the system undergoes a strong first-order transition since the energy difference between the two states is high and as a results the vacuum energy which is released into the radiation bath is very high. To understand and quantify these processes better, below we give a brief introduction to the theory of bubble nucleation based on refs. [11, 12, 26, 66, 67].

The computation of the decay rate (i.e. the tunneling rate) of the metastable state is based on the calculation of the imaginary part of effective potential at the metastable vacuum [66]. This rate per unit time per unit volume is written as [66]

$$\Gamma = A(T)e^{-S_E(T)}, \tag{7.1}$$

where the exponent is the euclidean action at finite temperature

$$S_E(T) = \int_0^{1/T} \mathrm{d}\tau \int \mathrm{d}^3x \left[\frac{1}{2}\left(\frac{d\phi}{d\tau}\right)^2 + \frac{1}{2}(\nabla\phi)^2 + V(\phi, T)\right], \tag{7.2}$$

*At the level of the effective potential at finite temperature is reflected in the decrease of the potential energy at the true minimum $\langle\phi\rangle = \varphi \neq 0$ with decreasing temperature (e.g. Fig. 6.1e, 6.1f).

for a scalar field $\phi(\mathbf{x}, \tau)$ which is periodic in imaginary time τ with period $\beta = T^{-1}$. The potential $V(\phi, T)$ is the effective potential at finite temperature. It should be defined such that at the false vacuum $V(\phi_f, T) = 0$. The fact that this theory is Euclidean can also be understood as a horizontal flip of the potential converting the local minima to local maxima. At $T = 0$, or $\beta \to \infty$, the classical solution to the euclidean action (7.2) with O(4) symmetry $\phi(r_4 = \mathbf{x}^2 + \tau^2)$ and boundary conditions [†]

$$\phi\Big|_{r_4 \to \infty} \to \phi_f, \quad \frac{\mathrm{d}\phi}{\mathrm{d}r_4}\Big|_{r_4=0} = 0 \tag{7.3}$$

is the so-called O(4) bounce solution or instanton solution which realizes the tunneling process at zero temperature. Although this is a classical solution, some quantum effects are taken into account since the effective potential is used in eq. (7.2). At finite temperature the symmetry of the bounce solution is broken to the O(3) symmetry because the period of the solution in imaginary time is finite [66]. For high temperatures the Euclidean action (7.2) is well approximated by the spatial Euclidean action S_3 [11]

$$S(T) \approx \frac{S_3(T)}{T} = \frac{1}{T} \int \mathrm{d}^3x \left[\frac{1}{2} (\nabla\phi)^2 + V(\phi, T) \right], \tag{7.4}$$

and using the O(3) symmetry we can cast the integral to

$$S_3(T) = 4\pi \int \mathrm{d}r\, r^2 \left[\frac{1}{2} \left(\frac{\mathrm{d}\phi}{\mathrm{d}r} \right)^2 + V(\phi, T) \right]. \tag{7.5}$$

The classical euclidean equation of motion following from that action is

$$\frac{\mathrm{d}^2\phi}{\mathrm{d}r^2} + \frac{2}{r^2} \frac{\mathrm{d}\phi}{\mathrm{d}r} - \frac{\mathrm{d}V_{\text{eff}}}{\mathrm{d}\phi} = 0, \tag{7.6}$$

where $r = |\mathbf{x}|$ is the spatial radius. The boundary conditions of the O(3) bounce solution read now

$$\phi\Big|_{r \to \infty} \to \phi_f, \quad \frac{\mathrm{d}\phi}{\mathrm{d}r}\Big|_{r=0} = 0. \tag{7.7}$$

The boundary conditions tells us that the field is in the true vacuum at the origin and in the false vacuum ϕ_f at infinite distance [11]. For a thermal field theory the nucleation rate per unit time per unit volume can be expressed as [26]

$$\Gamma(T) = \omega T^4 e^{-S_3(\phi,T)/T}, \tag{7.8}$$

where ω is a constant roughly of order $\mathcal{O}(1)$.

An important feature to characterize the bubbles is the thickness of their walls[‡]. We follow closely the discussion of ref. [26] by analyzing the scaling of the Euclidean action (7.5). Considering one bubble with radius R and $\phi = 0$ outside the bubble, we can write eq. (7.5) as

$$S_3(T) = 4\pi \int_0^R \mathrm{d}r\, r^2 \left[\frac{1}{2} \left(\frac{\mathrm{d}\phi}{\mathrm{d}r} \right)^2 + V(\phi, T) \right], \tag{7.9}$$

[†]We denote the false vacuum outside of the bubble as ϕ_f. In the literature one often finds that $\phi_f = 0$ since this is usually the case in thermal phase transitions.

[‡]The bubble walls separate the regions of the two phases $\phi_f = 0$ (false vacuum) and $\phi = \phi_m$ (true vacuum) of the field.

which scales like

$$S_3 \sim 2\pi R^2 \left(\frac{\delta\phi}{\delta R}\right)^2 \delta R + \frac{4\pi R^3 \langle V \rangle}{3} \tag{7.10}$$

where δR is the thickness of the bubble wall, $\delta\phi^2 \sim \phi_m^2$ and $\langle V \rangle$ is the average of the potential over the bubble volume. The first term can be interpreted as a surface term and the second term as a volume term. For temperatures slightly lower the T_c the height of the potential barrier $V(\phi_M, T)$ at the local maximum is large compared to depth of the potential $-V(\phi_m, T)$ at the global minimum ϕ_m. The minimization of S_3 at this temperature is therefore dominated by minimizing the volume term in the region around ϕ_M. This corresponds to configurations with thin wall bubbles $\delta R/R \ll 1$ and hence the field changes quickly from $\phi = 0$ outside the bubble to $\phi = \phi_m$ inside the bubble. If the nucleation happens at much lower temperatures $T \ll T_c$ the situation is different. The height of the potential barrier $V(\phi_M, T)$ at the local maximum is small compared to depth of the potential $-V(\phi_m, T)$ at the global minimum ϕ_m. Hence, the contribution of the volume term around the maximum ϕ_M is negligible and S_3 is dominated by the surface term. Minimizing the surface term amounts to thick bubble walls with $\delta R/R \sim \mathcal{O}(1)$.

We see that the details of bubble nucleation strongly depend on the shape of the potential at the temperature at which the nucleation happens. For this is reason it is important to find out when the nucleation rate is high enough to actually allow the nucleation in an expanding universe. This temperature is called the nucleation temperature T_n and is defined as the temperature at time t_n at which the probability to nucleate a single bubble within one horizon volume is $\mathcal{O}(1)$ [11],

$$\int_0^{t_n} \mathrm{d}t \frac{\Gamma}{H^3} \sim 1. \tag{7.11}$$

To derive an equation to estimate T_n we will use the decay rate (7.8) with $\omega = 1$ and consider the dynamics of an expanding universe during radiation domination. Since the typical energy scale for the electroweak phase transition is $\mathcal{O}(100\ \mathrm{GeV})$, the universe is actually in the radiation dominated era. During that epoch the Friedmann equation governing the evolution of the universe is

$$H(t)^2 = \frac{8\pi}{3M_{\mathrm{Pl}}^2}\rho_r, \tag{7.12}$$

and the energy density of radiation is

$$\rho_r(T) = \frac{g_*\pi^2}{30}T^4. \tag{7.13}$$

We assume that the relativistic degrees of freedom g_* are temperature independent during the time of the transition [§]. Assuming an adiabatic expansion of the universe $T \sim a^{-1}$ we then know by eq. (7.12) that the Hubble parameter scales as a^{-2} and hence

$$H(t) = H(t_0)\left(\frac{a(t_0)}{a(t)}\right)^2. \tag{7.14}$$

[§] A general formula is $g_*(T) = \sum_i g_B(T) + \frac{7}{8}\sum_i g_F(T)$, where g_B counts bosonic and g_F counts fermionic degress of freedom. For the SM at the electroweak scale $g_{\mathrm{SM}} = 106.75$ [26]

It follows that

$$t_0 = \int_0^{t_0} \mathrm{d}t = \frac{1}{H(t_0)} \int_0^{a_0} \frac{\mathrm{d}a}{a} \left(\frac{a}{a_0}\right)^2 = \frac{1}{2H(t_0)}. \tag{7.15}$$

Together with (7.12) we get an relation between time and temperature

$$t = \frac{1}{4\pi}\sqrt{\frac{45}{\pi g}}\frac{M_{\mathrm{Pl}}}{T^2} = \xi \frac{M_{\mathrm{Pl}}}{T^2}. \tag{7.16}$$

This allows to transform the time integral in (7.11) to an integral over temperature [26]

$$\int_{T_n}^{\infty} \frac{\mathrm{d}T}{T} \left(\frac{2\xi M_{\mathrm{Pl}}}{T}\right)^4 e^{-S_3(T)/T} \sim 1. \tag{7.17}$$

We will use this equation to determine the nucleation temperature.

With regard to gravitational wave production we are also interested in the approximate duration of the phase transition. We denote T_* as the temperature of the radiation bath at the time t_* at which the gravitational waves are produced. For typical transition without signifcant reheating one can approximate it by the nucleation temperature $T_* \approx T_n$ [10], as we will do throughout this thesis. We expand the euclidean action around the transition time

$$\frac{S_3(t)}{T} \approx \frac{S_3(t_*)}{T_*} - \beta(t - t_*), \tag{7.18}$$

where we defined

$$\beta = - \left.\frac{\mathrm{d}(S_3/T)}{\mathrm{d}t}\right|_{t=t_*}. \tag{7.19}$$

Then we see that $\Gamma(t) \sim e^{\beta t}$ and β might be interpreted as an approximate inverse time scale of the duration of the phase transition [11]. During radiation domination the ratio of this time scale to the Hubble time is expressed as

$$\frac{\beta}{H_*} = T_* \left.\frac{\mathrm{d}(S_3/T)}{\mathrm{d}T}\right|_{T=T_*}, \tag{7.20}$$

where we assumed an adiabatic expansion of the universe by writing $\mathrm{d}T(t)/\mathrm{d}t = -TH(t)$. If (7.20) is large the transition proceeds very fast compared to the cosmological time scale. For the gravitational wave signal we would also like to know how much energy is released during the phase transition. The latent heat ϵ is the free energy difference between the true vacuum and the false vacuum. It consists of the differencethe effective potential and additionaly by an entropy variation [12]

$$\epsilon = \left.(\Delta V + T\Delta s)\right|_{T=T_*} = \left.\left(\Delta V - T\Delta\frac{\partial V}{\partial T}\right),\right|_{T=T_*}, \tag{7.21}$$

where we used the general notation $\Delta f = f(\phi_{\mathrm{false}}) - f(\phi_{\mathrm{true}})$. In the limit of large supercooling $T_n \ll T_c$ the entropy variation is negligible $\epsilon \approx \Delta V$ and $\Delta V \sim v/T$ [14]. For the gravitational wave signal it is crucial to determine the ratio of ϵ to the energy density of radiation at the time of the transition

$$\alpha = \frac{\epsilon}{\rho_r^*}. \tag{7.22}$$

To sum up we aim to compute the nucleation temperature T_n, the time scale of the transition β/H_* and α for phase transition of the SU(2)cSM model and subsequently we will estimate stochastic gravitational wave signals in chapter 8.

7.1 Overshooting-Undershooting Method

To obtain results regarding the bubble nucleation we need to solve the equation of motion (7.24) with boundary conditions (7.7). The boundary condition can be translated to the numerically more convenient form

$$\left.\frac{\mathrm{d}\phi}{\mathrm{d}r}\right|_{r=0} = 0, \quad \left.\phi\right|_{r=0} = \phi_e, \tag{7.23}$$

where ϕ_e is the so-called escape point which is determined by the overshooting-undershooting method. In general, ϕ_e is the field value inside the bubble and is not necessarily equal to the true vacuum since the field does not always directly tunnel to this point as it is a less likely event. The overshooting-undershooting is basically a trial and error process to solve the equations of motion with the right escape point ϕ_e such that the original boundary conditions (7.7) are satisfied. We follow the discussion of ref. [11]. As already mentioned, the effective potential is flipped if we consider the equation of motion in euclidean space instead of Minkowski space. The correct choice of ϕ_e corresponds to case (a) in Fig. 7.1 where the field overcomes the friction force and comes to rest at the false vacuum $\phi = 0$ and hence satisfies $\phi \to 0$ if $r \to \infty$. If a value to the right of ϕ_e is chosen (case (b)) it overshoots the false vacuum and continues to $\phi \to -\infty$. In case (c), a value to the left of ϕ_e is chosen and the field can not overcome the friction force and undergoes instead a damped oscillation around the minimum of $-V(\phi)$. By a trial and error approach one can find numerically the right initial condition and for the bounce solution $\phi(r)$. The bounce solution for case (a) in the bottom panel of Fig. 7.1 is also called bubble profile since it shows the spatial profile of the bubbles.

7.2 Multi-Field Case

All previous statements were made for the case of only one scalar field. However, the SU(2)cSM contains two background fields and the effective potential is therefore two-dimensional. The effective potential can be reduced to one dimension if the Gildener-Weinberg method is used and the previously stated methods can be applied. This is the objective of section 7.3.
In the case of N scalar fields $\phi_1, \ldots, \phi_N$ we have N equation of motions

$$\frac{\mathrm{d}^2\phi_i}{\mathrm{d}r^2} + \frac{2}{r^2}\frac{\mathrm{d}\phi_i}{\mathrm{d}r} - \frac{\mathrm{d}V_{\text{eff}}}{\mathrm{d}\phi_i} = 0, \quad \text{for } i = 1, \ldots, N, \tag{7.24}$$

with $2N$ boundary conditions given by (7.7) for each field ϕ_i. In the case of two fields, the effective potential can be imagined as a mountain range. Multiple paths might connect two valleys. It might be the shortest path connecting the two valleys or there might be a path going through another valley in the vicinity. In a sense the situation is similar for bubble nucleation for two fields. Which path of nucleation in field space is realized most likely, depends on the value of the action $S_3(T)/T$ along that path. To find (numerically) the bounce solution minimizing the Euclidean action and satisfying all boundary conditions is more complicated than in the one field case. A first numerical approach to this problem was given in [68] and later among others for instance in [69]. We will use the numerical implementation of ref. [70] (AnyBubble) in section 7.4 to find the bounce solution for the two-dimensional effective potential of the SU(2)cSM and discuss the bubble profiles in more detail.

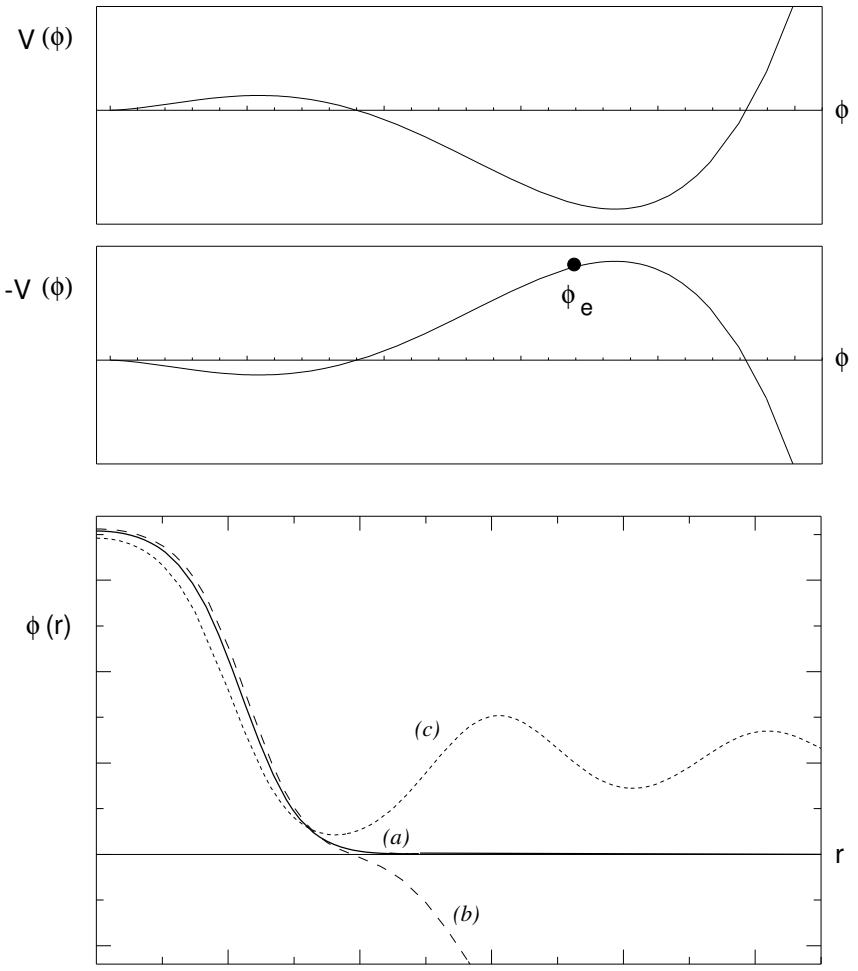

Figure 7.1: The top panel gives an example of an potential for temperatures below the critical temperature $T < T_c$ and the middle panel is the corresponding flipped potential. Bottom panel: three different solutions to the euclidean equation of motion. Case (a) corresponds to the correct bounce solution with $\phi\big|_{r=0} = \phi_e$ and case (b) and (c) illustrate overshooted and undershooted solutions, respectively. The figure is taken from ref. [11].

7.3 Results for the Gildener-Weinberg Case

In this section, we continue to examine the phase transition in Gildener-Weinberg case (section 6.3). To do that, we use the improved effective potential for temperatures $T < T_c \approx 360$ [GeV] and search for the two local minima: the false vacuum at $\rho = 0$ and the true vacuum at v_ρ. With the knowledge of these two points and the effective potential, we use the numerical implementation of [70] to solve for the O(3) bounce solutions. In Fig. 7.2 the bubble profiles for different temperatures are shown. At temperatures close to the critical temperatures (cf. Fig. 7.2b) the bubble walls are thin. This can be seen by the sharp transition from the true vacuum inside the bubble to the false vacuum outside the bubble. In contrast to that, for lower temperatures (cf. Fig. 7.2a) the bubble profiles indicate thicker bubble walls. These observations are in accordance with the scaling discussion we gave after eq. (7.10). To clarify this, we show the improved effective potentials in Fig. 7.3 for the cases considered in Fig. 7.2a. The plots reveal that the barrier of the potential is small compared to the depth of the potential at the global minimum, which leads to thick bubble walls.

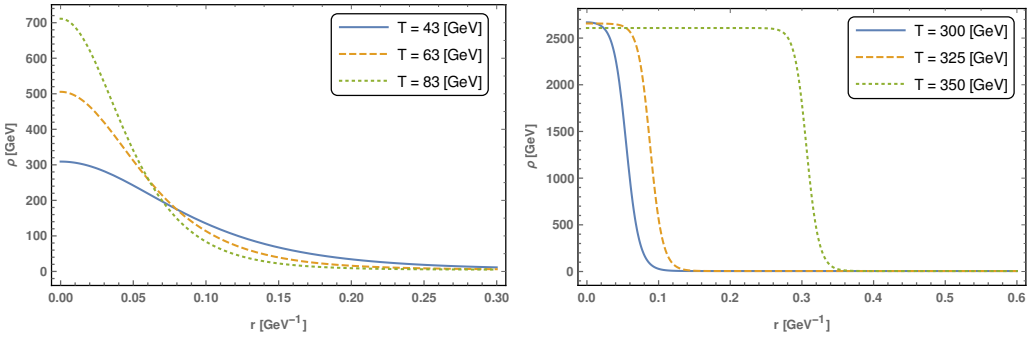

(a) (b)

Figure 7.2: Bubble profiles (solutions to eq. (7.24)) for different temperatures. Left panel: low temperatures with thick-walled bubble profiles. Right panel: Bubble profiles for thin-walled bubbles at higher temperatures closer to the critical temperature $T_c = 360$ GeV.

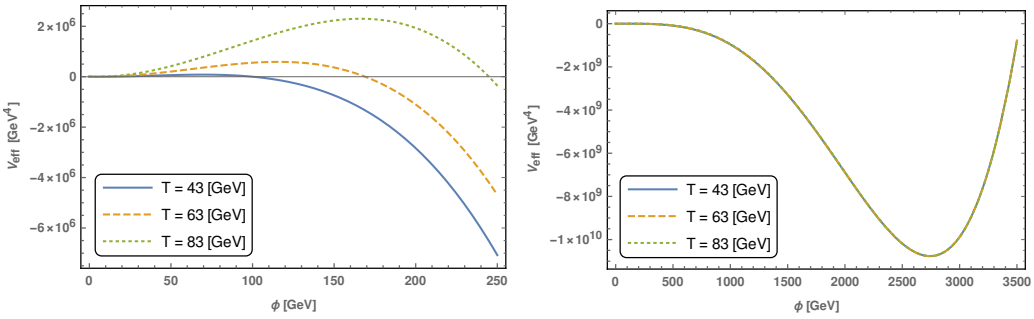

(a) (b)

Figure 7.3: Effective potentials for the temperatures in figure 7.2a. The left panel shows the potential around the false vacuum in higher resolution.

With the bubble profiles at hand, we can integrate eq. (7.5) numerically [70] to obtain the Euclidean action. This is done for temperatures $T < T_c$ in steps of $\Delta T = 1$ GeV down to

the temperature where the false vacuum at the origin becomes unstable. With these points we interpolate to obtain the scaling of $S_3(T)/T$ with temperature shown in Fig. 7.4. Using the condition (7.17) we obtain an estimate for the nucleation temperature

$$T_n \approx 40 \text{ GeV}. \tag{7.25}$$

Furthermore we compute the time scale of the transition by (7.20) and find

$$\frac{\beta}{H_*} \approx 390. \tag{7.26}$$

The result in (7.25) shows that the nucleation temperature is much lower than the critical temperature and assuming $T_c \approx T_n$ will yield wrong results. Hence the nucleation proceeds by formation of thick-wall bubbles (cf. Fig. 7.2a) and a large amount of supercooling can be expected. Furthermore, eq. (7.26) shows that the transition proceeds fast. The amount of supercooling is indeed large and leads to an extreme release of energy during the transition, quantified by the parameter

$$\alpha \approx 114, \tag{7.27}$$

telling us that the energy density released during the transition is roughly 100 times the radiation energy density at the time of the transition (cf. eq. (7.22)).

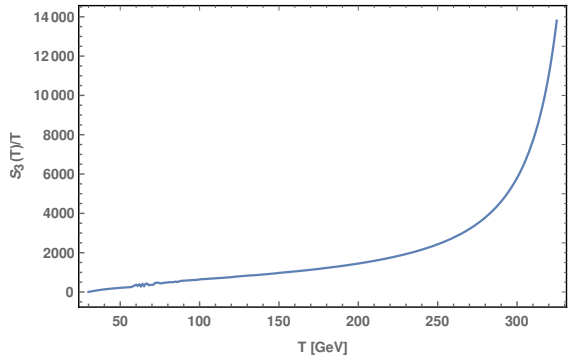

Figure 7.4: Euclidean action of the O(3) bounce solution for the Gildener-Weinberg case.

7.4 Results for Multi-Gap Case

In this section we study the nucleation of bubbles of the true vacuum in the full two-field setting. We have elaborated on the case of multiple scalar fields in section 7.2. The numerical implementaiton of ref. [70] allows us to also compute bubble profiles and the euclidean action in the multi-dimensional case. The conclusion from section 6.4.2 was that the phase transition of the SU(2)cSM at the chosen benchmark point is actually a multi-step transition. We denote points in field space by $\Phi = (h, \varphi)$ for the further discussion. To unfold the transition in the cosmological setting in chronological order, we have to start at high temperatures $T \to \infty$ where the system is in the symmetric phase denoted by $\Phi_f = (0, 0)$. With decreasing the temperature, the first transition is observed at $T_1 \approx 327$ GeV and the global minimum jumps mostly along the Φ direction to $\Phi_1 = (0, w_c)$. A second transition is then observed at $T_2 \approx 179$ GeV along the h direction to $\Phi_2 = (v_c, w_c)$. How the nucleation process is realized for this multi-step transition strongly depends on the nucleation temperature. We split this into two cases:

- If the nucleation temperature for the transition from Φ_f to Φ_1 is in the range $T_1 > T_n > T_2$, then the nucleation process is as follows. The fields will tunnel from Φ_0 to Φ_1 before the temperature drops below T_2 since the tunneling is efficient enough to nucleate in the expanding universe before the global minimum is formed at Φ_2 by the adiabatic cooling of the universe. If we then assume that T_n is not too close to T_2, we expect that the new phase Φ_1 fills completely the universe by nucleating bubbles before temperature T_1 is reached. After that one has to compute the tunneling rate from Φ_1 to Φ_2 and find a second nucleation temperature $T_n' < T_2$. To sum up, the bubble nucleation proceeds in two steps, first nucleating the phase Φ_1 and then nucleating the phase Φ_2.
- In the case of a nucleation temperature $T_n < T_2$ for the transition Φ_f to Φ_1, we know that a new global minimum is formed at Φ_2 before the tunneling from Φ_f to Φ_1 has started. Since the bounce solution has the boundary condition $\Phi \to \Phi_{\text{true}}$ as $r \to \infty$ we have to instead calculate the nucleation temperature for the transition from Φ_f to the true vacuum Φ_2. Which path connecting the Φ_f and Φ_2 is minimizing the euclidean action and hence giving the correct bubble profile depends on the effective potential at the nucleation temperature. This scenario has been studied for non-conformal models for instance in [68, 71]

To study the bubble nucleation with the two-dimensional effective potential obtained in section 6.4, we first have to determine which of the two aforementioned cases applies. First, we analyzed with the code of ref. [70] the nucleation rate for the transition Φ_f to Φ_1 and found that no bubbles can form for temperature above 179 GeV, i.e. eq. (7.17) is not satisfied. So, we conclude that case two applies and find the following quantities characterizing the bubble nucleation for the transition $\Phi_f \to \Phi_1$,

$$T_n \approx 58 \text{ GeV}, \tag{7.28}$$

$$\frac{\beta}{H_*} \approx 1400, \tag{7.29}$$

$$\alpha \approx 21. \tag{7.30}$$

Compared to the Gildener-Weinberg case, the difference between nucleation and critical temperate is smaller. Similarly, the latent heat α is smaller for this case, but still large enough to correspond to a large amount of supercooling. The time scale of the phase transition duration is roughly four times smaller than in the Gildener-Weinberg case. We conclude that the Gildener-Weinberg approach gives wrong estimates on the details of bubble nucleation for our model.

Furthermore, the bubble profile at the nucleation temperature in Fig. 7.5a displays the details of the bubble nucleation in the two field case. The additional scalar φ tunnels roughly along the $h = 0$ contour from the false vacuum to the escape point at roughly $\Phi_e = (h_e, \varphi_e) \approx (0, 350)$ GeV. The scalar fields then roll down towards the global minimum which is located roughly at the VEV $\Phi_0 \approx (v, w)$ for $T = 0$ (cf. Fig. 7.5b). In regard to production of gravitational waves a detailed study of the dynamics of the bubble expansion after the onset of nucleation is appropriate but beyond the scope of this thesis. The fields at the bubble wall might expierence a frictional force due to the interaction with the thermal plasma in the vicinity which slows down the veloctiy of bubble expansion. We refer the reader to ref. [72].

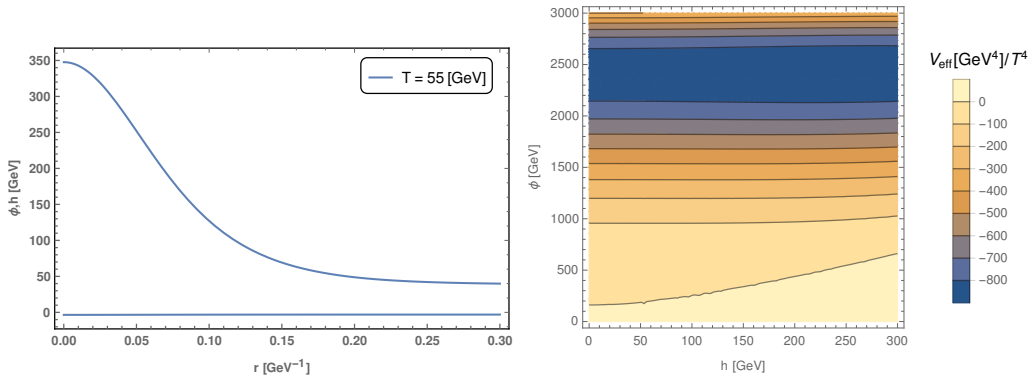

(a) (b)

Figure 7.5: The bubble profile (a) close to the nucleation temperature T_n for the two field case consists of two solutions: The h field with constant soloution $h(r) = 0$ and the φ field with a usual bubble profile. The contour plot (b) shows the effective potential at that temperature. Note that the bump along the φ direction is not visible due to the large depth of the potential at the true vacuum Φ_0.

Chapter 8

Prediction of Stochastic Gravitational Wave Background

The gravitational wave signals which are produced by cosmological phase transitions in the early universe are called stochastic gravitational wave background (SGWB) and are sourced by the collision of bubble walls. These backgrounds are stochastic because the gravitational waves are produced from numerous uncorrelated sources. If the gravitational waves are produced during a radiation dominated universe, where the horizon volume was much smaller than today, then the signal which we observe today is a superposition from uncoherent sources from different independent Hubble patches [12]. This would be exactly the case if gravitational waves are produced from bubble collisions during a first-order phase transition at the electroweak scale.

As final part of this thesis, we would like to estimate the SGWB produced by the first-order phase transitions we predicted for the SU(2)cSM. From these results we hope that the signal is strong enough to be measured by the LISA mission and thus offering an opportunity to rule out or approve (conformal) Higgs portal models. Before that, we would like to stress again that we only consider the benchmarkpoint (6.9). The details of the bubble nucleation encoded in the quantites T_n, β/H_* and α are model dependent. As a consequence, the SGWB is expected to be altered for different choices of paramters. An extensive analysis of the paramater space of the SU(2)cSM model and the resulting SGWB is desirable but is beyond the scope this thesis. Such systematic analyses can be found in the literature for various extensions of the SM for instance in ref. [15].

The predictions we give in this chapter should be read with caution, since we do not study all possible sources of gravitational waves and use common fitting formulas for the power spectra of SGWB used in the literature (e.g. ref. [10]) which might not apply to the very strong transitions we found in the previous chapter. In the context of strong first-order phase transitions at the electroweak scale, three processes involving the production of gravitational waves are expected [10]:

- The collision of bubble walls. In this case it is expected that the vacuum energy is mostly transformed to kinetic energy of the bubble expansion. Plasma effects are neglected. The expansion of a single bubble can not produce gravititaional waves due the spherical symmetry (Birkhoff's theorem). Therefore, the collision of bubbles is necessary to break the spherical symmetry.

- Sound waves in the plasma which are produced after the collision of bubble walls.
- Magnetohydrodynamic turbulences in the plasma after bubble collisions.

In general the three processes coexist and the total SGWB is approximately a linear combination of them. Which of the three sources give a significant contribution to the SGWB depends on the details of bubble nucleation. For a detailed treatment for all three sources we refer to [10] and references therein. In the following, we outline why we expect that only the first source is significant for the first-order phase transitions found in sections 6.3 and 6.4.

In the case of large supercooling (i.e. $\alpha \gg 1$) plasma effects are negligible and bubble wall will accelerate indefinetely since no friction forces are present in this approximation. The bubble wall velocity then quickly approaches the speed of light [10]. This case is also called a vacuum-dominated epoch since the energy density at that time is dominated by the vacuum energy at the global minimum. Furthermore, we assume that that the vacuum energy is transformed mostly to the kinetic energy of the scalar field (i.e. the velocity of the bubble wall). In other words, the plasma effect on the expansion of the bubbles are neglected in our results. This should be seen as an approximation since the vacuum energy can be transformed partly to the plasma, effectively slowing down the expansion of the bubbles. The two values we obtained for α in the Gildener-Weinberg (GW) case (section 7.3) and in the multi-gap (MG) case (section 7.4) display the large supercooling limit.

The method used to compute the power spectra of SGWB produced by bubble collision is called the envelope approximation. This approximation is based on the assumption that a fraction of the latent heat κ is deposited in a thin shell at the bubble wall and that most of the gravitational waves are produced by the collision of only two of these shells. The energy is expected to disperse quickly after the collision and further effects of collided shells on the uncollided ones are neglected [10]. With numerical simulations using the envelope approximation it is suggested that the power spectrum of the SGWB is given by [10]

$$h^2\Omega(f) = \frac{8}{10^5}\left(\frac{H_*}{\beta}\right)^2\left(\frac{\kappa\alpha}{1+\alpha}\right)^2\left(\frac{100}{g_*}\right)^{1/3}\left(\frac{0.11v_w^3}{0.42+v_w^2}\right)S_{\text{env}}(f), \tag{8.1}$$

where the spectral shape is defined by

$$S_{\text{env}}(f) = \frac{3.8(f/f_p)^{2.8}}{1+2.8(f/f_p)^{3.8}}, \tag{8.2}$$

and the peak frequency today is

$$f_p = 15.5\cdot 10^{-3}\text{mHz}\left(\frac{0.62}{1.8-0.1v_w+v_w^2}\right)\left(\frac{\beta}{H_*}\right)\left(\frac{T_*}{100\text{GeV}}\right)\left(\frac{g_*}{100}\right)^{1/6}. \tag{8.3}$$

The parameter $\kappa = \rho_\phi/\rho_{\text{vac}}$ is defined as the ratio of kinetic energy of the scalar field to the vacuum energy and v_w is the terminal bubble wall velocity. Interestingly, in the case of large supercooling $\alpha \gg 1$ the dependene of the spectrum on α drops out (cf. (8.1)). Moreover, a phase transition with short duration $\beta/H_* \gg 1$ decreases the intensity of the signal but increases the peak frequency f_p.

We will use eqs. (8.1), (8.2) and (8.3) for a phase transition in a vacuum-dominated epoch. As discussed, we set $\kappa = 1$ and $v_w = 1$ for this case. The power spectra are shown in Fig. 8.1 and other parameters used are summarized in table 8.1.

Table 8.1: Details of the gravitational wave spectra

	T_* [GeV]	β/H_*	α	f_p [mHz]	$h^2\Omega(f_p)$
GW	40	390	113	0.605	$8.148 \cdot 10^{-12}$
MG	58	1400	21	3.089	$5.867 \cdot 10^{-13}$

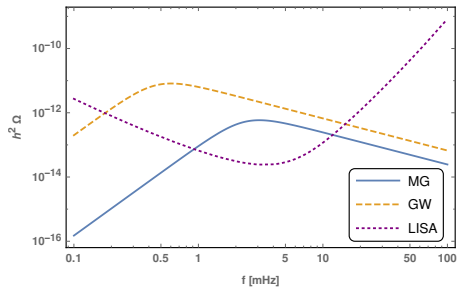

Figure 8.1: SGWB for the first-order phase transition of the Gildener-Weinberg (GW) case and the multi-gap (MG) case. Details can be found in table 8.1. The purple dotted line is the sensitivity curve of the LISA mission (obtained from Fig. 1 in ref. [10] for the configuration C1).

As a concluding remark, we would like to confront the obtained GW spectra with the LISA sensitivity. The sensitivity of LISA can be seen in Fig. 8.1 and were obtained from ref. [10]. The comparison with our results show that LISA could eventually measure the SGWB predicted for the SU(2)cSM. However, lower values of β/H_* are desirable to push the signal more within the detection range. The authors of ref. [16] projected the sensitivity of the LISA mission for the case of runaway bubbles in a vacuum dominated epoch (see Fig 8.2). In this case the GW signal only depends on two paramters of the phase transition: β/H_* and T_*. Again we see that our results (cf. table 8.1) the signals can potentially be detected by LISA. We would like to stress once more that we only considered one benchmark points of the SU(2)cSM model and other choices of parameters might lead to stronger SGWB. With our results we have shown that the first-order phase transition of the SU(2)cSM model is generally capable to lead to SGWB which could be detected by the LISA mission. Our results can be interpreted as a proof of concept for SGWB production of the SU(2)cSM.

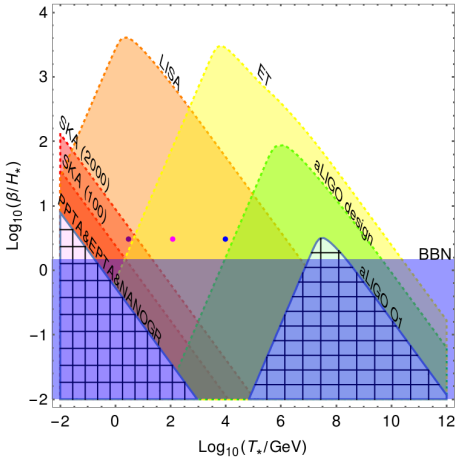

Figure 8.2: Projected sensitivity for the future gravitational wave experiment network with runaway bubbles in a vacuum-dominated epoch (i.e. $\alpha \gg 1, \kappa = 1, v_w = 1$). The colored regions indicate for which values of β/H_* and T_* the SGWB from collosion of runaway bubbles in a vacuum-dominated epoch can be detected with a signal-to-noise ratio > 10 by different experiments. The blue region is ruled out by BBN bounds. The results from table 8.1 are within the detection range of LISA. The figure is taken from ref. [16]

Conclusions

Physics beyond the SM is not yet observed directly but is necessary to give answers to unsolved problems in high-energy physics. The number of various extensions of the SM which are studied to address these problems is vast. The minimal supersymmetric SM has been popular field of study to address these problems, but the lack of experimental evidence for the minimal supersymmetric SM motivates the consideration of other options. With that motivation in mind, we study conformal models, where all masses are generated by radiative symmetry breaking (RSB). In particular, we have studied the SU(2)cSM which consists of the conformal SM extended by a scalar doublet and a hidden SU(2) gauge group. The main objective was to analyze potential first-order phase transitions at the electroweak scale and the resulting bubble nucleation and production of a stochastic gravitational wave background.

To do that, we have introduced a novel resummation technique utilizing the gap equation which is encoded in the 2PI formalism to obtain an improved effective potential which is reliable at high temperatures. In fact, the gap equation we derived does not rely on a high temperature expansion, but rather accounts for resummation at any temperature. In chapter 4 we have shown that the resummation is especially important at high temperatures to guarantee the validity of perturbation theory for a scalar toy model. In addition, the comparison with daisy resummation method shows that daisy resummation takes thermal corrections not accurately into account when the high temperature limit is not applicable. We extended this discussion in section 6.3.1 for the SU(2)cSM, which showed that the numerical difference between our approach to the common daisy resummation is significant. Moreover, we believe that the gap equation approach gives a theoretically more appealing framework to perform the resummations and directly obtain the improved effective potential. In addition, the class of diagrams which were resummed in our results is a broader class than the daisy diagrams. Application of this approach to obtain thermal corrected masses for gauge bosons and fermions is beyond the scope of this thesis and is left for future research. Furthermore, the relation between the gap equation improvement and the RG improvement should be studied in more detail in the future. In adittion, the finite momentum corrections in the gap equation that have been neglected in our results could be investigated. So far the finite momentum corrections to the self-energies of particles at finite temperature have not been studied yet in the context of electroweak phase transitions.

With the improved effective potential we have studied potential phase transitions in the early universe within the context of SU(2)cSM. We have performed the analysis for one benchmarkpoint from ref. [5] using three different approaches. Firstly we have used the approach of sequential symmetry breaking. Not surprisingly, it was found that the model does not entail a strong first-order phase transition. This could have been expected since

in sequential symmetry breaking the additional scalar acquires its VEV first, consituting an effective mass term for the Higgs doublet. Therefore, the symmetry breaking proceeds in the SM sector in the usual way and it has been shown that the SM does not entail a strong first-order electroweak phase transition but instead a crossover. Secondly, we used the Gildener-Weinberg method which is based on the assumption that the two-dimensional classical potential exhibits a flat direction at a certain renormalization scale. With that method and the help of the results from ref. [5] we could effectively reduce the two-dimensional potential to a one-dimensional potential which simplifies the introduced method of improving the effective potential by the 2PI gap equation. In this case, we confirmed that the SU(2)cSM entails a strong first-order phase transition. However, the Gildener-Weinberg method should be seen as an approximation scheme to the phase transition for models with multiple scalar fields and should be compared with results from the study of the full effective potential. These results were obtained in section 6.4. Here, we generalized the gap equation approach to multiple scalar fields and obtained the full effective potential with dependence on both background fields. The analysis of the global minimum with varying temperature points to the conclusion that the SU(2)cSM at the considered benchmark point entails a two-step transition. The phase transition which is approximately along the background field of the additional scalar fulfills the requirement for a strong phase transition. Hence, it is a strong first-order phase transition in the hidden sector. Comparing this result with the results from the Gildener-Weinberg method shows that the Gildener-Weinberg method, which is often used in the context of electroweak phase transition, in this particular case is a crude approximation and gives a false picture of the phase transition. However, if only a rough estimate for v_c/T_c is desired, it is a useful tool for models with extended scalar sector.

The indication of a strong first-order phase transition for the results from the Gildener-Weinberg method and the multi-gap equation approach motivated us to analyze the properties of bubble nucleation in the early universe. In both cases, it was found that the nucleation and the critical temperature are separated by more than 200 GeV. This leads to large supercooling of the true vacuum and as a consequence a lot of energy is released into the radiation bath during the phase transition. We expect that this energy is mostly converted into the kinetic energy of the bubble walls which are expanding with a velocity close to the speed of light. This feature is referred to as runaway-bubbles in a vacuum-dominated epoch. Based on this assumption we estimated the stochastic gravitational wave background from the bubble collisions with the additional assumptions that subsequent plasma effects, which could also produce gravitational waves are negligible. The results for both cases show that for the considered benchmark point of the SU(2)cSM bubble collisions induced by the first-order phase transition lead to the production of a stochastic gravitational wave background. A detailed analysis whether the assumption of runaway bubbles in a vacuum-dominated epoch is valid and whether plasma effects are negligible were not presented in this thesis. In addition, it was not studied whether the large energy release during the phase transition leads to considerable reheating of the thermal plasma and the consequences it has on the dynamics of bubble nucleation. These issues should be scrutinized in more detail but were not the main focus of this thesis.

Finally, we stress again that all presented results are only for one benchmark point of the SU(2)cSM. These preliminary results indicate that the phase transition could leave an observable imprint on the stochastic gravitational wave background. Therefore, in the future it would be interesting to scan the parameter space of the SU(2)cSM for regions where it can reproduce the physical Higgs mass, the Higgs VEV (e.g. ref. [5]) and give rise

to a strong first-order phase transition. With that analysis and eventual observation form stochastic gravitational wave backgrounds once could discriminated the parameter space of the SU(2)cSM. Moreover, it would be interesting to study other, more general, conformal extension of the SM, for instance with hidden gauge group $SU(N)_X$ and additional fermions in the hidden sector. In addition, a proper treatment of gauge fields would be appropriate for our results. One should include the pseudo-Goldstone bosons of our model and scrutinize the gauge dependence of the effective potential in future research.

The LISA mission is expected to launch in 2034 and the collected data might be of substantial importance for particle physics. It will offer new insights to physics beyond the SM and might enable targeted search for particles from the hidden sector at the LHC. Next to the implications for physics beyond the SM, the dawn of gravitational wave astronomy will also open a new window of cosmological observation. The cosmic microwave background is the earliest observation which can be made by detection of electromagnetic waves. With gravitational waves it is possible to observe the local universe in the epoch before recombination during which processes like inflation and reheating took place, which are not well understood yet.

Appendix A

High Temperature Expansion for J_B

In this appendix we derive the high temperature expansion which is valid for $m^2/T^2 \ll 1$ for the thermal function for bosons. We define the variable $y^2 = m^2/T^2$ and note the thermal function as

$$J_B(y^2) = \int_0^\infty dx x^2 \log\Big(1 - e^{\sqrt{x^2+y^2}}\Big). \tag{A.1}$$

We will follow the derivation of ref. [39]. At the boundary we find

$$J_B(0) = \int_0^\infty dx x^2 \log\big(1 - e^{-x}\big) = -\sum_{n=1}^{\infty} \int_0^\infty dx x^2 e^{-xn} = -2\zeta(4) = -\frac{\pi^4}{45}, \tag{A.2}$$

$$\frac{\partial}{\partial y^2} J_B\Big|_{y^2=0} = \int_0^\infty dx \frac{x/2}{e^x - 1} = \frac{1}{2}\zeta(2)\Gamma(2) = \frac{\pi^2}{12}. \tag{A.3}$$

For the next order in this expansion we need dimensional regularization where we set the dimension to $d = 3 - \epsilon$, then we obtain

$$\frac{\partial^2}{\partial (y^2)^2} J_B(y^2) = \frac{1}{4} \int_0^\infty dx \frac{x^{-\epsilon}}{\sqrt{x^2+y^2}} \frac{1}{e^{\sqrt{x^2+y^2}} - 1}. \tag{A.4}$$

Using the series $\coth(x) = \sum_{n=-\infty}^{\infty} \frac{x}{x^2+\pi^2 n^2}$ we obtain

$$\frac{\partial^2}{\partial (y^2)^2} J_B(y^2) = I_1(y^2) + I_2(y^2), \tag{A.5}$$

$$I_1(y^2) = \frac{1}{4} \int_0^\infty dx x^{-\epsilon} \sum_{n=-\infty}^{\infty} \frac{1}{(x^2+y^2) + \pi^2 n^2}, \tag{A.6}$$

$$I_2(y^2) = -\frac{1}{8} \int_0^\infty dx \frac{x^{-\epsilon}}{\sqrt{x^2+y^2}}. \tag{A.7}$$

For I_2 we obtain after expanding at $\epsilon = 0$

$$I_2(y^2) = -\frac{1}{8\epsilon} + \frac{1}{8}\log(y/2) + \mathcal{O}(\epsilon). \tag{A.8}$$

Integrating I_1 yields

$$\begin{aligned} I_1(y^2) &= \frac{\pi}{8}\sum_{n=-\infty}^{\infty}\left(y^2+4n^2\pi^2)\right)^{-(1+\epsilon)/2} \\ &= \frac{\pi}{8}\left(\frac{1}{y^{1+\epsilon}}+2\sum_{n=1}^{\infty}\left(y^2+4n^2\pi^2)\right)^{-(1+\epsilon)/2}\right) \\ &= \frac{\pi}{8y}+\frac{\pi^{-\epsilon}}{8}2^{-\epsilon}\zeta(1+\epsilon)+\underbrace{\frac{\pi}{4}\sum_{n=1}^{\infty}\left(\frac{1}{(2\pi n)^{1+\epsilon}}(y^2+4n^2\pi^2)\right)^{-(1+\epsilon)/2}-1)}_{=K(y^2)}\,. \end{aligned} \tag{A.9}$$

Using $(2\pi)^{-\epsilon}\zeta(1+\epsilon) = 1/8(1/\epsilon - \log(2\pi)+\gamma_E)+\mathcal{O}(\epsilon)$, we get

$$I_1+I_2 = \frac{1}{8}\log\Big(\frac{y}{2}\Big)+\frac{\pi}{4y}+\frac{3\gamma_e}{8}+K(y). \tag{A.10}$$

Integrating this twice with respect to y^2, keeping the boundary term in mind, the thermal function reads now

$$\begin{aligned} J_B(y^2) =& -\frac{\pi}{6}\left(\frac{m^2}{T^2}\right)^{3/2}-\frac{1}{32}\frac{m^4}{T^4}\log\frac{m^2}{a_bT^2}+J_B(0)+\frac{\partial}{\partial y^2}J_B\Big|_{y^2=0}y^2 \\ &+\int d(y^2)\int d(y^2)K(y) \\ =& -\frac{\pi^4}{45}+\frac{\pi^2}{12}\frac{m^2}{T^2}-\frac{\pi}{6}\left(\frac{m^2}{T^2}\right)^{3/2}-\frac{1}{32}\frac{m^4}{T^4}\log\frac{m^2}{a_bT^2} \\ &+\int d(y^2)\int d(y^2)K(y). \end{aligned} \tag{A.11}$$

Now we expand for $K(y)$

$$\begin{aligned} K(y) &= -\frac{\pi}{4}\sum_{n=1}^{\infty}\frac{1}{2\pi n}\sum_{m=1}^{\infty}\frac{(-1)^m}{m!}\left(\frac{1}{2}\right)_m x^m, \quad \text{for } x=\frac{y^2}{4\pi^2n^2}, \\ &= -\frac{1}{8\Gamma(\frac{1}{2}))}\sum_{m=1}^{\infty}\frac{(-1)^m}{m!}\Gamma\left(m+\frac{1}{2}\right)\left(\frac{y^2}{4\pi^2}\right)^m\zeta(2m+1). \end{aligned} \tag{A.12}$$

Integrating eq. (A.12) twice results in

$$\int d(y^2)\int d(y^2)K(y) = -2\pi^{7/8}\sum_{m=1}^{\infty}\frac{(-1)^m}{(m+2)!}\Gamma(m+\frac{1}{2})\left(\frac{y^2}{4\pi^2}\right)^{m+2}\zeta(2m+1). \tag{A.13}$$

Summing up all terms, we finally get the desired high temperature expansion

$$\begin{aligned} J_B(m^2/T^2) =& -\frac{\pi^4}{45}+\frac{\pi^2}{12}\frac{m^2}{T^2}-\frac{\pi}{6}\left(\frac{m^2}{T^2}\right)^{3/2}-\frac{1}{32}\frac{m^4}{T^4}\log\frac{m^2}{a_bT^2} \\ &+-2\pi^{7/8}\sum_{m=1}^{\infty}\frac{(-1)^m}{(m+2)!}\Gamma(m+\frac{1}{2})\left(\frac{y^2}{4\pi^2}\right)^{m+2}\zeta(2m+1). \end{aligned} \tag{A.14}$$

We can express the last term alternatively as

$$\begin{aligned}
&2\pi^{7/8}\sum_{m=1}^{\infty}\frac{(-1)^m}{(m+2)!}\Gamma(m+\frac{1}{2})\left(\frac{y^2}{4\pi^2}\right)^{m+2}\zeta(2m+1)\\
=&2\pi^{7/8}\sum_{m=1}^{\infty}\frac{(-1)^m}{(m+2)!}\Gamma(m+\frac{1}{2})\left(\frac{y^2}{4\pi^2}\right)^{m+2}\sum_{n=1}^{\infty}\frac{1}{n^{2m+1}}\\
=&\frac{\pi^4}{6}\sum_{n=1}^{\infty}\left(\frac{m^2}{4\pi^2nT^2}\right)^3{}_2F_1\left(1,\frac{3}{2};4,-\frac{m^2}{4\pi^2n^2T^2}\right). \qquad \text{(A.15)}
\end{aligned}$$

Hence, we can also write

$$\begin{aligned}
J_B(m^2/t^2) =&-\frac{\pi^4}{45}+\frac{\pi^2}{12}\frac{m^2}{T^2}-\frac{\pi}{6}\left(\frac{m^2}{T^2}\right)^{3/2}-\frac{1}{32}\frac{m^4}{T^4}\log\frac{m^2}{a_bT^2}\\
&+\frac{\pi^4}{6}\sum_{n=1}^{\infty}\left(\frac{m^2}{4\pi^2nT^2}\right)^3{}_2F_1\left(1,\frac{3}{2};4,-\frac{m^2}{4\pi^2n^2T^2}\right), \qquad \text{(A.16)}\\
a_b =&16\pi^2\exp\left(\frac{3}{2}-2\gamma_E\right). \qquad \text{(A.17)}
\end{aligned}$$

Appendix B

Sunset Diagram in the Gap Equation

This appendix concerns the computation of the so-called sunset diagram in the gap equation. To do that, we need to solve the Euclidean integral

$$S = \int \frac{\mathrm{d}^4p}{(2\pi)^4} \frac{1}{(k-p)^2 - m^2 + i\epsilon} \frac{1}{p^2 - m^2 + i\epsilon}. \tag{B.1}$$

With the definition $A = (k-p)^2 - m^2 + i\epsilon$ and $B = p^2 - m^2 + i\epsilon$ we can use the Feynman trick and write the integral as

$$\begin{aligned} S &= \int \frac{\mathrm{d}^4p}{(2\pi)^4} \int_0^1 \mathrm{d}x \, \frac{1}{(xA + (1-x)B)^2} \\ &= \int \frac{\mathrm{d}^4p}{(2\pi)^4} \int_0^1 \mathrm{d}x \, \frac{1}{(p^2 + x(k^2 - 2p\cdot k) - m^2 + i\epsilon)^2} \\ &= \int \frac{\mathrm{d}^4p}{(2\pi)^4} \int_0^1 \mathrm{d}x \, \frac{1}{((p-xk)^2 - x^2k^2 + xk^2 - m^2 + i\epsilon)^2} \\ &= \int \frac{\mathrm{d}^4p}{(2\pi)^4} \int_0^1 \mathrm{d}x \, \frac{1}{(p^2 + k^2x(1-x) - m^2 + i\epsilon)^2}. \end{aligned} \tag{B.2}$$

With the definition $a(k,x)^2 = m^2 - k^2x(1-x) + i\epsilon$ and under the assumption that the x and p integrals can be interchanged we get for a thermal field theory,

$$S = \int_0^1 \mathrm{d}x \, \frac{1}{\beta} \sum_{n=\infty}^{\infty} \int \frac{\mathrm{d}^3p}{(2\pi)^3} \frac{1}{(\omega_n^2 + \mathbf{p}^2 + a^2)^2} = 2\int_0^1 I_2(a(k,x)^2). \tag{B.3}$$

According to eq. (3.28) we obtain

$$S = \int_0^1 \mathrm{d}x \, \frac{1}{16\pi^2}\left(\frac{2}{\epsilon} - \gamma_E\right) - \frac{1}{16\pi^2}\log\left(\frac{a(k,x)^2}{4\pi\mu^2}\right) - \frac{1}{\pi^2}\left(\frac{\partial^2 J_B(y^2)}{\partial (y^2)^2}\right)\Big|_{y=a(k,x)/T}. \tag{B.4}$$

The two finite terms in eq. (B.4) we define as

$$S_1 = -\frac{1}{32\pi^2}\int_0^1 \mathrm{d}x \log\left(\frac{a(k,x)^2}{4\pi\mu^2}\right), \tag{B.5}$$

$$S_2 = -\frac{1}{2\pi^2}\int_0^1 \mathrm{d}x \left(\frac{\partial^2 J_B(y^2)}{\partial (y^2)^2}\right)\Big|_{y=a(x)/T}. \tag{B.6}$$

S_1 integral

In order to compute the integral S_1 we reintroduced the $i\epsilon$-prescription, to use the correct definition of the logarithm. We define the logarithm of a complex number z as the principal value logarithm

$$\log(z) = \ln(r) + i\varphi, \quad \text{where} \quad r = |r| \quad \text{and} \quad \varphi \in (-\pi, \pi]. \tag{B.7}$$

By this definition the branch cut of the complex logarithm is located on the negative real axis $(-\infty, 0]$. According to our $i\epsilon$-prescription, if the argument in the logarithm is negative, we take the limit from above. For the principal value logarithm this means that we can write

$$\begin{aligned} S_1 &= -\frac{1}{32\pi^2}\int_0^1 \mathrm{d}x \log\left(\frac{m^2 - k^2x(1-x) + i\epsilon}{4\pi\mu^2}\right) \\ &= -\frac{1}{32\pi^2}\int_0^1 \mathrm{d}x \left[\ln\left(\left|\frac{m^2 - k^2x(1-x)}{4\pi\mu^2}\right|\right) + i\pi\theta(k^2x(1-x) - m^2)\right]. \end{aligned} \tag{B.8}$$

For further evaluation of the integral we assume that M^2, k^2 and x are real. Then we can express the absolute value in eq. (B.8) by

$$\begin{aligned} S_1 = -\frac{1}{32\pi^2}\int_0^1 \mathrm{d}x \Bigg[&\theta(m^2 - k^2x(1-x)) \ln\left(\frac{m^2 - k^2x(1-x)}{4\pi\mu^2}\right) \\ &+ \theta(k^2x(1-x) - m^2)\left(\ln\left(\frac{k^2x(1-x) - m^2}{4\pi\mu^2}\right) + i\pi\right)\Bigg]. \end{aligned} \tag{B.9}$$

For the further computation we have to analyze the zeros of the function $f(x) = m^2 - k^2x(1-x)$ in the interval $[0,1]$. The zeros read

$$x_\pm = \frac{1}{2} \pm \sqrt{\frac{1}{4} - \frac{m^2}{k^2}}. \tag{B.10}$$

We split the location of the zeros in three cases:

$$\begin{cases} \text{(a)}\, \frac{m^2}{k^2} \geq \frac{1}{4} & \text{then} \quad \mathrm{Re}(x_\pm) = \frac{1}{2} \quad \text{and} \quad \theta(f(x)) = 1 \quad \forall x \in [0,1] \\ \text{(b)}\, 0 < \frac{m^2}{k^2} < \frac{1}{4} & \text{then} \quad 1 > x_+ > \frac{1}{2} > x_- > 0 \\ & \text{and} \quad \theta(f(x)) = 1 \quad \forall x \in [0, x_-] \cup [x_+, 1], \quad \theta(-f(x)) = 1 \quad \forall x \in [x_-, x_+] \\ \text{(c)}\, \frac{m^2}{k^2} = 0 & \text{then} \quad x_- = 0, x_+ = 1 \quad \text{and} \quad \theta(-f(x)) = 1 \quad \forall x \in [0,1] \end{cases} \tag{B.11}$$

Case (a)
In this case the only non-zero term in eq. (3.27) is the first one. After evaluating the step function we get

$$\begin{aligned} S_1 &= -\frac{1}{32\pi^2}\int_0^1 \mathrm{d}x \ln\left(\frac{m^2 - k^2x(1-x)}{4\pi\mu^2}\right) \\ &= -\frac{1}{32\pi^2}\int_0^1 \mathrm{d}x \left(\ln\left(\frac{m^2}{4\pi\mu^2}\right) + \ln\left(1 - \frac{k^2}{m^2}x(1-x)\right)\right). \end{aligned} \tag{B.12}$$

The first term can be easily integrated and in the second term we expand the logarithm,

$$S_1 = -\frac{1}{32\pi^2}\left(\ln\left(\frac{m^2}{4\pi\mu^2}\right) - \int_0^1 \mathrm{d}x \sum_{n=1}^{\infty} \frac{1}{n}\left(\frac{k^2}{m^2}x(1-x)\right)^n\right). \tag{B.13}$$

In the next step, we assume that the sum and the integral can be interchanged. Moreover, we use the integral

$$\int_0^1 \mathrm{d}x\, \frac{1}{n}\left(\frac{k^2}{m^2}x(1-x)\right)^n = \frac{\Gamma(n+1)^2}{n\Gamma(2n+2)}\left(\frac{k^2}{m^2}\right)^n, \tag{B.14}$$

which can be rewritten to

$$\frac{\Gamma(n)\Gamma(n+1)}{\Gamma(2n+2)}\left(\frac{k^2}{m^2}\right)^n. \tag{B.15}$$

The Legendre duplication formula tells us that $\Gamma(z)/\Gamma(2z) = \sqrt{\pi}2^{1-2z}\Gamma(z+1/2)^{-1}$. In eq. (B.15) we have $z = n+1$ and hence we obtain

$$\frac{\Gamma(n)\Gamma(n+1)}{\Gamma(2n+2)}\left(\frac{k^2}{m^2}\right)^n = \frac{\sqrt{\pi}}{2}\frac{\Gamma(n)}{\Gamma(n+\frac{3}{2})}\left(\frac{k}{2m}\right)^{2n}. \tag{B.16}$$

Summing now over n,

$$\sum_{n=1}^{\infty} \frac{\sqrt{\pi}}{2}\frac{\Gamma(n)}{\Gamma(n+\frac{3}{2})}\left(\frac{k}{2m}\right)^{2n} = 2\left(1 - \sqrt{\frac{4m^2}{k^2}-1}\arcsin\left(\frac{k}{2m}\right)\right). \tag{B.17}$$

Finally, we obtain for the integral in eq. (B.13)

$$S_1 = -\frac{1}{32\pi^2}\left(\ln\left(\frac{m^2}{4\pi\mu^2}\right) - 2\left(1 - \sqrt{\frac{4m^2}{k^2}-1}\arcsin\left(\frac{k}{2m}\right)\right)\right), \tag{B.18}$$

which is valid for $m^2/k^2 > 1/4$.

Case (b)

For the case (b), the square root in eq. (B.18) becomes imaginary and the inverse sine will be evaluated on its branch cut. Hence, we want to use the analytic continuation of the inverse sine to extend this result to case (b). We will use that

$$\arcsin(z) = -i\ln\left(iz + \sqrt{1-z^2}\right), \tag{B.19}$$

and thus

$$\sqrt{\frac{4m^2}{k^2}-1}\arcsin\left(\frac{k}{2m}\right) = \sqrt{1-\frac{4m^2}{k^2}}\ln\left(i\frac{k}{2m} + i\sqrt{\frac{k^2}{4m^2}-1}\right). \tag{B.20}$$

Writing $i = e^{i\pi/2}$ and using the principal value yields

$$\sqrt{\frac{4m^2}{k^2}-1}\arcsin\left(\frac{k}{2m}\right) = \sqrt{1-\frac{4m^2}{k^2}}\left[\ln\left(\frac{k}{2m} + \sqrt{\frac{k^2}{4m^2}-1}\right) + i\frac{\pi}{2}\right]. \tag{B.21}$$

With this result we find for S_1 in case (b)

$$S_1 = -\frac{1}{32\pi^2}\left(\ln\left(\frac{m^2}{4\pi\mu^2}\right) - 2\left(1 - \sqrt{1-\frac{4m^2}{k^2}}\left[\ln\left(\frac{k}{2m} + \sqrt{\frac{k^2}{4m^2}-1}\right) + i\frac{\pi}{2}\right]\right)\right), \tag{B.22}$$

where the only imaginary contribution is from the last term.

Case (c)
In this case we have $m = 0$ and thus

$$S_1 = -\frac{1}{16\pi^2}\int_0^1 \mathrm{d}x \ln\left(\frac{k^2 x(1-x)}{4\pi\mu^2}\right) + i\pi. \tag{B.23}$$

The integration yields

$$S_1 = -\frac{1}{16\pi^2}\left(\ln\left(\frac{k^2}{4\pi\mu^2}\right) - 2 + i\pi\right). \tag{B.24}$$

Appendix C

Gap Equation for the Higgs Boson in the SM

In this appendix we consider the gap equation

$$M^2(h,\varphi) = m_{h_1}^2(h,\varphi) + \Sigma \tag{C.1}$$

of the Higgs field in the SM with vanishing external momentum. The self energy due to interaction with other fields will be divided to a contribution coming from scalars, gauge bosons and fermions

$$\Sigma = \Sigma^{\phi} + \Sigma^{\mathrm{GB}} + \Sigma^{\psi}. \tag{C.2}$$

For each contribution, we split the self-energies to contribution coming from the bubble diagram and from the sunset diagram

$$\Sigma^i = \Sigma^i_B + \Sigma^i_S. \tag{C.3}$$

We derive the self-energies from the 2PI approach, i.e. we compute 2PI diagrams Γ^2 at two loop level with vertices in the shifted theory and use the resummed propagator G for the Higgs boson. For the propagators of other fields, we use the propagator at tree-level in the shifted theory. In this approach, self-energies are obtained by taking a derivative of Γ^2 with respect to G.

Scalar Fields

Bubble contribution

Here we consider the interaction of the Higgs field h_1 with itself

$$(-i)^2 \frac{3}{4}\lambda_1 \int \frac{\mathrm{d}^4k}{(2\pi)^4} G_{h_1}(k) \int \frac{\mathrm{d}^4p}{(2\pi)^4} G_{h_1}(p) \tag{C.4}$$

and with the three Goldstone bosons

$$(-i)^2 3 \frac{1}{2}\lambda_1 \int \frac{\mathrm{d}^4k}{(2\pi)^4} G_{GB}(k) \int \frac{\mathrm{d}^4p}{(2\pi)^4} G_{h_1}(p). \tag{C.5}$$

The symmetry factor of this diagram is 1/4 but there are three would-be Goldstone bosons which are running in the loop. So the two-loop 2PI diagrams involving only scalar fields are

$$V_2^{\phi,B} = -\frac{3\lambda_1}{4}\left[\int \frac{\mathrm{d}^4k}{(2\pi)^4} G_{h_1}(k) \int \frac{\mathrm{d}^4p}{(2\pi)^4} G_{h_1}(p) + 2\int \frac{\mathrm{d}^4k}{(2\pi)^4} G_{GB}(k) \int \frac{\mathrm{d}^4p}{(2\pi)^4} G_{h_1}(p)\right] \tag{C.6}$$

Now we can obtain the corresponding self energies by taking the derivative with respect to G_{h_1} and including the factor (-2) (cf. eq. (1.68))

$$\Sigma_B^{\phi}(h) = -2\frac{\partial V_2^{\phi,B}}{\partial G_{h_1}} = \frac{6\lambda_1}{4}\left[2\int \frac{\mathrm{d}^4k}{(2\pi)^4} G_{h_1}(k) + 2\int \frac{\mathrm{d}^4k}{(2\pi)^4} G_{GB}(k)\right]. \tag{C.7}$$

Using Feynman rules at finite temperature and including the factor (-2) this reads

$$\Sigma_B^{\phi}(h) = \frac{6\lambda_1}{4\beta}\sum_{n=\infty}^{\infty}\int \frac{\mathrm{d}^3k}{(2\pi)^3}\left[\frac{2}{\omega_n^2 + \mathbf{k} + M(h^2,\varphi^2)^2} + \frac{2}{\omega_n^2 + \mathbf{k} + m_{\mathrm{GB}}(h^2,\varphi^2)^2}\right]. \tag{C.8}$$

In terms of the integral defined in (3.27) this can be written as

$$\Sigma_B^{\phi}(h) = 6\lambda_1[I_1(M) + I_1(m_{\mathrm{GB}})], \tag{C.9}$$

where M is the tree-level mass of the Higgs boson and m_{GB} the tree-level mass of the Goldstone bosons. The expression for I_1 can be found in eq. (3.27)

Sunset Contribution

Here, we need the 3-point vertices which are given by $-i(\lambda_1 h)$ *. The symmetry factor of the sunset diagrams is 3. Also here we have two contributions. On the one hand, the two-loop sunset diagram only with Higgs propagators

$$(-i)^3 3(\lambda_1 h)^2 \int \frac{\mathrm{d}^4k}{(2\pi)^4}\int \frac{\mathrm{d}^4p}{(2\pi)^4} G_h(k)G_h(p)G_h(k-p), \tag{C.10}$$

and on the other hand, with two Goldstones and one Higgs propagator. The symmetry factor is 1, but there are 3 Goldstone Boson running in the loop. We obtain for that diagram

$$(-i)^3 3(\lambda_1 h)^2 \int \frac{\mathrm{d}^4k}{(2\pi)^4}\int \frac{\mathrm{d}^4p}{(2\pi)^4} G_h(k)G_{GB}(p)G_{GB}(k-p). \tag{C.11}$$

In total we have

$$V_2^{\phi,S} = -i3(\lambda_1 h)^2 \int \frac{\mathrm{d}^4k}{(2\pi)^4}\int \frac{\mathrm{d}^4p}{(2\pi)^4}[G_h(k)G_h(p)G_h(k-p) + G_h(k)G_{GB}(p)G_{GB}(k-p)], \tag{C.12}$$

so the self energy is

$$\Sigma_S^{\phi} = i6(\lambda_1 h)^2 \int \frac{\mathrm{d}^4k}{(2\pi)^4}[3G_h(k)G_h(k-p) + G_{GB}(k)G_{GB}(k-p)] \tag{C.13}$$

*One can derive this by working in the shifted theory.

We evaluate this first for zero momenta $p = 0$ and for Feynman rules at finite temperature,

$$\begin{aligned}\Sigma_S^{\phi} &= i6(\lambda_1 h)^2 \frac{i}{\beta} \sum_{n=\infty}^{\infty} \int \frac{\mathrm{d}^3 k}{(2\pi)^3} \left[3 \frac{1}{(\omega_n^2 + \mathbf{k}^2 + M^2)^2} + \frac{1}{(\omega_n^2 + \mathbf{k}^2 + m_{GB}^2)^2} \right] \\ &= -(\lambda_1 h)^2 [36 I_2(M) + 12 I_2(m_{GB})]. \end{aligned} \tag{C.14}$$

Note that a factor of $1/2$ was absorbed in the definition of I_2. The solution of I_2 (cf. eq. (3.28)) has a negative sign, so the contribution to the resummed mass will be positive.

Gauge Bosons

The interactions we need to consider here are described the Lagrangian

$$\mathcal{L} \supseteq \frac{g^2}{4}(h + h_1)^2 W_\mu^+ W^{-,\mu} + \frac{1}{2}\frac{g^2 + g'^2}{4}(h + h_1)^2 Z_\mu Z^\mu. \tag{C.15}$$

The vertices in the shifted theory which will be necessary in this section are given by

- $h_1^2 - W^2$-vertex: $i g_{\mu\nu} \frac{g^2}{4}$,
- $h_1^2 - Z^2$-vertex: $i g_{\mu\nu} \frac{g^2 + g'^2}{8}$,
- $h_1 - W^2$-vertex: $i g_{\mu\nu} \frac{g^2 h}{2}$,
- $h_1 - Z^2$-vertex: $i g_{\mu\nu} \frac{(g^2 + g'^2) h}{4}$.

Bubble Contribution

With the Feynman rules at hand, we can write down the two double bubble diagrams. We will include the overall factor $(-i)$. The diagram involving the Z gauge boson is

$$\begin{aligned} V_2^{Z,B} &= -i \frac{g^2 + g'^2}{8} \int \frac{\mathrm{d}^4 k}{(2\pi)^4} \frac{g^{\mu\nu}\left(g_{\mu\nu} - \frac{k_\mu k_\nu}{k^2}\right)}{k^2 - m_Z^2} \int \frac{\mathrm{d}^4 p}{(2\pi)^4} G_{h_1}(p) \\ &= -3i \frac{g^2 + g'^2}{8} \int \frac{\mathrm{d}^4 k}{(2\pi)^4} \frac{1}{k^2 - m_Z^2} \int \frac{\mathrm{d}^4 p}{(2\pi)^4} G_{h_1}(p). \end{aligned} \tag{C.16}$$

In the last line we performed the trace, which gives 3. Similarly, for the two W gauge bosons we find

$$V_2^{W,B} = -3i \frac{g^2}{4} \int \frac{\mathrm{d}^4 k}{(2\pi)^4} \frac{1}{k^2 - m_W^2} \int \frac{\mathrm{d}^4 p}{(2\pi)^4} G_{h_1}(p). \tag{C.17}$$

We now can obtain the self energy of the Higgs field due to interaction with the massive gauge bosons. It reads

$$\Sigma_B^{\mathrm{GB}}(h) = -\frac{12}{8} i (g^2 + g'^2) \int \frac{\mathrm{d}^4 k}{(2\pi)^4} \frac{1}{k^2 - m_Z^2} + \frac{12}{8} i g^2 \int \frac{\mathrm{d}^4 k}{(2\pi)^4} \frac{1}{k^2 - m_W^2} \tag{C.18}$$

Translating this expression to Feynman rules at finite temperature yields

$$\Sigma_B^{\mathrm{GB}}(h) = \frac{6}{4}(g^2 + g'^2) I_1(m_Z) + \frac{12}{4} g^2 I_1(m_W). \tag{C.19}$$

Sunset Contribution

The diagram involving the Z gauge boson is

$$-i\left(\frac{(g^2+g'^2)h}{4}\right)^2\int\frac{\mathrm{d}^4k}{(2\pi)^4}\int\frac{\mathrm{d}^4p}{(2\pi)^4}\frac{\left(g_{\mu\nu}-\frac{k_\mu k_\nu}{k^2}\right)\left(g_{\mu\nu}-\frac{(k-p)_\mu(k-p)_\nu}{(k-p)^2}\right)}{(k^2-m_Z^2)((k-p)^2-m_Z^2)}G_{h_1}(p). \tag{C.20}$$

Thus, for the self energy follows

$$\Sigma_S^Z(p)=2i\left(\frac{(g^2+g'^2)h}{4}\right)^2\int\frac{\mathrm{d}^4k}{(2\pi)^4}\frac{\left(g_{\mu\nu}-\frac{k_\mu k_\nu}{k^2}\right)\left(g_{\mu\nu}-\frac{(k-p)_\mu(k-p)_\nu}{(k-p)^2}\right)}{(k^2-m_Z^2)((k-p)^2-m_Z^2)}. \tag{C.21}$$

We evaluate this in the limit $p=0$,

$$\begin{aligned}\Sigma_S^Z(0)&=2i\left(\frac{(g^2+g'^2)h}{4}\right)^2\int\frac{\mathrm{d}^4k}{(2\pi)^4}\frac{\left(g_{\mu\nu}-\frac{k_\mu k_\nu}{k^2}\right)\left(g_{\mu\nu}-\frac{k_\mu k_\nu}{k)^2}\right)}{(k^2-m_Z^2)(k^2-m_Z^2)}\\&=6i\left(\frac{(g^2+g'^2)h}{4}\right)^2\int\frac{\mathrm{d}^4k}{(2\pi)^4}\frac{1}{(k^2-m_Z^2)^2}.\end{aligned} \tag{C.22}$$

At finite temperature this reads

$$\begin{aligned}\Sigma_S^Z(0)&=-12\left(\frac{(g^2+g'^2)h}{4}\right)^2I_2(m_Z)\\&=-\frac{3}{4}\left(g^2+g'^2\right)^2h^2I_2(m_Z).\end{aligned} \tag{C.23}$$

Similarly, for the W bosons we obtain

$$\Sigma_S^W(0)=-\frac{6}{4}8g^4h^2I_2(m_Z). \tag{C.24}$$

Top Quark

The interaction of the Higgs boson with the top quark is described by the Yukawa coupling in the SM Lagrangian

$$\mathcal{L}\supseteq\frac{y_t}{\sqrt{2}}(h+h_1)\bar{q}_tq_t, \tag{C.25}$$

where h is the vev of the Higgs field and y_t the Yukawa coupling constant of the top quark. The propagator of the top quark is

$$D_t(k)=\frac{i(\gamma\cdot k+m_t)}{k^2-m_t^2}. \tag{C.26}$$

The only 2PI diagram containing the Higgs and top quark field is at two-loop order the sunset diagram

$$V_2^\psi=-(-i)^3\frac{1}{2}\left(\frac{y_t}{\sqrt{2}}\right)^2\int\frac{\mathrm{d}^4k}{(2\pi)^4}\int\frac{\mathrm{d}^4p}{(2\pi)^4}G_{h_1}(p-k)\,\mathrm{Tr}[D_t(k)\cdot D_t(p)]. \tag{C.27}$$

Furthermore, we included an overall minus for the fermion loop. The trace is taken in spinor and color space. The corresponding self-energy for the Higgs boson is obtained by

$$\Sigma^{\psi}(h,k) = -2\frac{\partial V_2^{\psi}}{\partial G_{h_1}(k)}. \tag{C.28}$$

At zero momentum, that equation reduces to

$$\Sigma^{\psi}(h,0) = \frac{y_t^2}{2}\int \frac{\mathrm{d}^4k}{(2\pi)^4}\,\mathrm{Tr}[D_t(k)\cdot D_t(k)]. \tag{C.29}$$

The trace in color space can be performed trivially since the propagator is diagonal in this space and gives a factor of three. We are left with the trace in spinor space

$$\mathrm{Tr}[D_t(k)\cdot D_t(k)] = -\frac{3\,\mathrm{Tr}[(\gamma^\mu k_\mu + m)(\gamma^\nu k_\nu + m)]}{(k^2 - m_t(h)^2)^2}. \tag{C.30}$$

Since the trace of an odd number of gamma matrices vanishes, this simplifies to

$$\mathrm{Tr}[(\gamma^\mu k_\mu + m)(\gamma^\nu k_\nu + m)] = k_\mu k_\nu\,\mathrm{Tr}[\gamma^\mu\gamma^\nu] + m_t(h)^2\,\mathrm{Tr}[1], \tag{C.31}$$

and for a Dirac fermion this is equal to

$$4(k^2 + m_t(h)^2). \tag{C.32}$$

We write the integrand as

$$\begin{aligned} -12\frac{k^2 + m_t(h)^2}{(k^2 - m_t(h)^2)^2} &= -12\frac{k^2 - m_t(h)^2 + 2m_t(h)^2}{(k^2 - m_t(h)^2)^2} \\ &= -12\left(\frac{1}{(k^2 - m_t(h)^2)} + \frac{2m_t(h)^2}{(k^2 - m_t(h)^2)^2}\right). \end{aligned} \tag{C.33}$$

At finite temperatures eq. (C.29) gets replaced by

$$\Sigma^{\psi}(h,0) = 12i\frac{y_t^2}{2}\frac{i}{\beta}\sum_{n=\infty}^{\infty}\int \frac{\mathrm{d}^3k}{(2\pi)^3}\left(\frac{-1}{(\omega_n^2 + \mathbf{k} + m_t(h)^2)} + \frac{2m_t(h)^2}{(\omega_n^2 + \mathbf{k}^2 + m_t(h)^2)^2}\right), \tag{C.34}$$

where ω_n are here the fermionic Matsubara frequencies. We write eq. (C.34) as

$$\Sigma^{\psi}(h,0) = 12y_t^2\left[-J_1(m_t^2) + 2m_t(h)^2 J_2(m_t^2)\right], \tag{C.35}$$

where the J_a functions are defined by

$$J_a(m^2) = \frac{1}{2\beta}\sum_{n=\infty}^{\infty}\int \frac{\mathrm{d}^3k}{(2\pi)^3}\frac{1}{(\omega_n + \mathbf{k}^2 + m^2)^a}. \tag{C.36}$$

The finite parts of the two integral in eq. (C.35) in dimensional regularization are

$$J_1(m^2) = \frac{m^2}{32\pi^2}\left[\log\left(\frac{m^2}{\mu^2}\right) - 1\right] + \frac{T^2}{2\pi^2}\left.\frac{\partial J_F(y^2)}{\partial y^2}\right|_{y=m/T}, \tag{C.37}$$

$$J_2(m^2) = -\frac{1}{32\pi^2}\log\left(\frac{m^2}{\mu^2}\right) - \frac{1}{2\pi^2}\left.\frac{\partial^2 J_F(y^2)}{\partial (y^2)^2}\right|_{y=m/T}. \tag{C.38}$$

The overall contribution of the top quark to the gap equation is negative as expected.

Bibliography

[1] W. A. Bardeen, "On naturalness in the standard model", FERMILAB-CONF-95-301-T (1995).

[2] S. Coleman and E. Weinberg, "Radiative corrections as the origin of spontaneous symmetry breaking", Phys. Rev. D **7**, 1888 (1973).

[3] T. G. Steele and Z.-W. Wang, "Is radiative electroweak symmetry breaking consistent with a 125 gev higgs mass?", Phys. Rev. Lett. 110 (2013) 151601 (2012) 10.1103/PhysRevLett.110.151601, arXiv:1209.5416v3 [hep-ph].

[4] V. Elias, R. B. Mann, D. G. C. McKeon, and T. G. Steele, "Radiative electroweak symmetry-breaking revisited", Phys.Rev.Lett. 91 (2003) 251601 (2003) 10.1103/PhysRevLett.91.251601, arXiv:hep-ph/0304153v2 [hep-ph].

[5] L. Chataignier, T. Prokopec, M. G. Schmidt, and B. Swiezewska, "Systematic analysis of radiative symmetry breaking in models with extended scalar sector", (2018), arXiv:1805.09292v1 [hep-ph].

[6] D. A. Kirzhnits, "Weinberg model in the hot universe", JETP Lett. **15**, [Pisma Zh. Eksp. Teor. Fiz.15,745(1972)], 529 (1972).

[7] K. Kajantie, M. Laine, K. Rummukainen, and M. Shaposhnikov, "Is there a hot electroweak phase transition at m(h) larger or equal to m(w)?", Phys.Rev.Lett.77:2887-2890,1996 (1996) 10.1103/PhysRevLett.77.2887, arXiv:hep-ph/9605288v1 [hep-ph].

[8] G. W. Anderson and L. J. Hall, "The Electroweak phase transition and baryogenesis", Phys. Rev. **D45**, 2685 (1992).

[9] http://sci.esa.int/lisa/.

[10] C. Caprini, M. Hindmarsh, S. Huber, T. Konstandin, J. Kozaczuk, G. Nardini, J. M. No, A. Petiteau, P. Schwaller, G. Servant, and D. J. Weir, "Science with the space-based interferometer elisa. ii: gravitational waves from cosmological phase transitions", (2015) 10.1088/1475-7516/2016/04/001, arXiv:1512.06239v2 [astro-ph.CO].

[11] R. Apreda, M. Maggiore, A. Nicolis, and A. Riotto, "Gravitational waves from electroweak phase transitions", Nucl.Phys. B631 (2002) 342-368 (2001) 10.1016/S0550-3213(02)00264-X, arXiv:gr-qc/0107033v1 [gr-qc].

[12] C. Grojean and G. Servant, "Gravitational waves from phase transitions at the electroweak scale and beyond", Phys.Rev.D75:043507,2007 (2006) 10.1103/PhysRevD.75.043507, arXiv:hep-ph/0607107v1 [hep-ph].

[13] F. Sannino and J. Virkajärvi, "First order electroweak phase transition from (non)conformal extensions of the standard model", Phys. Rev. D 92, 045015 (2015) (2015) 10.1103/PhysRevD.92.045015, arXiv:1505.05872v2 [hep-ph].

[14] L. Marzola, A. Racioppi, and V. Vaskonen, "Phase transition and gravitational wave phenomenology of scalar conformal extensions of the standard model", Eur. Phys. J.

C 77, 484 (2017) (2017) 10.1140/epjc/s10052-017-4996-1, arXiv:1704.01034v2 [hep-ph].

[15] D. Croon, V. Sanz, and G. White, "Model discrimination in gravitational wave spectra from dark phase transitions", (2018), arXiv:1806.02332v1 [hep-ph].

[16] D. G. Figueroa, E. Megias, G. Nardini, M. Pieroni, M. Quiros, A. Ricciardone, and G. Tasinato, "Lisa as a probe for particle physics: electroweak scale tests in synergy with ground-based experiments", (2018), arXiv:1806.06463v1 [astro-ph.CO].

[17] R. R. Parwani, "Resummation in a hot scalar field theory", Phys.Rev.D45:4695,1992; Erratum-ibid.D48:5965,1993; Phys.Rev.D48:5965,1993 (1992) 10.1103/PhysRevD.45.469510.1103/PhysRevD.48.5965, arXiv:hep-ph/9204216v1 [hep-ph].

[18] J. R. Espinosa, M. Quirós, and F. Zwirner, "On the phase transition in the scalar theory", Phys.Lett.B291:115-124,1992 (1992) 10.1016/0370-2693(92)90129-R, arXiv:hep-ph/9206227v1 [hep-ph].

[19] J. R. Espinosa, M. Quiros, and F. Zwirner, "On the nature of the electroweak phase transition", Phys.Lett.B314:206-216,1993 (1992) 10.1016/0370-2693(93)90450-V, arXiv:hep-ph/9212248v4 [hep-ph].

[20] M. E. Carrington, "Effective potential at finite temperature in the standard model", Phys. Rev. D **45**, 2933 (1992).

[21] G. Amelino-Camelia and S.-Y. Pi, "Self-consistent improvement of the finite-temperature effective potential", Phys. Rev. D **47**, 2356 (1993).

[22] S. Weinberg, *The quantum theory of fields*, Vol. Volume II Modern Applications (Cambridge University Press, 1996).

[23] S. Coleman, *Aspects of symmetry: selected erice lectures* (Cambridge Universtiy Press, 1988).

[24] V. A. Miransky, *Dynamical symmetry breaking in quantum field theories* (World Scientific Publishing Co., 1993).

[25] R. Jackiw, "Functional evaluation of the effective potential", Phys. Rev. D **9**, 1686 (1974).

[26] M. Quiros, "Finite temperature field theory and phase transitions", (1999), arXiv:hep-ph/9901312v1 [hep-ph].

[27] B. Swiezewska, "Higgs boson and vacuum stability in models with extended scalar sector", PhD thesis (University of Warsaw, 2016).

[28] J. M. Cornwall, R. Jackiw, and E. Tomboulis, "Effective action for composite operators", Phys. Rev. D **10**, 2428 (1974).

[29] J. Berges, "Introduction to nonequilibrium quantum field theory", AIP Conf.Proc.739:3-62,2005 (2004) 10.1063/1.1843591, arXiv:hep-ph/0409233v1 [hep-ph].

[30] J. Berges, S. Borsányi, U. Reinosa, and J. Serreau, "Nonperturbative renormalization for 2pi effective action techniques", Annals of Physics **320**, 344 (2005).

[31] N. Landsman and C. van Weert, "Real- and imaginary-time field theory at finite temperature and density", Physics Reports **145**, 141 (1987).

[32] R. H. Brandenberger, "Quantum field theory methods and inflationary universe models", Rev. Mod. Phys. **57**, 1 (1985).

[33] M. L. Bellac, *Thermal field theory (cambridge monographs on mathematical physics)* (Cambridge University Press, 2010).

[34] M. B. Einhorn and D. T. Jones, "A new renormalization group approach to multiscale problems", Nuclear Physics B **230**, 261 (1984).

[35] L. Chataignier, T. Prokopec, M. G. Schmidt, and B. Swiezewska, "Single-scale renormalisation group improvement of multi-scale effective potentials", JHEP 03 (2018) 014 (2018) 10.1007/JHEP03(2018)014, arXiv:1801.05258v2 [hep-ph].

[36] E. Braaten and R. D. Pisarski, "Soft amplitudes in hot gauge theories: a general analysis", Nuclear Physics B **337**, 569 (1990).

[37] P. Arnold and O. Espinosa, "The effective potential and first-order phase transitions: beyond leading order", Phys.Rev.D47:3546,1993; Erratum-ibid.D50:6662,1994; Phys.Rev.D50:6662,1994 (1992) 10.1103/PhysRevD.47.354610.1103/PhysRevD.50.6662, arXiv:hep-ph/9212235v2 [hep-ph].

[38] A. Pilaftsis and D. Teresi, "Symmetry improved 2pi effective action and the infrared divergences of the standard model", 2015 J. Phys.: Conf. Ser. 631 012008 (2015) 10.1088/1742-6596/631/1/012008, arXiv:1502.07986v1 [hep-ph].

[39] L. Dolan and R. Jackiw, "Symmetry behavior at finite temperature", Phys. Rev. D **9**, 3320 (1974).

[40] A. Fowlie, "A fast C++ implementation of thermal functions", (2018) 10.1016/j.cpc.2018.02.015, arXiv:1802.02720 [hep-ph].

[41] K. A. Meissner and H. Nicolai, "Conformal symmetry and the standard model", Phys.Lett.B648:312-317,2007 (2006) 10.1016/j.physletb.2007.03.023, arXiv:hep-th/0612165v4 [hep-th].

[42] K. A. Meissner and H. Nicolai, "Conformal symmetry and the standard model", Phys.Lett.B648:312-317,2007 (2006) 10.1016/j.physletb.2007.03.023, arXiv:hep-th/0612165v4 [hep-th].

[43] K. A. Meissner and H. Nicolai, "Effective action, conformal anomaly and the issue of quadratic divergences", Phys.Lett.B660:260-266,2008 (2007) 10.1016/j.physletb.2007.12.035, arXiv:0710.2840v2 [hep-th].

[44] P. H. Chankowski, A. Lewandowski, K. A. Meissner, and H. Nicolai, "Softly broken conformal symmetry and the stability of the electroweak scale", Mod. Phys. Lett. A, Vol. 30, No. 2 (2015), 1550006 (2014) 10.1142/S0217732315500066, arXiv:1404.0548v2 [hep-ph].

[45] A. Lewandowski, K. A. Meissner, and H. Nicolai, "Conformal standard model, leptogenesis and dark matter", Phys. Rev. D 97, 035024 (2018) (2017) 10.1103/PhysRevD.97.035024, arXiv:1710.06149v2 [hep-ph].

[46] R. Hempfling, "The next-to-minimal coleman-weinberg model", Physics Letters B **379**, 153 (1996).

[47] T. Hambye and A. Strumia, "Dynamical generation of the weak and dark matter scale", Physical Review D **88** (2013) 10.1103/PhysRevD.88.055022, arXiv:1306.2329v1 [hep-ph].

[48] C. D. Carone and R. Ramos, "Classical scale-invariance, the electroweak scale and vector dark matter", Physical Review D **88** (2013) 10.1103/PhysRevD.88.055020, arXiv:1307.8428v3 [hep-ph].

[49] V. V. Khoze, C. McCabe, and G. Ro, "Higgs vacuum stability from the dark matter portal", Journal of High Energy Physics **2014** (2014) 10.1007/jhep08(2014)026, arXiv:1403.4953v2 [hep-ph].

[50] A. Karam and K. Tamvakis, "Dark matter and neutrino masses from a scale-invariant multi-higgs portal", Phys. Rev. D 92, 075010 (2015) (2015) 10.1103/PhysRevD.92.075010, arXiv:1508.03031v3 [hep-ph].

[51] V. V. Khoze and A. D. Plascencia, "Dark matter and leptogenesis linked by classical scale invariance", Journal of High Energy Physics **2016** (2016) 10.1007/JHEP11(2016)025, arXiv:1605.06834v2 [hep-ph].

[52] K. Kannike, "Vacuum stability conditions from copositivity criteria", (2012) 10.1140/epjc/s10052-012-2093-z, arXiv:1205.3781v3 [hep-ph].

[53] T. Robens and T. Stefaniak, "Lhc benchmark scenarios for the real higgs singlet extension of the standard model", Eur.Phys.J. C76 (2016) no.5, 268 (2016) 10.1140/epjc/s10052-016-4115-8, arXiv:1601.07880v2 [hep-ph].

[54] T. Robens and T. Stefaniak, "Status of the higgs singlet extension of the standard model after lhc run 1", EPJC (2015) 75:105 (2015) 10.1140/epjc/s10052-015-3323-y, arXiv:1501.02234v2 [hep-ph].

[55] A. Ilnicka, T. Robens, and T. Stefaniak, "Constraining extended scalar sectors at the lhc and beyond", Published in Mod.Phys.Lett. A33 (2018) no.10n11, 1830007 (2018) 10.1142/S0217732318300070, arXiv:1803.03594v2 [hep-ph].

[56] C. Englert, T. Plehn, D. Zerwas, and P. M. Zerwas, "Exploring the higgs portal", Phys.Lett.B703:298-305,2011 (2011) 10.1016/j.physletb.2011.08.002, arXiv:1106.3097v2 [hep-ph].

[57] J. R. Espinosa, T. Konstandin, J. M. No, and M. Quiros, "Some cosmological implications of hidden sectors", Phys.Rev.D78:123528,2008 (2008) 10.1103/PhysRevD.78.123528, arXiv:0809.3215v2 [hep-ph].

[58] J. M. Cline, S. Kraml, G. Laporte, and H. Yamashita, "Electroweak phase transition and lhc signatures in the singlet majoron model", JHEP 0907:040,2009 (2009) 10.1088/1126-6708/2009/07/040, arXiv:0905.2559v1 [hep-ph].

[59] J. Elias-Miro, J. R. Espinosa, and T. Konstandin, "Taming infrared divergences in the effective potential", (2014) 10.1007/JHEP08(2014)034, arXiv:1406.2652v1 [hep-ph].

[60] S. P. Martin, "Taming the goldstone contributions to the effective potential", Phys. Rev. D 90, 016013 (2014) (2014) 10.1103/PhysRevD.90.016013, arXiv:1406.2355v2 [hep-ph].

[61] L. D. Rose, C. Marzo, and A. Urbano, "On the fate of the standard model at finite temperature", (2015) 10.1007/JHEP05(2016)050, arXiv:1507.06912v2 [hep-ph].

[62] P. Basler and M. Muhlleitner, "Bsmpt - beyond the standard model phase transitions -a tool for the electroweak phase transition in extended higgs sectors", (2018), arXiv:1803.02846v1 [hep-ph].

[63] M. Sher, "Electroweak higgs potential and vacuum stability", Physics Reports **179**, 273 (1989).

[64] A. Eichhorn, H. Gies, J. Jaeckel, T. Plehn, M. M. Scherer, and R. Sondenheimer, "The higgs mass and the scale of new physics", (2015) 10.1007/JHEP04(2015)022, arXiv:1501.02812v1 [hep-ph].

[65] E. Gildener and S. Weinberg, "Symmetry breaking and scalar bosons", Phys. Rev. D **13**, 3333 (1976).

[66] A. Linde, "Decay of the false vacuum at finite temperature", Nuclear Physics B **216**, 421 (1983).

[67] J. Ignatius, "Cosmological phase transitions", (1993), arXiv:hep-ph/9312293v1 [hep-ph].

[68] S. J. Huber, P. John, and M. G. Schmidt, "Bubble walls, cp violation and electroweak baryogenesis in the mssm", Eur.Phys.J.C20:695-711,2001 (2001), arXiv:hep-ph/0101249v2 [hep-ph].

[69] T. Konstandin and S. J. Huber, "Numerical approach to multi dimensional phase transitions", JCAP 0606 (2006) 021 (2006) 10.1088/1475-7516/2006/06/021, arXiv:hep-ph/0603081v2 [hep-ph].

[70] A. Masoumi, K. D. Olum, and B. Shlaer, "Efficient numerical solution to vacuum decay with many fields", (2016) 10.1088/1475-7516/2017/01/051, arXiv:1610.06594v3 [gr-qc].

[71] V. Barger, P. Langacker, M. McCaskey, M. J. Ramsey-Musolf, and G. Shaughnessy, "Lhc phenomenology of an extended standard model with a real scalar singlet", Phys.Rev.D77:035005,2008 (2007) 10.1103/PhysRevD.77.035005, arXiv:0706.4311v1 [hep-ph].

[72] G. D. Moore and T. Prokopec, "How fast can the wall move? a study of the electroweak phase transition dynamics", Phys.Rev.D52:7182-7204,1995 (1995) 10.1103/PhysRevD.52.7182, arXiv:hep-ph/9506475v2 [hep-ph].